

UNIVERSITY OF CALIFORNIA, SAN DIEGO

**High Efficiency Broadband Envelope-Tracking Power Amplifiers**

A dissertation submitted in partial satisfaction of the requirements for the  
degree Doctor of Philosophy

in

Electrical Engineering (Electronic Circuits and Systems)

by

Jonmei Johana Yan

Committee in charge:

Peter M. Asbeck, Chair  
Prabhakar Bandaru  
James Buckwalter  
Chung K. Cheng  
Lawrence E. Larson

2013

Copyright ©

Jonmei Johana Yan, 2013

All rights reserved.

The dissertation of Jonmei Johana Yan is approved, and it is acceptable in quality and form for publication on microfilm and electronically:

---

---

---

---

---

Chair

University of California, San Diego

2013

## DEDICATION

*To my parents who have always been there supporting me and probably secretly led me to this path by giving me a multi-meter at age 5, microscope at age 6, and a computer at age 7.*

父母一直以來是我生活中的良師。  
在他們潛移默化下, 造就了今天的我。  
感謝他們付出無私的愛。

## EPIGRAPH

To myself, I am only a child playing  
on the beach, while vast oceans of  
truth lie undiscovered before me.

*Isaac Newton*

We cannot solve our problems with the same  
thinking we used when we created them.

*Albert Einstein*

Vision without execution is delusion.

*Thomas Edison*

# TABLE OF CONTENTS

Signature Page .....	iii
Dedication .....	iv
Epigraph .....	v
Table of Contents .....	vi
List of Figures .....	viii
List of Tables .....	xiii
Acknowledgments .....	xiv
Vita .....	xviii
Abstract of the Dissertation .....	xxii
<b>Chapter 1 Introduction .....</b>	<b>1</b>
1.1 Base-station Power Amplifiers .....	1
1.1.1 Peak-to-Average Ratio Reduction for Multi-carrier Transmission.....	3
1.2 High Efficiency Power Amplifier for High Peak-to-Average-Power Signals.....	5
1.2.1 Doherty Power Amplifiers.....	5
1.2.2 Outphasing Power Amplifiers.....	7
1.2.3 ET/EER Power Amplifiers .....	8
1.3 Scope of the Dissertation .....	9
<b>Chapter 2 Envelope Tracking Power Amplifier System.....</b>	<b>13</b>
2.1 Introduction.....	13
2.2 Envelope Tracking Power Amplifier Architecture .....	14
2.2.1 Envelope Supply Waveform Shaping .....	16
2.2.2 Envelope Tracking Power Amplifier Efficiency .....	17
2.2.3 Dynamic Power Supply Efficiency.....	18
2.2.4 RF Power Amplifier Efficiency under Envelope-Tracking .....	21
2.3 Broadband Test-bench Implementation.....	25
2.3.1 Calibration Equalization for Broadband Flat Linear Response .....	31
2.3.2 Memoryless Digital Pre-distortion Implementation .....	36
2.4 Envelope Tracking Power Amplifier Performance.....	38
2.4.1 UHF Envelope Tracking Power Amplifier .....	39
2.4.2 Band 14 - 780 MHz Envelope Tracking Power Amplifier .....	45
2.4.3 2.14 GHz Envelope Tracking Power Amplifier.....	50
2.4.4 Envelope Tracking Power Amplifiers for Mm-wave .....	56
2.5 Summary .....	61
2.6 Acknowledgments.....	63
<b>Chapter 3 Envelope Tracking Power Amplifiers Under Average Power Back-off.....</b>	<b>65</b>
3.1 Introduction.....	65
3.2 Envelope Tracking Operation in Back-off.....	68
3.3 Average Power Efficiency in Back-off.....	73
3.3.1 Power Amplifier Efficiency at Various Output Powers.....	73
3.3.2 Average Efficiency with Modulated Signals .....	76

3.4	Scalable DPD Model for Average Power Back-off.....	79
3.5	Modeling of Long Term Envelope Tracking Power Amplifier Performance.....	84
3.5.1	Base-Station Average Output Power .....	87
3.6	Summary .....	91
3.7	Acknowledgments.....	92
Chapter 4 Broadband Envelope Tracking Power Amplifier .....		93
4.1	Introduction.....	93
4.2	Broadband GaN Power Amplifier .....	96
4.2.1	Stacked Power Amplifier Design.....	97
4.2.2	RC Feedback Implementation.....	100
4.2.3	GaN Stacked Power Amplifier with RC Feedback Performance Results.....	103
4.3	Push-pull Broadband GaN Power Amplifier .....	107
4.3.1	Stacked Feedback Design .....	111
4.3.2	Broadband Balun Design .....	112
4.3.3	Push-pull Power Amplifier Implementation and Performance Results .....	113
4.4	Multi-Octave Envelope Tracking Power Amplifier Design .....	118
4.4.1	Broadband Envelope Tracking Power Amplifier Design .....	118
4.4.2	Broadband Envelope Tracking Power Amplifier Implementation .....	122
4.4.3	Broadband Envelope Tracking Power Amplifier Performance Results .....	126
4.5	Summary .....	129
4.6	Acknowledgments.....	133
Chapter 5 Adaptive De-troughing for Wide Modulation Bandwidth Signal .....		134
5.1	Introduction.....	134
5.2	Power Supply Waveform Engineering Implementation .....	136
5.3	Effects on Dynamic Power Supply Performance.....	148
5.4	Effects on RF Power Amplifier Efficiency.....	150
5.5	Digital Pre-distortion for “Adaptively De-troughed” ET Power Amplifiers.....	152
5.6	Adaptively De-troughed Envelope Tracking Power Amplifier Performance....	155
5.7	Summary .....	157
5.8	Acknowledgements.....	159
Chapter 6 Conclusion and Future Work .....		160
6.1	Dissertation Summary.....	160
6.2	Future Work.....	162
6.2.1	Envelope Tracking Power Amplifier Modeling.....	162
6.2.2	Reconfigurable Broadband Envelope Tracking Power Amplifier .....	163
6.2.3	Hybrid Supply Modulator for Broad Modulation Bandwidth Signals.....	164
6.2.4	Envelope Supply Path Equalizer and Linearization.....	164
References.....		165

## LIST OF FIGURES

Figure 1.1: Efficiency vs. output power for Class A, Class B, and Envelope Tracking.....	3
Figure 1.2. Effect of high PAPR on power amplifier efficiency .....	4
Figure 1.3: Doherty power amplifier .....	6
Figure 1.4: Basic outphasing power amplifier configuration. ....	7
Figure 1.5: Block diagram of the radar transmitter using EER/ET high power amplifier..	8
Figure 2.1: Block diagram of the envelope tracking power amplifier (left) and constant supply power amplifier (right) and comparison of the energy dissipation. ....	15
Figure 2.2: Time domain representation of the envelope supply signal before (blue) and after (magenta) de-toughing. ....	16
Figure 2.3: Envelope spectral response of a 10 MHz LTE signal. ....	18
Figure 2.4: Schematic block diagram of the dynamic supply modulator. ....	19
Figure 2.5: Printed circuit board of a representative dynamic modulator outputting 28V peak envelope voltage with up to 100-W average output power. ....	21
Figure 2.6. Envelope tracking trajectory as a result of dynamically varying the drain supply voltage. ....	23
Figure 2.7. Gain performance as a function of output power for a constant drain power amplifier at various supply voltages. ....	24
Figure 2.8. Detailed schematic diagram of the Mark II broadband linearization test-bench for broadband power amplifiers. ....	28
Figure 2.9: Mark II system implementation with 100 MHz bandwidth .....	29
Figure 2.10: Measured response of the 100 MHz broadband test-bench with a 40 MHz 64-QAM signal on a straight-through measurement without calibration, resulting in significant memory effects (~8% EVM). ....	31
Figure 2.11: Calculated transfer function (top: magnitude and bottom: phase – wrapped) of the normalized received signal and the normalized transmit signal. The horizontal axis is frequency in MHz. ....	33
Figure 2.12: Calculated inverse FIR filter (top: magnitude and bottom: phase – wrapped) in red and calculated transfer function of the path. The horizontal axis is frequency in MHz. ....	34
Figure 2.13: Measured response of the 100 MHz broadband test-bench with a 40 MHz 64 QAM signal on a straight-through measurement after equalization calibration, resulting in ~1% EVM. ....	35
Figure 2.14. Digital pre-distortion system .....	36
Figure 2.15: Amplifier model .....	36



Figure 2.16: Single-ended Si-LDMOS UHF PA fixture tuned to 295 MHz, placed under envelope tracking with a high power dynamic supply modulator .....	40
Figure 2.17. Instantaneous measurement of the drain current, drain voltage, and RF output for instantaneous drain efficiency.....	40
Figure 2.18: Output spectral response of the single push-pull UHF power amplifier (Specifications: -33 dBc / -43 dBc). .....	41
Figure 2.19: Dual modulator balance push-pull ET power amplifier, fed with a single signal generator. ....	42
Figure 2.20: Output spectral response of the balanced single push-pull UHF power amplifier. (Specifications: -33 dBc / -43 dBc).....	43
Figure 2.21: Output spectral response of the balanced single push-pull UHF power amplifier with a 1.2 MHz notch placed in the middle of the SA-WCDMA signal. .	44
Figure 2.22: RF3934 RF power amplifier fixture tuned to 780 MHz operation.....	45
Figure 2.23: Measured AM-AM, AM-PM, and spectrum with a single carrier WCDMA signal, centered at 780 MHz before and after memory compensated digital pre-distortion. ....	47
Figure 2.24: Measured AM-AM, AM-PM, spectrum, and constellation diagram with a 16 QAM 10 MHz LTE signal, centered at 780 MHz before and after memory compensated digital pre-distortion.....	48
Figure 2.25: Measured instantaneous output amplitude and phase (normalized) vs. input amplitude, prior to pre-distortion (up) and after pre-distortion (down).....	54
Figure 2.26: Top: Measured spectrum of the 5 MHz bandwidth 3.5-dB PAPR WCDMA signal before digital pre-distortion (a) and after DPD (b). Bottom: Measured spectrum of the 5-MHz 3.5-dB PAPR SA-WCDMA signal before DPD (c) and after DPD (d). ....	55
Figure 2.27: Mm-wave ET power amplifier system. ....	56
Figure 2.28: Q-band MMIC power amplifier under envelope tracking.....	57
Figure 2.29: AM-AM and AM-PM characteristics before digital pre-distortion under both constant drain and envelope tracking conditions. ....	60
Figure 2.30: Output power spectrum before digital pre-distortion (red), after memoryless DPD (blue), and after memory compensation (green). ....	61
Figure 3.1: Normalized traffic profile as a function of time over a 24-hour period. ....	66
Figure 3.2: Efficiency performance of power amplifiers as a function of output power..	67
Figure 3.3: Back-off implementation algorithm. ....	68
Figure 3.4: Normalized $V_{env}$ versus normalized $V_{in}$ at the different back-off levels.....	69
Figure 3.5: Supply envelope voltage for different back-off power levels as a function of time, while maintaining the ET de-troughing relationship .....	71

Figure 3.6: Measurement setup for calibration for power back-off.....	72
Figure 3.7: Measured versus calculated envelope supply voltages .....	72
Figure 3.8: Average efficiency using a single carrier 7.54 dB PAPR WCDMA signal as the average output power was backed-off up to -10 dB for an ideal Class B, ideal Doherty (with 78.5% peak eff.), Doherty (with 60% peak eff.) and measured ET results. ....	74
Figure 3.9: Left axis: "Instantaneous" efficiency vs. output power of measured ET PA, normalized to peak power. Right axis: PDF of a 7.54 dB single carrier WCDMA signal at full power, -3 dB, -6 dB, and -10 dB average power back-off.....	78
Figure 3.10: Relationship surface between output power, input voltage, and supply voltage of a RFPA. The ET-HPA follows a single trajectory as depicted by the blue line.....	80
Figure 3.11: Implementation to determine the AM-AM and AM-PM characteristics by using two data sets (at full power and at -7 dB) concatenated together to generate a single LUT capable of scaling with average output power.....	81
Figure 3.12: Probability density function of the modulated 7.54 dB PAPR WCDMA signal at 0 dB and at -7 dB back-off. ....	81
Figure 3.13: Normalized AM-AM (top) and AM-PM (bottom) measured at full power (blue) and at 7 dB back-off (red) used to generate a single scalable LUT. ....	82
Figure 3.14: Implementation of the open loop pre-distorted signal for various power back-off levels.....	83
Figure 3.15: AM-AM (top) and AM-PM (bottom) at 2 dB back-off using the scalable open loop DPD.....	85
Figure 3.16: AM-AM (top) and AM-PM (bottom) at 9 dB back-off using the scalable open loop DPD.....	86
Figure 3.17: Normalized traffic as a function of the time in the day over 24 hours.....	88
Figure 3.18: Probability density function of the number of users over a 24-hr period in a given cell in which the maximum number of users is 128. ....	89
Figure 3.19: Probability density function of average output power in a 40W base-station based on the traffic profile described in Figure 3.17. ....	90
Figure 4.1: Schematic of the proposed stacked GaN power amplifier with RC feedback. ....	97
Figure 4.2: Simulated DC IV curve of a stacked GaN FET structure. ....	99
Figure 4.3: Comparison of the input return loss of the conventional stacked PA without RC feedback and with RC feedback. ....	102
Figure 4.4: Comparison of the gain of the conventional stacked PA without RC feedback and with RC feedback.....	103

Figure 4.5: Micrograph of the fabricated GaN power amplifier IC.....	104
Figure 4.6 Measurement setup and implemented GaN broadband PA.....	105
Figure 4.7: Extracted stability factor and stability measure based on measured S-parameters.....	106
Figure 4.8: CW Measurements of the GaN PA IC under a constant drain bias of 40V, biased in Class AB, illustrating the drain efficiency, gain, and output power across the frequency band of interest.....	108
Figure 4.9: Measured drain efficiency, gain, and output power of the GaN PA IC under a constant drain bias of 40V, biased in Class AB, using a 6.6 dB PAPR WCDMA signal, across the frequency band of interest.....	109
Figure 4.10: Schematic and photo of the push-pull power amplifier. The amplifier measures to be 80 mm x 80 mm.....	110
Figure 4.11: Geometry of the balun.....	112
Figure 4.12: Simulated and measured result of back-to-back configuration.....	113
Figure 4.13: Simulated and measured S-parameter of the single IC and measured and simulated stability factor of the single IC.....	114
Figure 4.14: Measured output power, gain, and drain efficiency as a function of input power at 1500 MHz.....	115
Figure 4.15: Measured output power, gain, and drain efficiency as a function of frequency, corresponding to maximum PAE point.....	116
Figure 4.16: Normalized envelope shaping function, corresponding to 42 V peak and 12 V minimum envelope.....	120
Figure 4.17: De-troughed envelope signal, with 42.3 V peak and 23.2 V rms, applied onto the drain of the RFPA in the time domain.....	120
Figure 4.18: CW Measurements of the GaN PA under single-tone excitation at 752 MHz as a function of output input power for various drain biases.....	121
Figure 4.19: CW Measurements of the GaN PA under single-tone excitation as a function of frequency from 500 MHz to 1750 MHz at a drain bias of 23V with -3.72V gate bias.....	122
Figure 4.20: High voltage envelope amplifier block diagram.....	123
Figure 4.21: Measured average efficiency, gain, and output power of the GaN ETPA across frequency band of interest with -3.72 V gate bias.....	125
Figure 4.22: Measured envelope modulator efficiency as a function of output power, measured using the representative de-troughed envelope signal on various resistive loads.....	127
Figure 4.23: Output spectrum before and after DPD at 752 MHz.....	128
Figure 4.24: Measured AM-AM after DPD at 752 MHz.....	131

Figure 4.25: Measured AM-PM after DPD at 752 MHz. ....	131
Figure 5.1: Spectral response of a 10 MHz LTE envelope signal. ....	137
Figure 5.2: Spectral response of a 20 MHz LTE envelope signal. ....	137
Figure 5.3: Histogram of the slew-rate into and out of the modulator. ....	139
Figure 5.4: Histogram of the slew-rate of a 10 MHz and 20 MHz LTE supply envelope waveform. ....	140
Figure 5.5: Example of a cubic spline interpolation used after “adaptive de-troughing” in the time domain; showing the original envelope, the new envelope supply waveform using cubic spline interpolation for a downward slope (top) and upward slope (bottom).....	144
Figure 5.6: Normalized envelope versus normalized RF amplitude signal after adaptive de-troughing. ....	146
Figure 5.7: Power spectral density after adaptive de-troughing. ....	147
Figure 5.8: Histogram of a representative 20 MHz LTE-A signal after "adaptive de-troughing". ....	147
Figure 5.9: Power spectral density of the adaptively de-troughed envelope in MATLAB, input into the envelope amplifier, and output of the envelope amplifier to a 6 ohms load.....	149
Figure 5.10: Comparison of the envelope amplifier input and output.....	150
Figure 5.11: Time domain representation after adaptive de-troughing such that 95% of the waveform’s slew-rate is contained within 400 V/us. ....	151
Figure 5.12: Relationship surface between output power, input voltage, and supply voltage of a RFPA with “standard de-troughing” (blue) and under “adaptive de-troughing” (magenta). ....	155
Figure 5.13: Measured AM-AM, AM-PM, and constellation of the adaptively de-troughed 20 MHz signal after digital pre-distortion. ....	158

## LIST OF TABLES

Table 2.1: Summary of results for 780 MHz ET power amplifier.....	46
Table 2.2: Summary of results for the 2140 MHz Envelope Tracking power amplifier with a 5 MHz WCDMA signal. ....	51
Table 2.3: Summary of results of the Q-band Envelope Tracking power amplifier.....	58
Table 3.1: Measured power back-off at the output of the RF PA demonstrates the precision of the digital control, performed digitally in DSP.....	73
Table 3.2: Summary of measured linearity results at various back-offs.....	84
Table 3.3: Energy usage of a base-station over 24 hour period.....	91
Table 4.1: Examples of wideband wireless communication systems and frequency allocations for LTE systems.....	94
Table 4.2: Comparison of broadband RF power amplifiers .....	117
Table 4.3: Summary of broadband ET PA results .....	129
Table 4.4: Comparison of reported broadband power amplifiers .....	132
Table 4.5: Comparison of reported broadband power amplifiers performance under high PAPR signals. ....	132
Table 5.1: Measurements with a 6 Ohms resistive load. ....	148
Table 5.2: Summary of measurement results of a 10 MHz LTE signal and an “adaptatively de-troughed” 20 MHz LTE signal .....	158

## ACKNOWLEDGMENTS

First, I would like to give my gratitude to my chair and advisor, Professor Peter M. Asbeck, for his guidance, advice, supervision, and support throughout the entire process of this dissertation and its research efforts. I am grateful for his continuous efforts to challenge our minds, provide us with feedback on papers and presentations, and advice on various aspects of our career. I appreciate his patience and understanding throughout my graduate career and truly value how he always looks out for the best interest of all his graduate students and fellow colleagues. The opportunity to speak about our research to various veterans of the field has made our group unique and has become a priceless experience to many of us. I sincerely thank him for being an excellent advisor and also a professional figure I can hold in high regards.

I would like to give my gratitude to Professor James Buckwalter, Professor Chung K. Cheng, Professor Prabhakar Bandaru, and Professor Lawrence Larson for serving on my committee. Over the past few years, it has been my pleasure to be acquainted and to have the opportunity to work as a TA for some of their classes.

I would also like to give my gratitude to Donald F. Kimball for all his support and guidance throughout my graduate career. Through interacting with him, I have realized a great mentor makes a great difference. I thank him for sharing many great ideas and insights that have changed my way of thinking. His enthusiasm, diligence, and knowledge of engineering, as well as many other areas, have inspired me. I thank him for being one of the best mentors I'll ever have.

I would like to give my gratitude to Houman Ghajari for his support. He has been very understanding with my graduate career. I thank him for always having my best interest in mind, for being flexible with my time, and for giving me the opportunity to continue my working experience. With his guidance, the experience of writing proposals, speaking with sponsors, and working with other business-oriented efforts have become an invaluable part of my career. I thank him for being a great supervisor as well as an great friend.

I would like to thank Paul Draxler for his support and guidance. He has not only been a great friend, but also one of the best mentors. His assistance in MATLAB and linearization has been truly invaluable to me. Like an older brother, his words have guided me through many challenges in both engineering and other aspects of my life. I am grateful for his optimism and to have shared many stressful yet happy moments.

I would like to thank all the many past and present members of HSDG group, my MaXentric colleagues, and all those who I have met throughout my graduate career for the invaluable advice, support, and friendship. In particular, I thank Anthony Tang, Toshifumi Nakatani, Hayg Dabag, Jefy Jayamon, Varish Diddi, Young-pyo Hong, Chin Hsia, Cuong Vu, Nick Farich, Paul Theilmann, Andre Metzger, Myoungbo Kwak, Pavel Kolinko, and Sataporn Pornpromlikit for being pressure relievers and keeping me sane.

Most importantly, I would like to thank my parents, Henry and Kinny, sisters, Lucy and Stephanie, and hubby-to-be, Matthew Chen for their continuous support. I have very much enjoyed trying to explain my research to my parents and the future plans I have for my career. I know they will always be there to listen and provide me guidance towards the road I will walk on. I am grateful for all the sacrifices they've made in order

for me to be where I am today. Even when times were tough, they always tried to provide all education related requests I had as a child. My parents have been the greatest parents I could have asked for and I am grateful to have the opportunity to show them my gratitude. As for my sisters, they are my best friends. I very much enjoyed how they look up to me and it has given me motivation to be my best. They always have me in mind and look out for me whenever times have been busy for me. Whenever a time crunch occurs, I can be certain that my sisters or Matthew will help take care of all the chores and food will be ready for me. The times we've spent studying for exams, working on projects, and finishing up homework was always memorable. I am grateful to have someone I can discuss my research with and get feedback from. I'm grateful to have met Matthew who enhance my strengths and compensate for all my weaknesses.

In chapter 2, some of the materials are as they appear in “A High Efficiency 780 MHz GaN Envelope Tracking Power Amplifier”, Jonmei J. Yan, Paul Theilmann, and Donald F. Kimball, published in IEEE Compound Semiconductor Integrated Circuit Symposium 2012, in “Efficiency Enhancement of mm-Wave Power Amplifiers Using Envelope Tracking”, Jonmei J. Yan, Calogero D. Presti, Donald F. Kimball, Young-pyo Hong, Chin Hsai, Peter M. Asbeck, and James Schellenberg, published in IEEE Microwave and Wireless Components Letters, Vol. 21 No. 3, and in “High-efficiency, high-linearity envelope tracking power amplifier for mobile UHF applications”, Jonmei J. Yan, Donald F. Kimball, Chin Hsia, Hsuan-yu Pan, Scott Ricketts, and Houman Ghajari, published in IEEE MILCOM 2010. The contributions from the co-authors are appreciated. The author of this dissertation was the primary investigator and primary author for these publications.



In chapter 3, some of the materials are as they appear in “Digital Pre-distortion of Envelope Tracking Power Amplifiers under Average Power Back-off and Long-Term Average Power Efficiency for Base-Station Applications”, Jonmei J. Yan, Paul Draxler, Calogero D. Presti, Donald F. Kimball and Peter M. Asbeck, published in the International Journal of Microwave and Wireless Technologies, 2013 Issue 2. The contributions from the co-authors are appreciated. The author of this dissertation was the primary investigator and primary author for this publication.

In chapter 4, some of the materials are as they appear in “Design of a 4-W Envelope Tracking Power Amplifier With More Than One Octave Carrier Bandwidth”, Jonmei J. Yan, Chin Hsia, Donald F. Kimball and Peter M. Asbeck, published in IEEE Journal of Solid-State Circuits, Vol. 47, No. 10 and in “Broadband High PAE GaN Push-Pull Power Amplifier for 500 MHz to 2.5 GHz Operation”, Jonmei J. Yan, Young-pyo Hong, Shintaro Shinjo, Kenji Mukai, and Peter M. Asbeck, submitted and accepted to the International Microwave Symposium 2013, June 2013. The contributions from the co-authors are appreciated. The author of this dissertation was the primary investigator and primary author for this publication.

In chapter 5, some of the materials are as they appear in “Enabling Wide Modulation Bandwidth for Envelope Tracking Power Amplifiers Through the Use of DSP”, Jonmei J. Yan, Paul Draxler, Donald F. Kimball and Peter M. Asbeck, published in GoMACTech Conference 2012. The contributions from the co-authors are appreciated. The author of this dissertation was the primary investigator and primary author for this publication.

## VITA

- 2005 Bachelor of Science, Electrical and Computer Engineering, University of California, San Diego, CA
- 2009 Master of Science. Electrical Engineering (Electronic Circuits and Systems), University of California, San Diego, CA
- 2013 Doctor of Philosophy, Electrical Engineering (Electronic Circuits and Systems), University of California, San Diego, CA

## PUBLICATIONS

Yan, Jonmei J.; Hong, Young-pyo; Shinjo, Shintaro; Mukai, Kenji; Asbeck, Peter M., "Broadband High PAE GaN Push-Pull Power Amplifier for 500 MHz to 2.5 GHz Operation," *International Microwave Symposium (IMS), 2013 IEEE*, June 2013.

Yan, Jonmei J.; Draxler, Paul J.; Presti, Calogero D.; Kimball, Donald F.; Asbeck, Peter M., "Digital predistortion of envelope-tracking power amplifiers under average power back-off and long-term average power efficiency for base-station applications," *International Journal of Microwave and Wireless Technologies*, vol. 5, pp.171-177, April 2013.

Yan, Jonmei J.; Draxler, Paul J.; Kimball, Donald F.; Asbeck, Peter M., "Enabling Wide Modulation Bandwidth for Envelope Tracking Power Amplifiers Through the Use of DSP", *2013 Government Microcircuit Applications & Critical Technology Conference*, 11-14 March 2013.

Theilmann, Paul; Vu, Coung; Yan, Jonmei J.; Kimball, Donald F., "High Efficiency Wideband Envelope Amplifier for Handheld and Manpack Power Amplifiers", *2013 Government Microcircuit Applications & Critical Technology Conference*, 11-14 March 2013.

Kheirkhahi, Alireza; Yan, Jonmei J.; Asbeck, Peter M.; Larson, Lawrence E., "RF Power Amplifier Efficiency Enhancement by Envelope Injection and Termination for Mobile Terminal Applications," *Microwave Theory and Techniques, IEEE Transactions on* , vol.61, no.2, pp.878,889, Feb. 2013.

Kimball, Donald F.; Yan, Jonmei J.; Theilmann, Paul; Hassan, Muhammad; Asbeck, Peter M.; Larson, Lawrence E., "Efficient and wideband envelope amplifiers for envelope tracking and polar transmitters," *Power Amplifiers for Wireless and Radio Applications (PAWR), 2013 IEEE Topical Conference on* , vol., no., pp.13,15, 20-20 Jan. 2013.

- Yan, Jonmei J.; Hsia, Chin; Kimball, Donald F.; Asbeck, Peter M., "Design of a 4-W Envelope Tracking Power Amplifier With More Than One Octave Carrier Bandwidth," *Solid-State Circuits, IEEE Journal of*, vol.47, no.10, pp.2298,2308, Oct. 2012.
- Yan, Jonmei J.; Theilmann, Paul; Kimball, Donald F., "A High Efficiency 780 MHz GaN Envelope Tracking Power Amplifier," *Compound Semiconductor Integrated Circuit Symposium (CSICS), 2012 IEEE*, 14-17 Oct. 2012.
- Hassan, Muhammad; Olson, Chris; Kovac, Dave; Yan, Jonmei J.; Nobbe, Dan; Kelly, Dylan; Asbeck, Peter M.; Larson, Lawrence E., "An Envelope-Tracking CMOS-SOS Power Amplifier with 50% Overall PAE and 29.3 dBm Output Power for LTE Applications," *Compound Semiconductor Integrated Circuit Symposium (CSICS), 2012 IEEE*, 14-17 Oct. 2012.
- Yan, Jonmei J.; Draxler, Paul J.; Asbeck, Peter M., "Extending the Bandwidth of Envelope Amplifiers Through Selective Detrouching", *Power Amplifier Symposium, 2012 IEEE*, 17-18 Sept. 2012.
- Draxler, Paul J.; Yan, Jonmei J.; Asbeck, Peter M., "Modeling and DPD of Dynamic Supply RFLPA Using Polynomial Expansion", *Power Amplifier Symposium, 2012 IEEE*, 17-18 Sept. 2012.
- Kwak, Myoungbo; Kimball, Donald F.; Presti, Calogero D.; Scuderi, Antonino; Santagati, Carmelo; Yan, Jonmei J.; Asbeck, Peter M.; Larson, Lawrence E., "Design of a Wideband High-Voltage High-Efficiency BiCMOS Envelope Amplifier for Micro-Base-Station RF Power Amplifiers," *Microwave Theory and Techniques, IEEE Transactions on*, vol.60, no.6, pp.1850-1861, June 2012.
- Draxler, Paul J.; Yan, Jonmei J.; Kimball, Donald F.; Asbeck, Peter M., "Digital predistortion for envelope tracking power amplifiers," *Wireless and Microwave Technology Conference (WAMICON), 2012 IEEE 13th Annual*, 15-17 April 2012.
- Kwak, Myoungbo; Jeong, Jinseong; Hassan, Muhammad; Yan, Jonmei J.; Kimball, Donald F.; Asbeck, Peter M.; Larson, Lawrence E., "High efficiency wideband envelope tracking power amplifier with direct current sensing for LTE applications," *Power Amplifiers for Wireless and Radio Applications (PAWR), 2012 IEEE Topical Conference on*, 15-18 Jan. 2012.
- Hsia, Chin; Zhu, Anding; Yan, Jonmei J.; Draxler, Paul J.; Kimball, Donald F.; Lanfranco, Sandro; Asbeck, Peter M., "Digitally Assisted Dual-Switch High-Efficiency Envelope Amplifier for Envelope-Tracking Base-Station Power Amplifiers," *Microwave Theory and Techniques, IEEE Transactions on*, vol.59, no.11, pp.2943,2952, Nov. 2011.
- Yan, Jonmei J.; Hsia, Chin; Kimball, Donald F.; Asbeck, Peter M., "GaN Envelope Tracking Power Amplifier with More Than One Octave Carrier Bandwidth," *Compound Semiconductor Integrated Circuit Symposium (CSICS), 2011 IEEE*, 16-19 Oct. 2011.
- Draxler, Paul J.; Yan, Jonmei J.; Asbeck, Peter M., "Receive Band Noise in Envelope Tracking Systems", *Power Amplifier Symposium, 2011 IEEE*, Sept. 2011.

Hassan, Muhammad; Kwak, Myoungbo; Leung, Vincent W.; Hsia, Chin; Yan, Jonmei J.; Kimball, Donald F.; Larson, Lawrence E., Asbeck, Peter M., "High efficiency envelope tracking power amplifier with very low quiescent power for 20 MHz LTE," *Radio Frequency Integrated Circuits Symposium (RFIC), 2011 IEEE* , 5-7 June 2011.

Kwak, Myoungbo; Kimball, Donald F.; Presti, Calogero D.; Scuderi, Antonino; Santagati, Carmelo; Yan, Jonmei J.; Asbeck, Peter M.; Larson, Lawrence E., "Wideband high efficiency envelope tracking integrated circuit for micro-base station power amplifiers," *Radio Frequency Integrated Circuits Symposium (RFIC), 2011 IEEE* , 5-7 June 2011.

Yan, Jonmei J.; Presti, Calogero D.; Kimball, Donald F.; Hong, Young-pyo; Hsia, Chin; Asbeck, Peter M., Schellenberg, James, "Efficiency Enhancement of mm-Wave Power Amplifiers Using Envelope Tracking," *Microwave and Wireless Components Letters, IEEE* , vol.21, no.3, pp.157,159, March 2011.

Yan, Jonmei J.; Hsia, Chin; Kimball, Donald F., "High Efficiency Envelope Tracking GaN HEMT Power Amplifiers for MUOS Handheld and Man-pack Applications", *2011 Government Microcircuit Applications & Critical Technology Conference*, 21-24 March 2011.

Kim, Bumjin; Schellenberg, James; Yan, Jonmei J.; Kimball, Donald F.; Watkins, Edward, "A Linear, High-Efficiency GaN Power Amplifier Operating at 74 GHz", *2011 Government Microcircuit Applications & Critical Technology Conference*, March 2011.

Yan, Jonmei J.; Kimball, Donald F.; Hsia, Chin; Pan, Huaun-yu; Ricketts, Scott; Ghajari, Houman, "High-efficiency, high-linearity envelope tracking power amplifier for mobile UHF applications," *MILITARY COMMUNICATIONS CONFERENCE, 2010 - MILCOM 2010* , Oct. 31 2010-Nov. 3 2010.

Yan, Jonmei J.; Asbeck, Peter M., "High Efficiency Broadband GAN Power Amplifier IC Spanning from UHF to L-BAND," *Power Amplifier Symposium, 2010 IEEE*, 13-14 Sept. 2010.

Kimball, Donald F.; Yan, Jonmei J.; Draxler, Paul J.; Hsia, Chin; Asbeck, Peter M., "High Efficiency RF line-up for UMTS WCDMA RF Chain". *Power Amplifier Symposium, 2010 IEEE*, 13-14 Sept. 2010.

Hsia, Chin; Kimball, Donald F.; Draxler, Paul J.; Yan, Jonmei J.; Asbeck, Peter M., "Wideband High Efficiency Envelope Tracking Power Amplifiers Using High Voltage GaAs HBTs", *Power Amplifier Symposium, 2010 IEEE*, 13-14 Sept. 2010.

Yan, Jonmei J.; Draxler, Paul J.; Kimball, Donald F.; Asbeck, Peter M.; Steinbeiser, Craig, "Operation of Envelope Tracking Base-Station Amplifiers Under Average-Power Back-off", *Power Amplifier Symposium, 2009 IEEE*, 19-20 Jan. 2009.

Yan, Jonmei J.; Draxler, Paul J.; Kimball, Donald F.; Asbeck, Peter M., "High-Efficiency Envelope Tracking High Power Amplifier under Average Power Back-Off Operation",

2009 *Government Microcircuit Applications & Critical Technology Conference*, 16-19 March 2009.

Zhu, Anding; Draxler, Paul J.; Yan, Jonmei J.; Brazil, Thomas J.; Kimball, Donald F.; Asbeck, Peter M., "Open-Loop Digital Predistorter for RF Power Amplifiers Using Dynamic Deviation Reduction-Based Volterra Series", *Microwave Theory and Techniques, IEEE Transactions on* , vol.56, no.7, pp.1524,1534, July 2008.

Hsia, Chin; Kimball, Donald F.; Draxler, Paul J.; Yan, Jonmei J.; Asbeck, Peter M.; Kinney, J.; Toulouse, Eric; Wood, John, "High Efficiency LDMOS Power Amplifier for Wireless Base Stations using Envelope Tracking", *2008 TECHCON*, Nov. 2008.

Draxler, Paul J.; Zhu, Anding; Yan, Jonmei J.; Kolinko, Pavel; Kimball, Donald F.; Asbeck, Peter M., "Quantifying Distortion of RF Power Amplifiers for Estimation of Predistorter Performance", *Microwave Symposium Digest, 2008 IEEE MTT-S International* , 15-20 June 2008.

Kimball, Donald F.; Hsia, Chin; Draxler, Paul J.; Yan, Jonmei J.; Asbeck, Peter M. "66% PAE Envelope Tracking GAN Power Amplifier for EDGE Base stations Applications," *Power Amplifier Symposium, 2008 IEEE*, 21-22 Jan. 2008.

Hsia, Chin; Kimball, Donald F.; Draxler, Paul J.; Yan, Jonmei J.; Asbeck, Peter M.; Kinney, J.; Toulouse, Eric; Wood, John, "High Efficiency Envelope Tracking Overdriven Class-A LDMOS Power Amplifier for Base Station Applications", *Power Amplifier Symposium, 2008 IEEE*, 21-22 Jan. 2008.

# ABSTRACT OF THE DISSERTATION

## **High Efficiency Broadband Envelope-Tracking Power Amplifiers**

by

Jonmei Johana Yan

Doctor of Philosophy in Electrical Engineering (Electronic Circuits and Systems)

University of California San Diego, 2013

Peter M. Asbeck, Chair

In order to meet the increasing demand for higher data rates while maximizing spectral efficiency, modern wireless communication systems transmit complex non-constant envelope modulation signals with high peak-to-average ratio (PAPR). As a result, conventional power amplifiers must be operated in back-off, leading to a significant efficiency reduction. Various power amplifier architectures (i.e. Doherty, outphasing, and envelope tracking) have been demonstrated to achieve high efficiency for these high PAPR signals. Unlike the other architectures, the envelope tracking power amplifier (ETPA) makes an excellent candidate for multi-band multi-frequency use, while maintaining high efficiency for high PAPR and under average power back-off, as it is fundamentally immune to changes in the frequency of the carrier; it depends only on the envelope of the RF signal. This dissertation focuses on the design of envelope tracking power amplifiers for enabling broadband wireless communication systems.

First, a test-bench for evaluating broadband ETPAs is described. A calibration routine, acting as a pre-equalizer, is used to achieve a flat linear response over the entire

instantaneous bandwidth of the system, resulting in less than 1% EVM for a 40 MHz LTE signal. Performances of envelope tracking power amplifiers on this test-bench at various frequencies from UHF to millimeter-wave are evaluated, and record efficiencies are demonstrated.

Next, this dissertation describes how in under practical usage, the power transmitted fluctuates as a function of the load demands over time. The long-term efficiency of the ETPA is evaluated using Monte-Carlo simulations based on a projected time-varying power profile. Compared to a Doherty PA with the same peak efficiency, the ETPA can provide more than 1.4x reduction in overall energy consumed. The ETPA thus provides significant opportunities for system energy savings under realistic operation.

Thirdly, to accommodate the wide range of carrier frequencies required for numerous emerging wireless systems, a multi-octave RFPA based on a compact GaN stacked IC with RC feedback is designed, fabricated, and evaluated. Multi-octave ET operation was demonstrated from 500 to 1750 MHz with >25% efficiency. Compared to its constant drain voltage counterpart, >2x improvement in RFPA efficiency is observed in ET.

Lastly, while the ETPA provides advantages such as broad carrier bandwidths and high efficiency under back-off operation, one of the main challenges in ETPA design lies in accommodating wide modulation bandwidths. Adaptive de-troughing, a digital signal processing approach for extending the modulation bandwidth capability of an existing dynamic power supply, is described and evaluated. Measurements demonstrated the ability to extend ET operation to 20 MHz LTE signals. In addition, ~5-6% modulator

efficiency enhancement was measured when comparing “standard” to “adaptive” detrouching supply waveforms.



# Chapter 1

## Introduction

The exponentially increasing demand from consumers for various multimedia services and the crowded frequency spectrum allocation has led to the development of high spectral efficiency communication signals in order to accommodate these high throughput and large capacity demands. However, a resulting by-product of these signals is its non-constant envelope modulation and high peak-to-average power ratios (PAPRs). To satisfy the stringent linearity requirements (such as out-of-band interference such as ACPR and in-band distortion such as EVM) imposed by the communication standard, the power amplifier is operated most of the time at a significant back-off, resulting in a large reduction in efficiency. In this chapter, a brief review of the requirements on base-station power amplifiers will be discussed. In addition, architectures for achieving high efficiency for high PAPR signals and their design consideration will be introduced.

### 1.1 Base-station Power Amplifiers

The design of base-station power amplifiers requires careful consideration and trade-offs of its bandwidth, efficiency, and linearity performance. High linearity is

required in these communication systems in order to minimize signal distortion, reduce bit error rate, improve spectral efficiency, and reduce adjacent channel interference. As a result, in order to maintain linearity, most conventional power amplifiers operate at power levels backed-off from the saturated power level. However, backing-off from saturated power level reduces the power-added efficiency (PAE). Low-efficiency power amplifiers consume large amounts of power and dissipate large quantities of unwanted heat, resulting in expensive and large thermal compensation circuitry or systems. Therefore, the PAE of the power amplifier greatly impacts the size, weight, power consumption, and reliability of the total system.

The problem is further complicated as the increasing demand for higher data rates and larger signal bandwidth, while maintaining signal integrity, lead to the use of signals with non-constant envelope and high peak-to-average signal ratio. In conventional fixed bias power amplifiers, the maximum efficiency occurs at saturation, with a single-tone signal. As the power amplifier operates at power levels away from saturation, the efficiency degrades. This creates an issue in the presence of multi-tone signals, due to their high peak-to-average characteristics, where the average power is well below saturation. If the peak signal level corresponds to the 1dB compression point, then the average power level results in lower efficiency with moderate linearity. On the other hand, if the average power level corresponds to the compression point, then peak power levels will drive the amplifier into saturation, creating larger nonlinearities. Class A power amplifiers have a theoretical drain efficiency of 50%, while Class B power amplifiers have a theoretical power drain efficiency of 78.5%. Both amplifier classes have adequate linearity, but their maximum efficiency occurs at saturation. The high peak

to average ratio (i.e. envelope peak factor) or non-Rayleigh amplitude envelope distribution results in operation far from saturation, so the drain efficiency drops to 10% and 32% for Class A and Class B power amplifiers, respectively, for signals with 6 dB PAPR (peak-to-average ratio), as depicted in Figure 1.1. The inefficiency of Class A, Class AB and B amplifiers with next generation wireless signals highlights the need for new approaches to solving this problem. It is also widely accepted that although linearity and efficiency are competing constraints, signal processing may be used to simultaneously maximize both. The theory is that invertible, i.e. non-saturating nonlinearities may be corrected with techniques such as feed-forward and pre-distortion. Obtaining high efficiency, high linearity power amplifiers, known to be the largest power consumer in the transmit chain, is a major desire for many systems designers. Not only will efficient systems consume less energy, but will also lower the heat dissipation since most of the power lost is converted to heat. Lower heat dissipation has the added benefit of minimizing size and mass by reducing the amount of required cooling components.

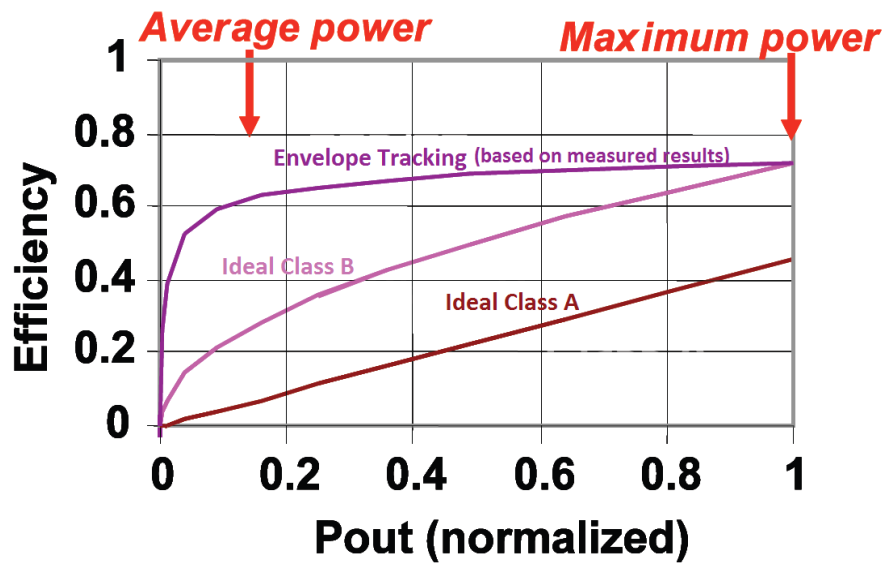


Figure 1.1: Efficiency vs. output power for Class A, Class B, and Envelope Tracking.

### 1.1.1 Peak-to-Average Ratio Reduction for Multi-carrier Transmission

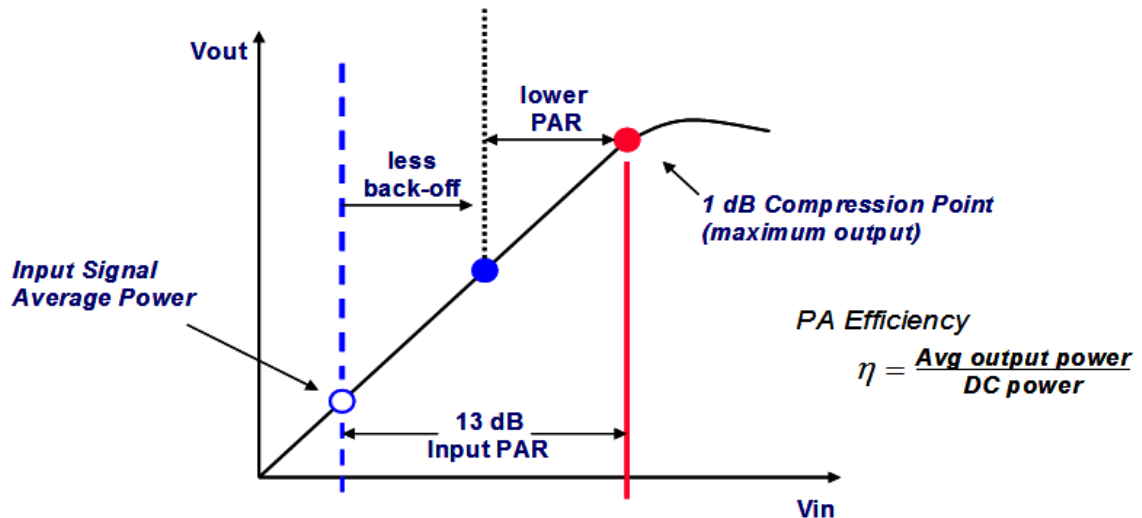


Figure 1.2. Effect of high PAPR on power amplifier efficiency

To understand the effects of high peak-to-average power ratio (PAPR) on an amplifier's efficiency, a signal with up to eight simultaneous tones is considered. The combined input signal when all eight tones are in-phase can potentially cause high peak-to-average power drive levels. Setting the average power at maximum efficiency, hence at the compression point, leads to amplifier saturation at peak power levels, creating nonlinearities. To prevent intermodulation distortion, the amplifier must operate at even larger input power back-off, where the efficiency is low.

Crest factor reduction to decrease the PAPR while maintaining sufficient linearity margin can be used to increase efficiency while trading-off a small amount of in-band linearity such that linearity specifications can still be met. Parameterized algorithm can be developed to effectively deal with the diversity without fundamental changes in the algorithmic functional blocks. Various PAPR reduction techniques such as amplitude

clipping and filter, tone reservation, coding, selected mapping, and tone injection have been studied [6]-[10]. In order to select the appropriate PAPR reduction technique, a set of criteria of PAR reduction must be used. For the purpose of this dissertation, a simplified band-pass de-cresting algorithm is used such that in-band linearities such as EVM are still satisfied after de-cresting.

## **1.2 High Efficiency Power Amplifier for High Peak-to-Average-Power Signals**

In recent years, various efficiency enhancement techniques targeting systems with high PAPR signals have been investigated. Among them are the Doherty, outphasing, envelope elimination restoration (EER), and envelope tracking (ET). These techniques can improve efficiency while maintaining linearity at power back-off operation. This section highlights some of the underlying theory and design considerations behind these techniques.

### **1.2.1 Doherty Power Amplifiers**

The basic Doherty power amplifier consists of a carrier amplifier and a peaking amplifier, as shown in Figure 1.3. The input signal is passed through a power divider, splitting the power equally to each amplifier with a  $90^\circ$  phase difference. After amplification, the outputs of the two amplifiers are combined via a quarter-wave transmission line that acts as an impedance inverter. As a result of using active load modulation on the carrier amplifier via the peaking amplifier attached to the quarter-wave impedance transformer, high efficiency in the presence of signals with high PAPR can be

achieved. At low output powers, the carrier amplifier, typically biased in Class AB, is presented with a modulated load impedance and operated into a relatively higher impedance, thereby, achieving high efficiency. As the carrier amplifier approaches its saturation power, typically around 6 dB backed-off from the peak output power of the overall Doherty PA, the peaking amplifier begins to deliver power. Hence, the impedance seen by the carrier amplifier reduces, allowing the carrier amplifier to achieve high efficiency without hard saturation. The peaking amplifier is biased in a high efficiency class of operation, typically Class C. There are other alternative implementations of the Doherty amplifier such as the 3-way Doherty, asymmetric Doherty, etc., that have been investigated to provide high efficiency for next generation LTE systems.

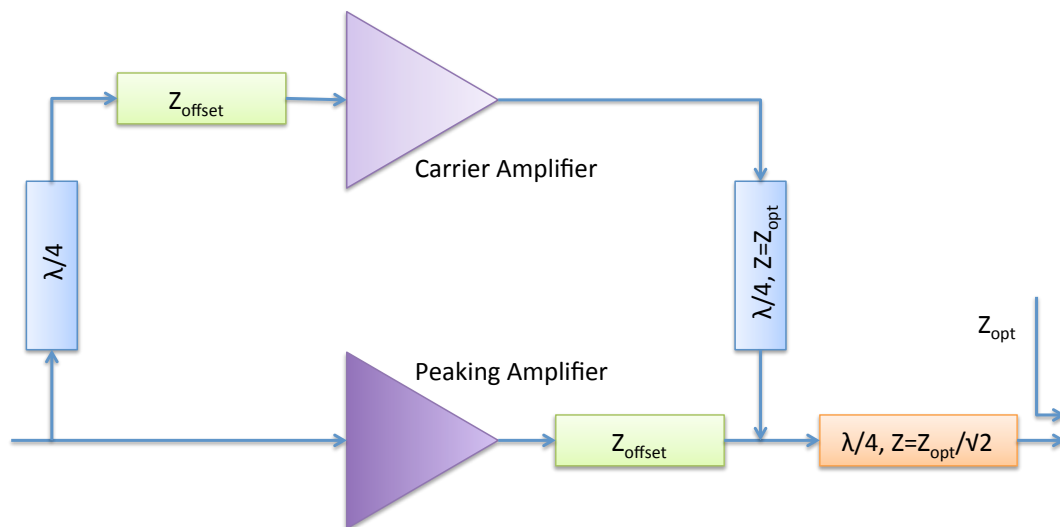


Figure 1.3: Doherty power amplifier

## 1.2.2 Outphasing Power Amplifiers

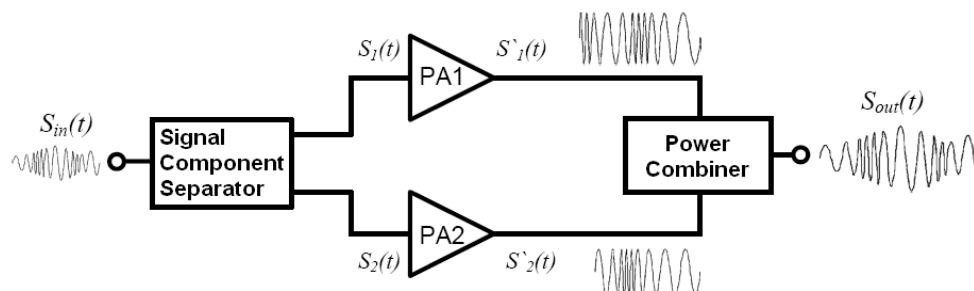


Figure 1.4: Basic outphasing power amplifier configuration.

The outphasing power amplifier, shown in Figure 1.4, consists of two amplifiers, driven with constant envelope signals, whose outputs are combined in such a way as to produce the desired signal. By varying the relative phases between the two input signals, the output summation can achieved the desired envelope and phase variation in the modulated output signal. In recent years, the two input signals with relative phases have been more commonly implemented using DSP approaches, making it a much simpler implementation. As a result of the constant envelope input signals, it is possible to use switching mode power amplifiers to realize very high efficiency operation. In addition, in theory, a linear output of the outphasing power amplifier can be obtained through combining the outputs of the switching mode power amplifiers, regardless of the nonlinear characteristics of the individual amplifiers. However, in practice, challenges arise from the ability to implement well-balanced paths with matching conditions between the two amplifiers, resulting in incomplete cancellation of the out-of-phase signals, and therefore, distortions are generated. Other implementation challenges lie in the phase and amplitude imbalance of the combiner, power losses, and amplifier switching losses. These issues become even more challenging as the bandwidth,

operation frequency, and output power increase, and the linearity specifications to become more stringent.

### 1.2.3 ET/EER Power Amplifiers

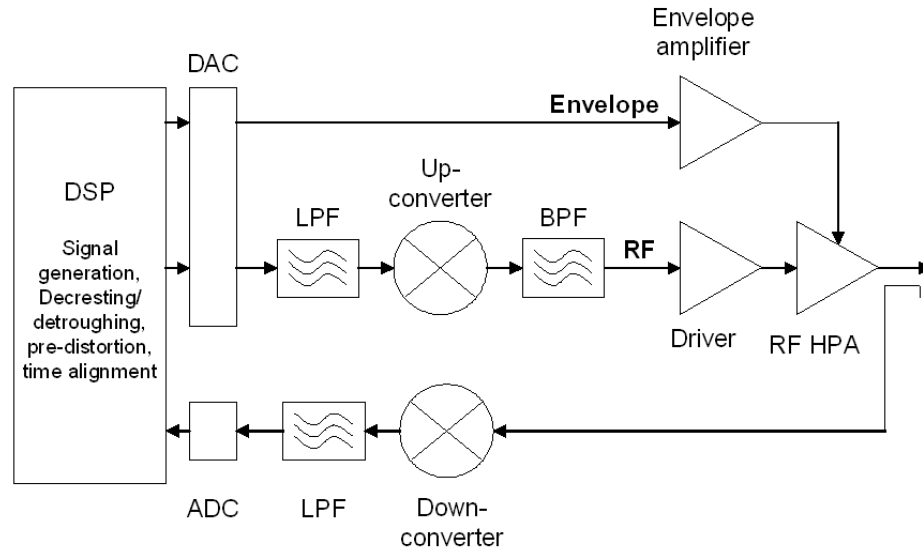


Figure 1.5: Block diagram of the radar transmitter using EER/ET high power amplifier.

The envelope elimination restoration (EER), first developed by Leonard R. Kahn in 1952, and envelope tracking (ET) power amplifier uses power supply modulation to achieve high efficiency, as depicted in Figure 1.5. In the EER configuration, the high power amplifier (HPA) operates as a switching mode power amplifier, driven by constant envelope signals. The phase information of the modulated signal is contained in the RF input path while the envelope amplifier or supply modulator via the supply path provides the amplitude information. In theory, very high efficiency can be obtained by using a high efficiency supply modulator and a switching mode power amplifier to amplify the constant envelope signals without degrading the PAPR. However, the linearity of the signal is strongly dependent on the supply modulator that is used to restore the envelope



information of the modulated signal. Time alignment between the RF phase signal and the amplitude envelope signal at the output of the HPA is extremely crucial and has a dramatic influence on the linearity of the power amplifier.

Another similar configuration is the envelope tracking (ET) power amplifier. In the ET configuration, a fully modulated signal is presented to the input of the HPA. Unlike EER, the HPA is biased below deep saturation. As a result, although the envelope path does contain amplitude information, the supply modulator behaves more like a power supply rather than an amplifier. In addition, since the amplitude information is contained in the RF input under ET, the envelope supply waveform can be “de-trouged” to prevent gain collapse and sensitivity to time misalignment, an advantage over EER. By tracking the envelope with the drain voltage, the ET HPA keeps the RF transistor operating continuously at  $P_{-1dB}$  or  $P_{-2dB}$  power levels where the HPA efficiency is high. A key component to achieve high overall ET efficiencies is the development of an efficient and high fidelity envelope amplifier or supply modulator. The signal fidelity at the output of the envelope amplifier is important to ensure that ACPR and spurious emission specifications are met.

## **1.3 Scope of the Dissertation**

Envelope tracking power amplifiers have received much research and development attention as promising candidates for future broadband wireless communication systems. The need to achieve even wider bandwidths while maintaining high efficiency and linearity performance under full power and in power back-off has

motivated the research of this dissertation. This dissertation is dedicated to exploring the development of broadband envelope tracking power amplifiers for micro- and macro-base-station applications. The challenge is to demonstrate high efficiency performance while satisfying system linearity specifications. The objectives of this dissertation are to analyze practical issues for envelope tracking power amplifiers in terms of bandwidth, efficiency, linearity and back-off operation and provide solutions for better performance. The dissertation is organized as follows:

In Chapter 2, the envelope tracking power amplifier system is analyzed. A test-bench for evaluating broadband performance and back-off operation is described. A pre-equalization routine is developed to provide a broadband flat linear response over the entire instantaneous bandwidth of the system. Measurement results demonstrate an improvement from 8% EVM to 1% EVM with a 40 MHz signal as a result of utilizing pre-equalization. Using this test-bench, envelope tracking power amplifiers implemented at various carrier frequencies from UHF to mm-wave are studied and evaluated for maximum performance. At UHF, a single push-pull amplifier with 85W of output power was measured to have better than 63% drain efficiency. In addition, the implementation of a dual modulator approach for extremely high output powers is shown to provide better than 60% efficiency at 150 W, which includes the losses of the input and output hybrid divider/combiners. At the 780 MHz band, a GaN envelope tracking power amplifier, demonstrating record efficiency of  $\sim 70\%$  with 28.6 W of output power and 13.5 dB of gain, is presented. This illustrates the potential of GaN FETs, under envelope tracking, for next generation LTE power amplifier systems. The application of ET to millimeter wave power amplifiers for efficiency enhancement is also shown to lead to an

increase of more than 5.7 times in MMIC PA efficiency under ET, when compared to a fixed drain bias; measurements were done with a 20-MHz 7.6-dB PAPR 64-QAM signal. These results indicate that ET offers a promising solution for the design of high efficiency power amplifiers in the millimeter-wave regime.

In Chapter 3, envelope tracking power amplifier operation under average power back-off is investigated. A scalable digital pre-distortion model is developed to achieve linearity performance as the average power is backed-off. Its long-term efficiency based on a projected time-varying power profile is analyzed using Monte-Carlo simulations and its performance is compared to other power amplifier architectures. For ET amplifiers, less than 2x reduction in efficiency was measured as average power was decreased over a 10 dB range. Using the scalable DPD model, high efficiency and linearity envelope tracking power amplifier under average power back-off is demonstrated and its performance advantages are discussed. Calculations of long-term efficiency indicate that, compared to an ideal Doherty amplifier with the same peak efficiency, ET amplifiers can provide more than 1.4x reduction in overall energy consumed. Thus, envelope tracking provides significant opportunities for system energy savings under realistic operating conditions.

In Chapter 4, broad carrier bandwidth envelope tracking power amplifiers are investigated. The design of broadband RF power amplifiers using gallium nitride (GaN) technology is discussed. Leveraging the intrinsic characteristics of GaN, stacked FETs with RC feedback are utilized to demonstrate efficiencies for CW (continuous-wave) tones greater than 50% with more than 12 W of output power across a 3:1 bandwidth from 500 MHz to 1750 MHz when terminated directly to 50 ohms at both the input and

the output. A push-pull broadband power amplifier using a low-loss broadband balun is also evaluated. Spanning from 500 MHz to 2.5 GHz, the broadband push-pull hybrid power amplifier demonstrated power added efficiencies (PAE) greater than 47% including the loss of the balun, with output powers range between 12.5-18.2 W and greater than 16 dB gain measured across the band. Finally, a compact GaN stacked power amplifier IC with RC feedback is operated under envelope tracking to demonstrate multi-octave carrier bandwidth capability. As a representative modulated signal, a 6.6 dB PAPR single-carrier WCDMA signal is used as the carrier frequency is tuned across the band. The overall efficiency of the envelope tracking power amplifier was between 25% - 31% with 10.3 dB - 13.9 dB gain from 500 MHz to 1750 MHz, including the dissipation of the modulator. Compared to its constant drain counterpart, using the same WCDMA signal, more than 2x improvement in average efficiency in the RFPA is observed as a result of operating in envelope tracking (as compared to constant drain mode).

Lastly, in Chapter 5, “adaptive de-troughing”, an approach using digital signal processing to extend the modulation bandwidth capability of a dynamic supply modulator, is investigated. Its effect on RF power amplifier efficiency and dynamic supply performance is analyzed. Digital pre-distortion for linearizing the adaptively de-troughed envelope tracking system is described. Adaptive de-troughing is used to extend the capabilities of an existing envelope amplifier in terms of its bandwidth and slew-rate capability to support a 20 MHz LTE-A signal with very little efficiency penalty. Measurement results also show that approximately 5-6% increase in efficiency was measured when compared to conventional “standard de-troughed” envelope supply waveforms for a 10 MHz LTE-A signal.

# Chapter 2

## Envelope Tracking Power Amplifier System

### 2.1 Introduction

Power amplifier (PA) efficiency for high PAPR signals is an ongoing area of research. PA efficiency determines the power consumption, size, and battery lifetime of a radio. Various techniques have been explored to increase the efficiency of power amplifiers for high PAPR signals (such as OFDM). One area of research is the Envelope Elimination and Restoration (EER) technique, which was first developed by Leonard R. Kahn in 1952 and later enhanced by others. Unlike the EER technique that faces issues due to the origin crossings in the IQ signal space diagram, the Envelope Tracking (ET) technique does not limit the amplitude modulation of the RF signal, as is the case in EER, and may be biased below deep saturation. These modifications to the EER technique may be desirable in OFDM applications where origin crossings occur. Similar to the EER PA, the supply voltage of the RF PA is varied dynamically to track the envelope of

the signal, providing the appropriate DC supply signal and keeping the RF transistor operating continuously at power levels close to saturation. This results in a dramatic increase in RF power amplifier (RFPA) efficiency. Since the DC supply power is changing with the input envelope supply waveform, the overall transmitter will consume lower DC power in low output power regions. When the transmitter is not transmitting, the DC power is not provided to the transmitter, minimizing the power consumption in the system and improving the overall system efficiency.

In this chapter, the envelope tracking architecture and its overall efficiency will be discussed. Its effects on the dynamic supply modulator and RF power amplifier efficiency performance are analyzed. A broadband test-bench for evaluating envelope tracking power amplifiers as well as linearization techniques was developed. Performance measurements from UHF to mm-wave on the broadband test-bench using the envelope tracking technique are demonstrated.

## **2.2 Envelope Tracking Power Amplifier Architecture**

In conventional constant bias power amplifiers, the maximum efficiency occurs at saturation, with a single-tone signal. As the output power of the power amplifier backs-off from the saturation point the efficiency degrades. This creates an issue in the presence of high PAPR signals where the envelope of the transmitted signal varies as a function of time. Thus, the difference between the DC power provided and the envelope power transmitted can be characterized as energy dissipation, as depicted in Figure 2.1.

On the other hand, the ET power amplifier architecture allows the operator to utilize only as much power as necessary to provide the amplified output. As shown in Figure 2.1 for the conventional power amplifier, a constant voltage is provided to the amplifier regardless of the output power, leading to considerable amount of unnecessary power consumption, depending on the class of operation. By dynamically varying the voltage supplied to the power amplifier such that it tracks the envelope of the RF signal, the power consumption can be significantly reduced. High efficiency is achieved in this manner by keeping the power amplifier in saturation most of the time where the efficiency is highest.

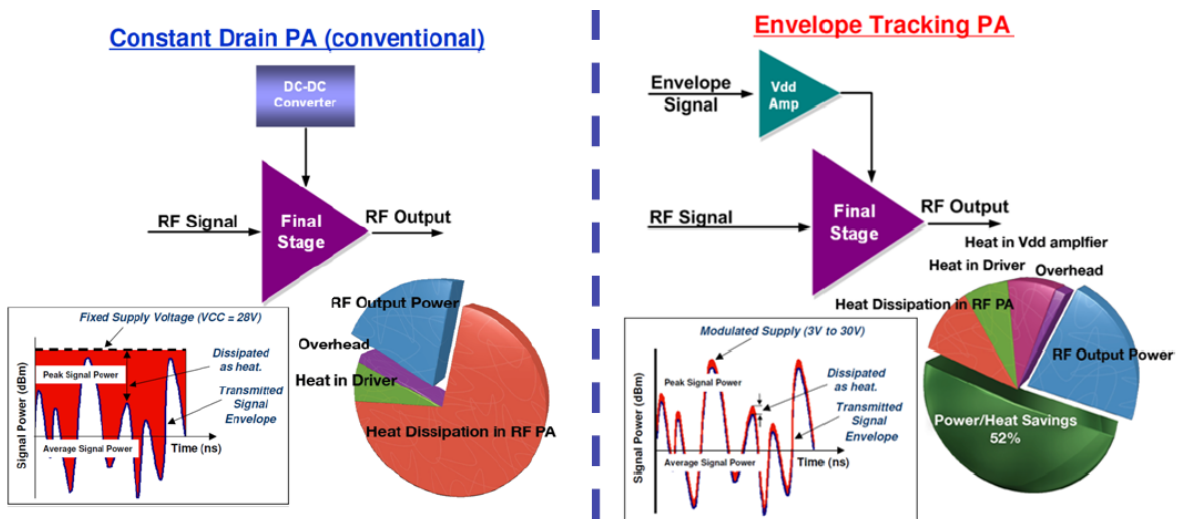


Figure 2.1: Block diagram of the envelope tracking power amplifier (left) and constant supply power amplifier (right) and comparison of the energy dissipation.

The envelope tracking architecture incorporates the use of a dynamic supply modulator and a RF power amplifier. The dynamic supply modulator (AKA. envelope amplifier, envelope modulator, or Vdd amplifier) is used to provide a modulated power supply in accordance to the envelope of the transmitted signal to the PA, dramatically decreasing the heat dissipation and reducing the junction temperatures at these devices

for better reliability. The fully modulated RF signal is fed to the input of the RF PA. As a result of reduced time spent during the higher peak envelope voltages, in envelope tracking, higher dynamic peak voltages can be achieved when compared to constant drain configurations. In addition, the envelope tracking power amplifier will generally have increased maximum output power for a given RF transistor periphery due to lower junction temperatures.

### 2.2.1 Envelope Supply Waveform Shaping

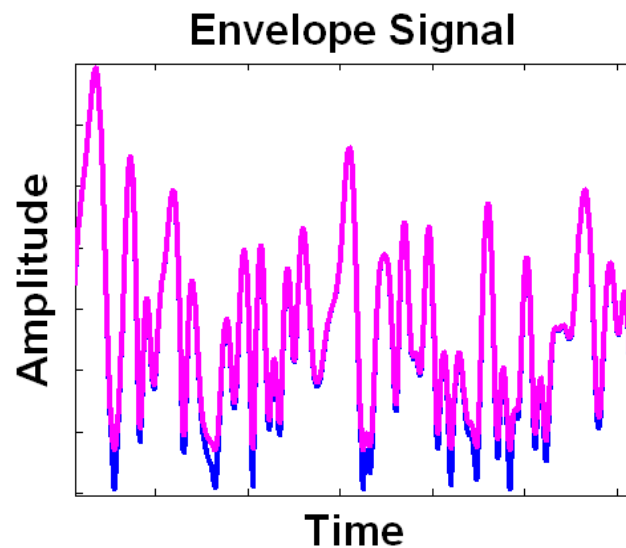


Figure 2.2: Time domain representation of the envelope supply signal before (blue) and after (magenta) de-troughing.

The envelope supply waveform supplied to the collector/drain of the power amplifier is shaped such that a linear relationship between the amplitude of the modulated RF signal and the envelope supply exists at the medium and high power levels. At the low input voltage levels, the supply waveform is de-troughed in order to avoid gain collapse, as depicted in Figure 2.2. In addition, de-troughing reduces the bandwidth of the envelope supply waveform and the ET system's sensitivity to time misalignment. The



de-troughed value was chosen to be near the knee voltage of the power amplifier. The transition between the linear region and the de-troughed value is adjusted to maximize efficiency and minimize nonlinearities and memory effects. The choice of the envelope voltage  $V_{env}(t)$  used in the ETPAs in this dissertation can be expressed as:

$$V_{env}(t) = V_{DD,max} \cdot \left[ |x_{in}(t)| + b \cdot e^{-\frac{|x_{in}(t)|}{b}} \right], \quad (2.1)$$

where  $V_{DD,max}$  is the peak envelope voltage,  $|x_{in}(t)|$  is the normalized input RF signal amplitude, and  $b$  is the “de-troughing” ratio, given by  $\frac{V_{DD,min}}{V_{DD,max}}$ , where  $V_{DD,min}$  is chosen to be close to the knee voltage of the RFPA.

## 2.2.2 Envelope Tracking Power Amplifier Efficiency

As shown in Figure 2.1, the envelope tracking power amplifier comprises both the dynamic supply modulator and the RF power amplifier. To accurately account for any dissipation in the dynamic supply modulator, it is necessary to include the efficiency of the envelope modulator in the calculation of the overall envelope tracking power amplifier efficiency. Hence, the overall efficiency of the ETPA can be approximated as the product of the RFPA efficiency ( $\eta_{RFPA}$ ) and the envelope modulator efficiency ( $\eta_{EA}$ ), given by:

$$\eta_{ETPA} = \eta_{EA} * \eta_{RFPA}. \quad (2.2)$$

Thus, it is important to maintain high efficiency for both the RF PA and the envelope modulator in order to maximize the overall envelope tracking power amplifier efficiency.

### 2.2.3 Dynamic Power Supply Efficiency

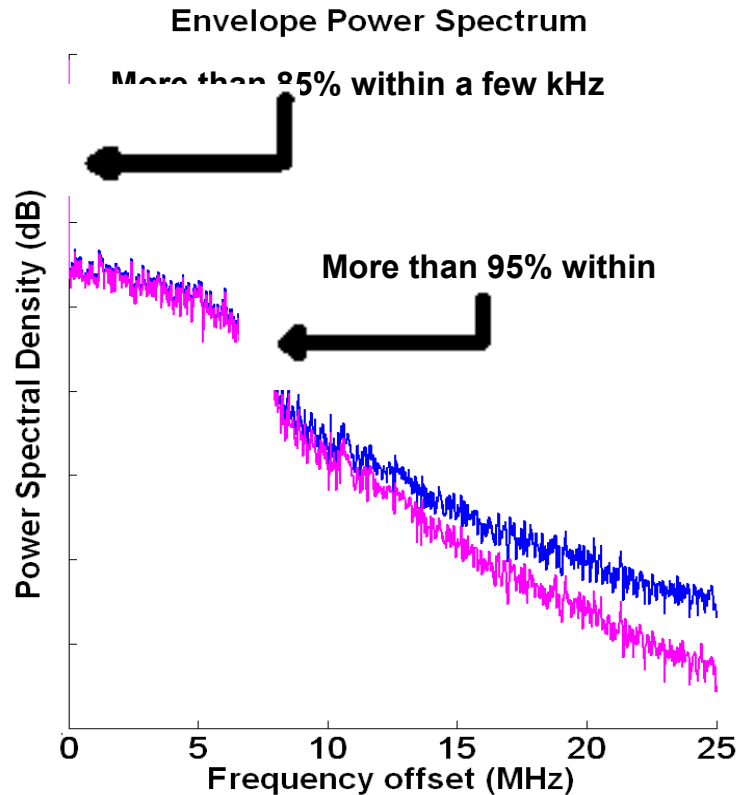


Figure 2.3: Envelope spectral response of a 10 MHz LTE signal.

By observing the spectrum of the envelope supply waveform, Figure 2.3 shows that more than 85% of the envelope power lies in the spectral region from DC up to a few hundred kHz. This portion of the power can be provided by a high efficiency switcher stage, resulting in a high efficiency dynamic modulator design. A high efficiency dynamic supply modulator can be realized by utilizing a linear stage operated in parallel with a switcher stage as shown schematically in Figure 2.4. The linear stage operates as a voltage source with an operational amplifier implemented in a feedback loop to maintain linearity. Essentially designed as a high efficiency buck converter, the switcher stage provides the majority of the current to the RF power amplifier. The hysteretic current

feedback control is used to provide a smooth power split between the linear stage and the switcher stage. A hysteretic current sense stage couples the linear and the switcher stages by detecting the net current out of the linear stage to control the switching behavior of the switcher stage. The switching waveform produced is highly correlated to the envelope supply waveform and approximates a delta-sigma modulation. The signal fidelity at the output of the dynamic supply modulator is important to ensure that ACPR and spurious emission specifications are met. Hence, the linear stage acts as an auxiliary current source to sink and source any additional necessary current needed to minimize the overall error between the desired current and the current provided by the switcher stage.

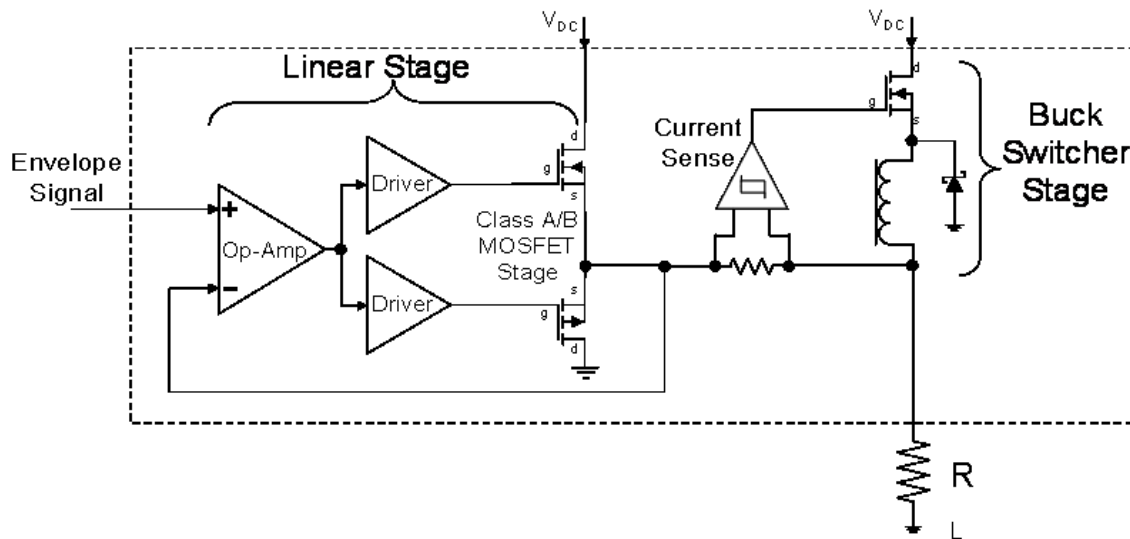


Figure 2.4: Schematic block diagram of the dynamic supply modulator.

The dynamic supply modulator efficiency can be expressed as:

$$\eta_{EA} = \frac{P_{out,env}}{P_{DC,env}} = \frac{P_{out,env}}{P_{out,env} + P_{loss}}, \quad (2.3)$$

where  $P_{out,env}$  is the output envelope power into the load or RFPA and  $P_{DC,env}$  is the DC power drawn by the modulator. The DC power consumption of the modulator can be expressed as the summation of the power delivered to the load ( $P_{out,env}$ ) and the power loss dissipated as heat ( $P_{loss}$ ). The power loss in the modulator can be characterized into two types of loss: static and dynamic, such that

$$P_{loss} = P_{loss,static} + P_{loss,dyn}. \quad (2.4)$$

The dynamic power loss of the dynamic modulator varies and is dependent on the characteristics of the signal and loading condition. As mentioned previously, the dynamic modulator contains two stages that work in parallel. While the switcher stage is used to provide the majority of the current (occurring at low frequencies), the linear stage must work in conjunction to source or sink any differences in the current drawn by the load. The switcher stage is designed to switch with a maximum frequency in the range of a few MHz's. Hence, as the modulation bandwidth of the signal increases, the amount of compensation needed from the linear stage also increases. Extra current produced by the switcher stage must be sunk by the linear stage and constitutes as a dynamic power loss, which is dependent on the signal characteristics. Additionally, the extra power sourced by the linear stage is subject to the losses from the linear stage such as on-resistance. The static power loss is constant and independent of signal characteristics and loading conditions, such as the quiescent power of the linear stage. Thus, as the output envelope power  $P_{out,env}$  decreases, while the dynamic power loss  $P_{loss,dyn}$  does decrease, the static power loss  $P_{loss,static}$  remains constant. Hence,  $P_{loss}$  becomes relatively large as  $P_{out,env}$

decreases, resulting in lower overall modulator efficiency. This is particularly true for signals with higher PAPR. Consequently, the RMS (root-mean-square) voltage of the envelope supply waveform is reduced, lowering the average output envelope power. Shown in Figure 2.5 is the fabricated PCB design of a 100-W dynamic supply modulator.

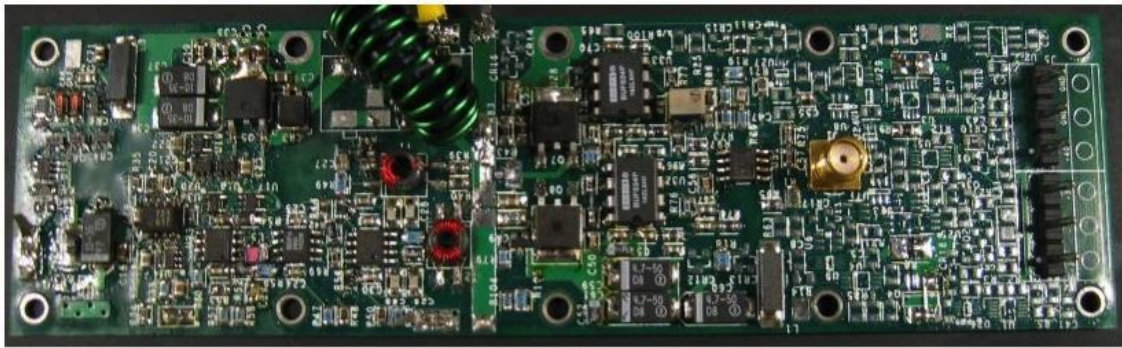


Figure 2.5: Printed circuit board of a representative dynamic modulator outputting 28V peak envelope voltage with up to 100-W average output power.

## 2.2.4 RF Power Amplifier Efficiency under Envelope-Tracking

In the presence of a non-constant envelope signal, the efficiency of the RF power amplifier is dominated by its performance corresponding to the average value of the signal. For a signal with a PAPR of  $\rho$  dB, the average envelope supply voltage at the drain of the RFPA can be expressed as:

$$\langle V_{Env,avg} \rangle = 10^{-\frac{\rho}{20}} * (V_{Env,max} - V_{Env,min}) + V_{Env,min}, \quad (2.5)$$

where  $V_{Env,max}$  is the peak envelope supply voltage and  $V_{Env,min}$  is the minimum envelope supply voltage. Hence, the RFPA characteristics is dominated by its performance at a supply voltage of  $\langle V_{Env,avg} \rangle$ . Continuous-wave (CW) measurements are

performed to provide an estimated performance expectation. The CW data was taken under various constant supply voltages, ranging from the peak envelope voltage to the minimum envelope voltage. Due to the relationship between the supply voltage and the input signal, the average RF power amplifier efficiency can be found by analyzing the performance of the RFPA with respect to the envelope supply voltage. When the RFPA is placed under envelope tracking, the expected output power, gain, and efficiency correspond closely to those measured under a supply voltage of  $\langle V_{Env,avg} \rangle$ . Figure 2.6 and Figure 2.7 depict the efficiency and gain, respectively, of a particular GaN power amplifier, measured at various constant drain supply voltages. For example, the average envelope supply voltage was approximately 12.65 V for an envelope supply waveform of a 7 dB single carrier WCDMA signal with a peak envelope voltage of 28 V and a minimum envelope voltage of 2.8 V. Based on the measured results in Figure 2.6 and Figure 2.7, the RFPA is expected to achieve approximately 72% drain efficiency, 15-17 dB of gain, and 40-50 W of output power. The dynamic supply modulator that would supply such power range (~70 W) achieves efficiencies in the low 70%, resulting in approximately 50% overall envelope tracking power amplifier efficiency with about 15-17 dB of gain at 40-50 W of output power. In addition to determining the relationship between the supply envelope voltage and input RF signal, optimization is also performed to maximize gain and thereby increase PAE (power-added-efficiency). These procedures yield a first order design and analysis of the constant drain power amplifier when operated under envelope tracking.

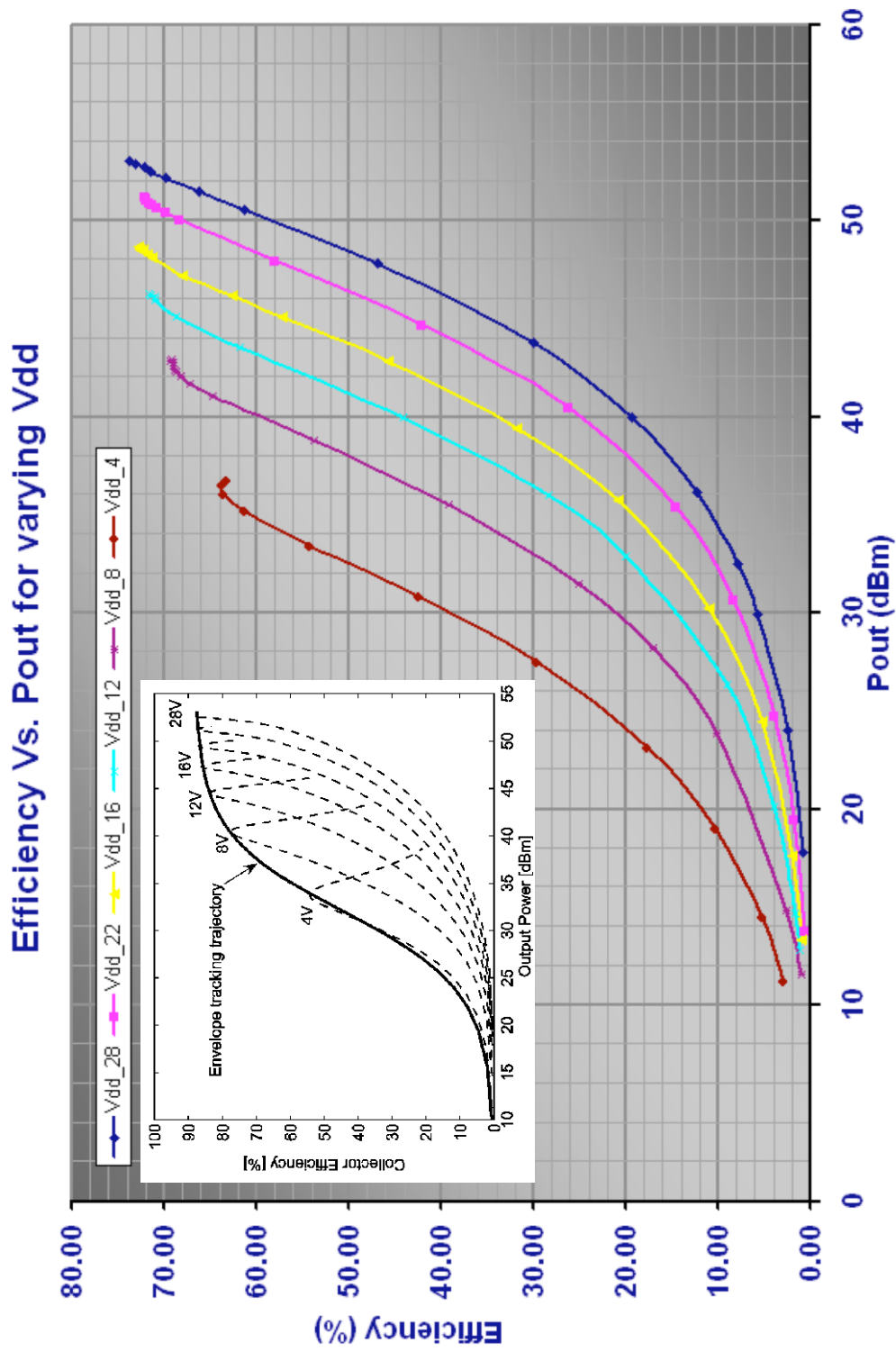


Figure 2.6. Envelope tracking trajectory as a result of dynamically varying the drain supply voltage.

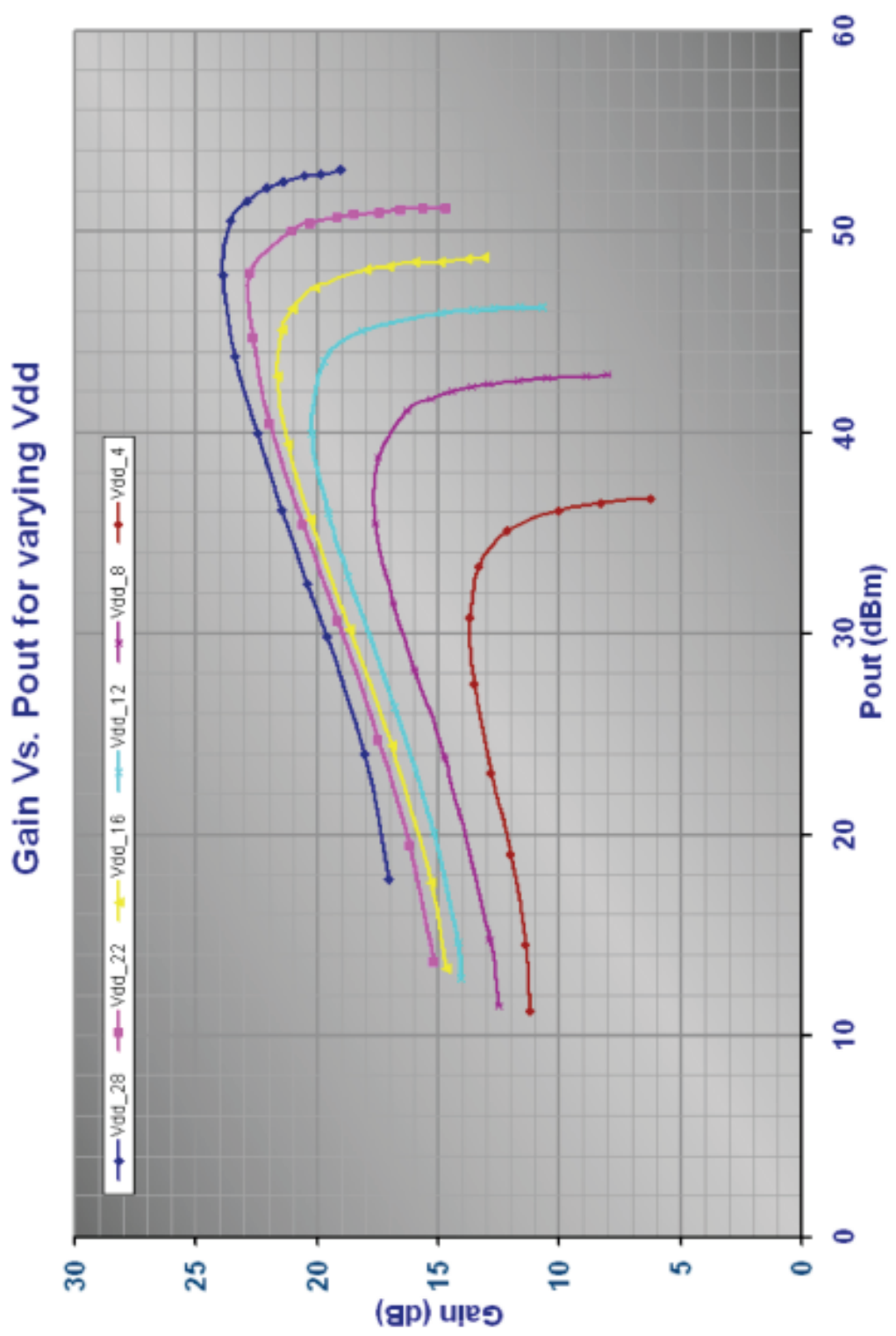


Figure 2.7. Gain performance as a function of output power for a constant drain power amplifier at various supply voltages.



## 2.3 Broadband Test-bench Implementation

The 4G OFDMA downlink signals have a PAPR of 7-11 dB, and data service transmissions will vary between the at the maximum permissible power and average back-off to achieve desired data rates and throughput. Energy consumption will increase as a result of the proliferation of popular consumer applications. To further increase capacity, micro-base-stations with tower mounted and wall mounted remote radio heads are increasing in popularity. High efficiency high power amplifiers with high linearity are necessary for these applications to eliminate noisy fans and air-conditioning, lower roof rentals, and increase reliability. It is widely accepted that although linearity and efficiency are competing constraints, signal processing may be used to simultaneously maximize both. The theory is that invertible nonlinearities may be corrected with techniques such as feed-forward and pre-distortion. Consequently, the ability to characterize an amplifier's nonlinearities and minimize their impact through signal processing using digital pre-distortion (DPD algorithms and closely related crest-factor reduction algorithms) has become paramount to remain competitive in the wireless communications market.

Digital pre-distortion (DPD) is a linearization technique that is performed in the digital signal-processing (DSP) domain. Because the correction is applied at the input of the power amplifier, insertion loss considerations, typically considered in other linearization techniques, are less critical. From the digital pre-distorter's perspective, the power amplifier is a black box, making this technique applicable across carrier

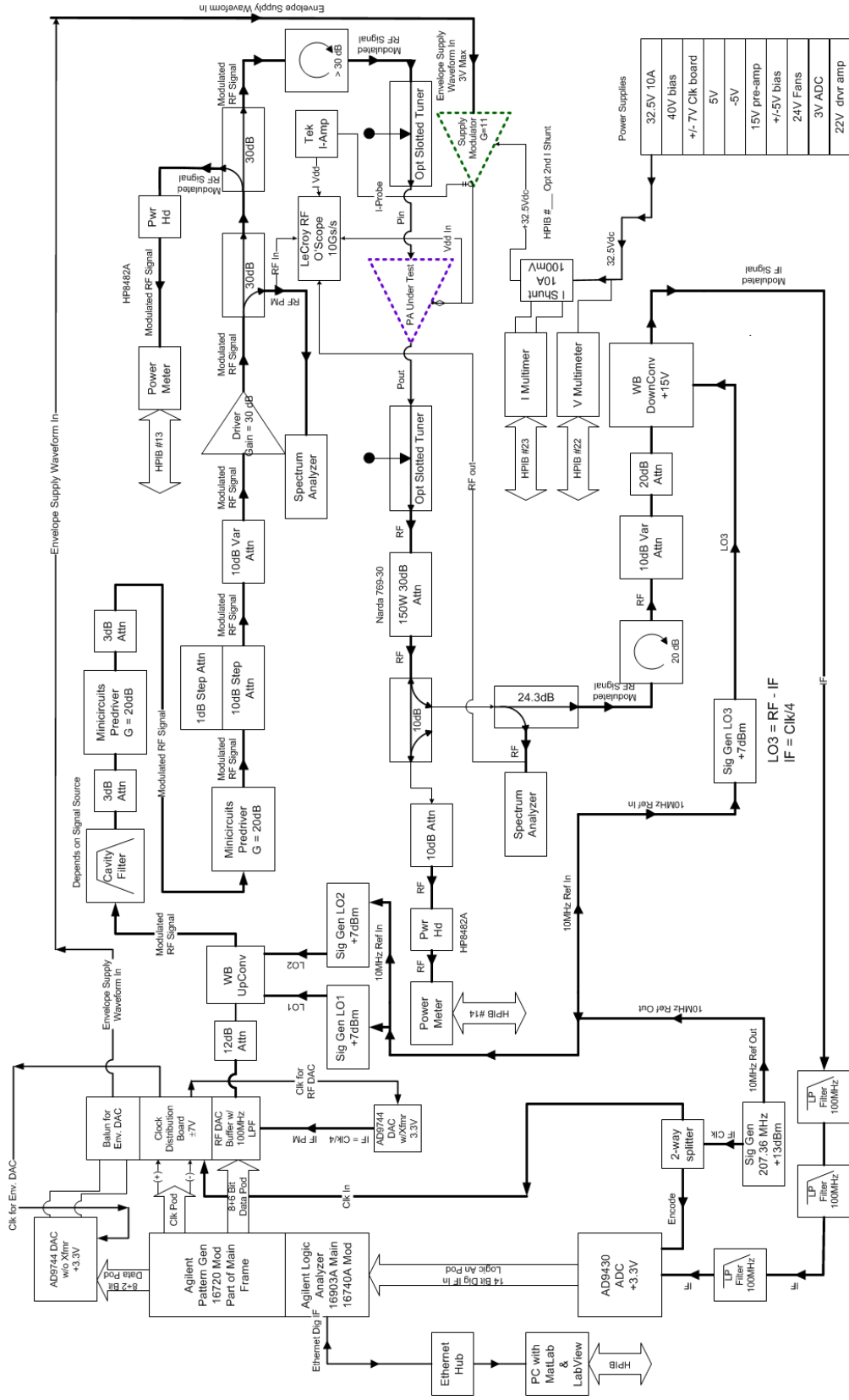
frequencies, power levels, device technology, amplifier technology, classes of operation, and operating conditions. DPD works in a complementary fashion with multi-tone dithering, and may even be used in conjunction with more exotic amplifier schemes such as Doherty and Envelope Tracking. In addition, another advantage of the DPD system over an analog pre-distorter is accurate and repeatable correction of AM-PM distortion. An analog pre-distorter can correct for AM-AM distortion, but often has unreliable AM-PM performance in the presence of different combinations of tones over wide bandwidths. Hence, linearization via DPD is very appropriate for implementation with a broadband power amplifier test-bench

The first generation power amplifier test-bench was designed to operate with 44 MHz of instantaneous bandwidth, support signals up to 10 MHz wide if digital pre-distortion is used. In addition, it was designed to operate solely at 2.14 GHz. However, in order to be able to support a broadband power amplifier, it is necessary to develop a test-bench that can support signals greater than 20 MHz of modulation bandwidth with the ability to perform digital pre-distortion. In addition, the test-bench needs to have the ability to test the power amplifier over a wide tunable carrier range, from UHF to 4 GHz.

In building such a test-bench capable of pre-distorting signals with up to 20 MHz of modulation bandwidth, it is necessary to have 100 MHz of instantaneous bandwidth in order to account for 5th order distortion products. By the Nyquist theorem, this requires at least 200 MSps DACs and ADCs. Figure 2.8 and Figure 2.9 depicts the schematic and the implemented 2nd generation (Mark II) broadband power amplifier and linearization test-bench, respectively, that was implemented (by the author in collaboration with Donald Kimball and Pavel Kolinko) for the research of this dissertation. It is designed to

support power amplifier operation in EER, ET, and classical constant bias mode. To accommodate wide carrier bandwidths, broadband up- and down-converters were built. The up-converter was designed in a heterodyne structure to ensure images were far enough apart to be filtered out. Direct down-conversion was used for the down-converter. In addition to its versatility in bandwidth and mode of operation, the test-bench also lends itself to being a platform for testing new DPD algorithms implemented in MATLAB. The system itself is independent of the linearization technique used. Many various linearization techniques, including look-up tables, behavioral modeling, Volterra-series based pre-distortion, memory mitigation, etc., have been found to be compatible for this system. The system has a tunable bandwidth from 100 MHz to 3.5 GHz with data vector patterns for up to 220 samples (~5 us) in depth and utilizes two 210 MSps 14-bit DACs and one 210 MSps 12-bit ADC.

In order to preserve the signal integrity of the clock signal, custom buffer circuitry was designed to provide sufficient drive levels to the clock of the ADC and DACs. In addition, most high speed COTS (commercial-off-the-shelf) DACs have differential output signals, which are converted to a single-end output via a balun. This works well for the RF path, which is AC-coupled. However, for the envelope supply path (to the dynamic supply modulator), which contains DC components and whose bandwidth extends to 5-7 times the modulation bandwidth, the low frequency cutoff of these baluns adds complication to the implementation of the wideband test-bench for ETPAs. To overcome this challenge, custom circuitry utilizing a low distortion difference amplifier is used in place of the balun and designed to drive the envelope input to the dynamic supply modulator.



Mark II High Power PA RF Test Set Up for UCSD, 100MHz BW

Figure 2.8. Detailed schematic diagram of the Mark II broadband linearization test-bench for broadband power amplifiers.

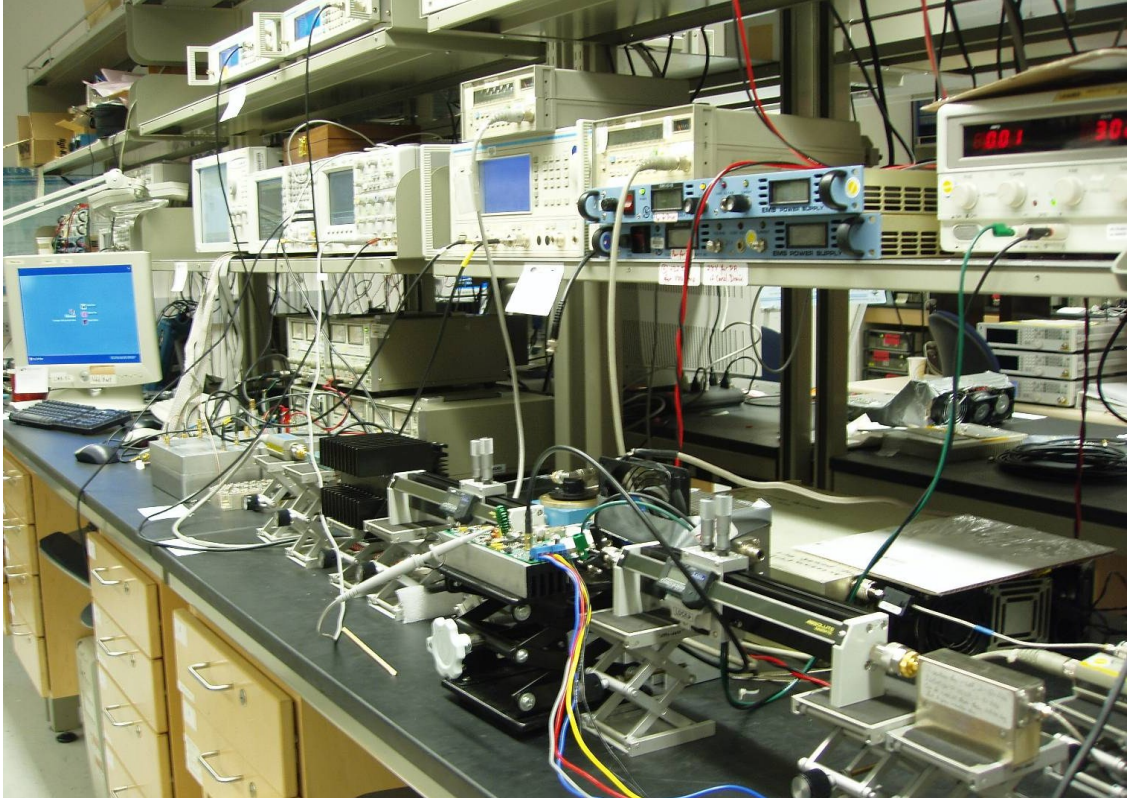


Figure 2.9: Mark II system implementation with 100 MHz bandwidth

For envelope tracking, in order to provide a dynamic envelope supply to the RF PA, a de-troghed envelope supply waveform is generated in the digital domain and converted to analog using a DAC, clocked at 207.36 MHz. A low-pass filter is used to reject the images generated by the DACs. In addition, the digital signal processing is used to generate the baseband fully modulated signal, centered at 51.84 MHz with 100 MHz of pre-distortion bandwidth. Sub-sample time alignment between the envelope path and the RF path can be adjusted in the digital domain to ensure that the envelope supply voltage reaches the collector/drain of the device at the same time as the RF signal for minimal distortion and optimized efficiency. To bring the fully modulated signal to the desired RF center frequency, a wideband heterodyne up-conversion scheme is performed. Up-conversion to millimeter wave frequencies can also be facilitated with an additional

mixer. The band-pass filter after the up-conversion is used to reject any harmonic content generated by the mixers. The output of the RF PA is sampled and down-converted back to IF via direct down-conversion and sampled by the ADC for analysis in the digital domain for digital pre-distortion (DPD). After proper alignment of the desired ideal modulated signal and the distorted output signal, look-up-tables (LUTs) are generated based on the measured amplitude and phase with respect to the amplitude of the desired signal (AM-AM and AM-PM, respectively). Applying the intended signal through the inverse of the LUT generates a pre-distorted memory-less signal to be applied to the input of the RFPA. In addition to memoryless distortions, power amplifiers exhibit distortion components that are dependent on past outputs. These deterministic memory effects generated by the ETPA itself are inherent to the power amplifier's class of operation, dependent on the results of the dynamic behavior of the system, and/or induced by the dynamic modulator itself. To generate a memory compensated pre-distorted signal, an approach of successive approximation can be used [2]-[3]. A key point in such an approach is system repeatability, a necessary condition in order to quantify and separate the memory effects due to the randomness of noise (non-deterministic) and the true memory (deterministic) of the ETPA. Another important challenge in the development of a broadband PA test-bench is to ensure spectral flatness over the entire instantaneous bandwidth. Over a wide instantaneous bandwidth of 100 MHz, spectral variations, as a result of filters and other components in the RF path, occur. These variations appear like memory effects in the measurement. To ensure that the measured memory effects attribute mainly to the memory of just random noise and

the RFPA under test, a wideband calibration routine is implemented to compensate for these spectral variations in the RF path.

### 2.3.1 Calibration Equalization for Broadband Flat Linear Response

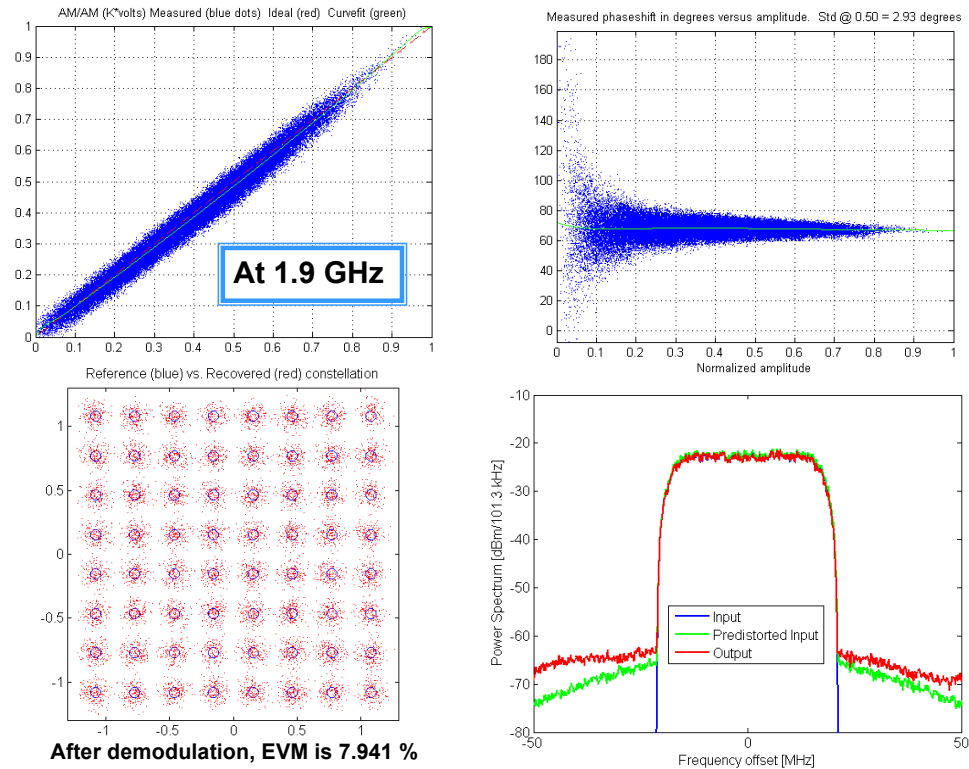


Figure 2.10: Measured response of the 100 MHz broadband test-bench with a 40 MHz 64-QAM signal on a straight-through measurement without calibration, resulting in significant memory effects (~8% EVM).

One major challenge in developing this broadband test-bench is the ability to achieve spectral flatness over the entire bandwidth. Variations in the spectral domain result in memory artifacts in the straight-through environment, as depicted in Figure 2.10. As illustrated in the AM-AM and AM-PM plots with a 40 MHz signal over the 100 MHz pre-distortion bandwidth, the straight-through of the system behaves in the linear manner.

However, a significant amount of memory can be observed, noted by the spread, resulting in ~8% EVM (error vector magnitude). These artifacts are due mostly to the amplitude and phase variation as a function of frequency in the filters and mixers of the RF transmit path on the wideband test-bench. Another source of the memory results from the non-flat response of the DAC. Hence, it is desirable to separate and correct for these artifacts in order to accurately characterize and pre-distort the nonlinearities of the power amplifier under test.

A calibration routine is developed to address these issues. The routine generates a frequency dependent equalizer based on a FIR filter to calibrate out the variations in the transfer function of the transmit path. The first issue arises from the non-flat response of the DAC sampling a digital baseband signal in which the analog output at higher frequencies are attenuated more than those at lower frequencies. Because the DAC output operates by holding the last voltage value over the whole sampling period of  $1/f_s$ , this results in the multiplication of the frequency response of the input signal of the DAC with a sinc envelope function in the frequency domain, given by:

$$H_{DAC}(f) = \frac{\sin\left(\frac{\pi f}{f_s}\right)}{\frac{\pi f}{f_s}} \quad (2.6)$$

One method to calibrate out this sinc envelope is by generating a  $1/\text{sinc}(x)$  frequency boost function in the digital signal processing before the DAC. Hence, the pre-equalization FIR filter implemented incorporates the inverse sinc function to equalize the DAC's inherent sinc frequency response.



To determine the frequency responses of the other components (i.e., filters and mixers) whose responses differ when operated under large signal versus small signal in the transmit path, a calibration signal is generated based on the desired modulated signal. A frequency chirp is added to the modulated signal to characterize the transfer function of the system as a function of frequency. The received signal through the transmit path is measured and recorded. A transfer function estimate  $H_{system}(j\omega)$  between the normalized transmitted signal  $\hat{X}(j\omega)$  and the normalized time-aligned received signal  $\hat{Y}(j\omega)$  is calculated in MATLAB, giving

$$H_{system}(j\omega) = \frac{\hat{Y}(j\omega)}{\hat{X}(j\omega)} \quad (2.7)$$

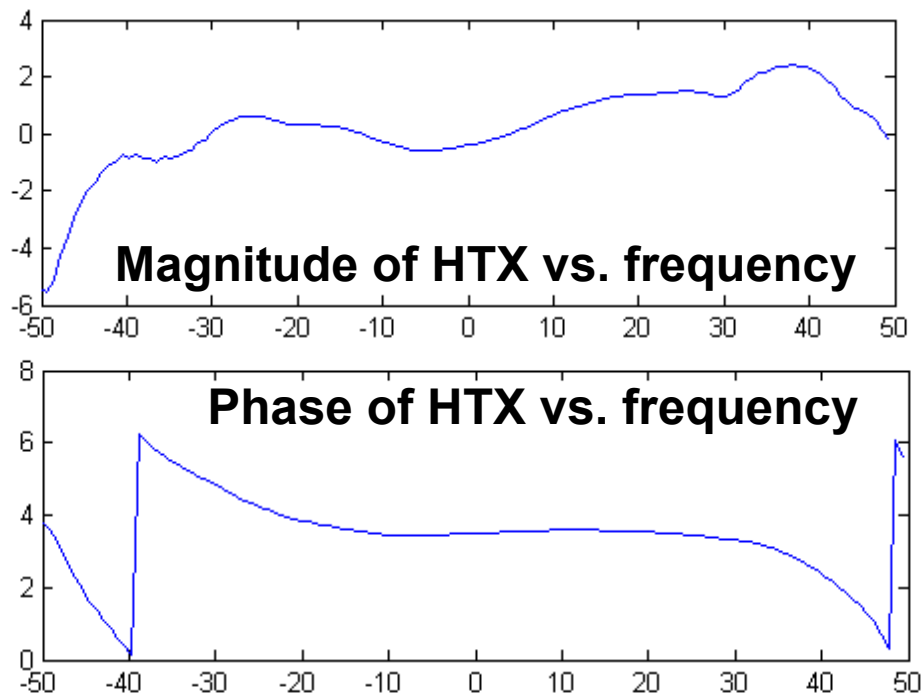


Figure 2.11: Calculated transfer function (top: magnitude and bottom: phase – wrapped) of the normalized received signal and the normalized transmit signal. The horizontal axis is frequency in MHz.

Shown in Figure 2.11 is the example transfer function, both magnitude and phase, calculated from the measured chirped 40-MHz 64-QAM signal through the 100-MHz broadband test-bench system. In this particular frequency setup, approximately 8 dB of magnitude variation with more than  $2\pi$  radians of phase change was observed over 100 MHz. This contributes significantly to the straight-through response of the system, which results in significant memory effects as shown in Figure 2.10.

A complex and nonlinear phase FIR filter can be determined in MATLAB such that its response is the band-limited inverse of the system response, given by:

$$H_{filter}(f) = H_{system}^{-1}(f) \quad .(2.8)$$

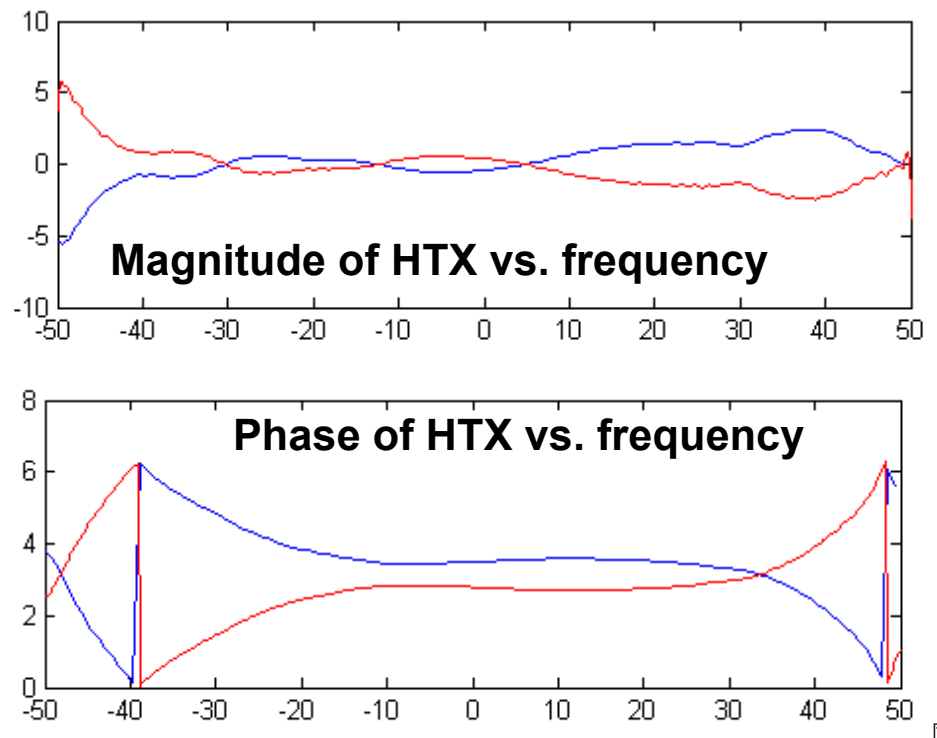


Figure 2.12: Calculated inverse FIR filter (top: magnitude and bottom: phase – wrapped) in red and calculated transfer function of the path. The horizontal axis is frequency in MHz.

Shown in Figure 2.12 is the response of the designed 128-order inverse FIR filter. The original transmit signal is passed through this calibration filter before being sent to the DAC and through the transmit chain. Using this pre-equalization filter, compared to the non-calibrated case with  $\sim 8\%$  EVM, better than  $1\%$  EVM was achieved with excellent spectral flatness and significant reduction in the spread in the amplitude and phase for a 40-MHz signal over 100 MHz of pre-distortion bandwidth, as depicted in Figure 2.13.

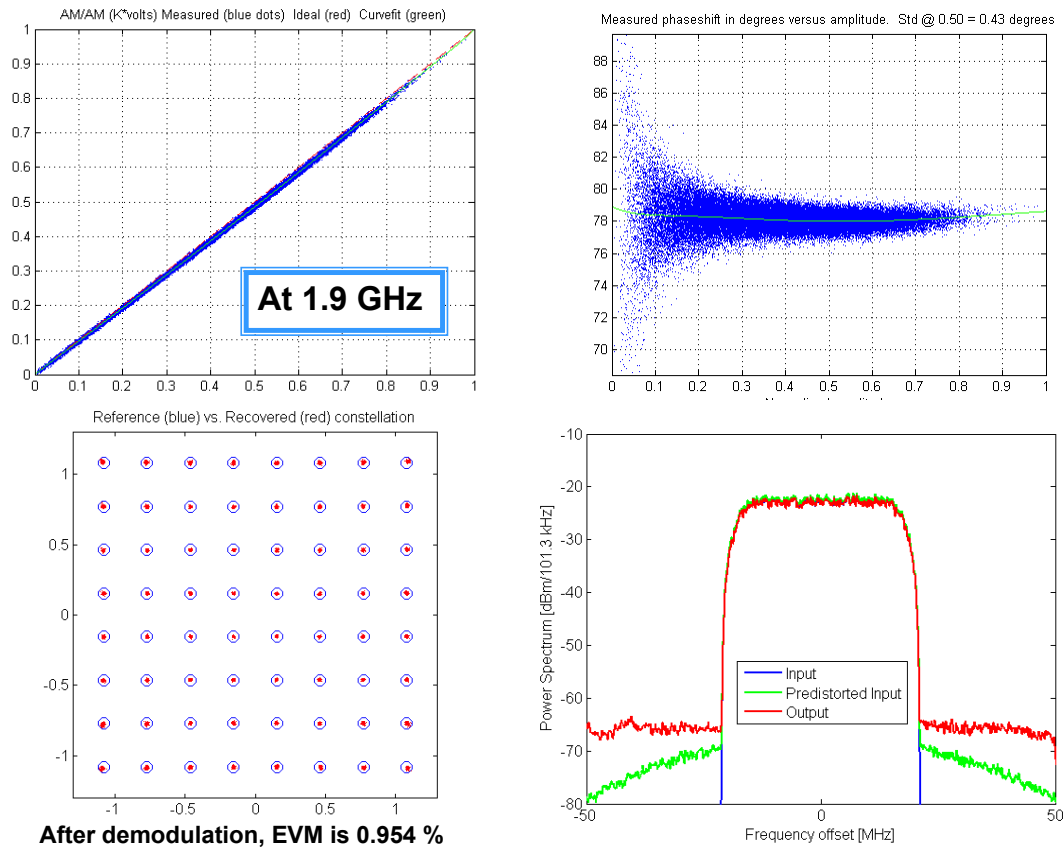


Figure 2.13: Measured response of the 100 MHz broadband test-bench with a 40 MHz 64 QAM signal on a straight-through measurement after equalization calibration, resulting in  $\sim 1\%$  EVM.

### 2.3.2 Memoryless Digital Pre-distortion Implementation

If an amplifier's transfer function is known or can be measured, the signal entering the amplifier may be intelligently modified, or pre-distorted, in an inverse fashion, such that after amplification the desired output is achieved, as shown in Figure 2.14.

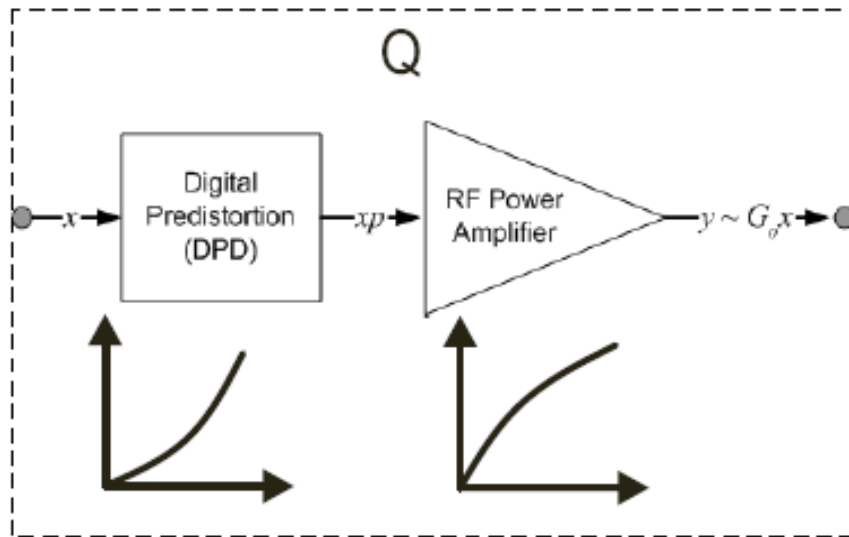


Figure 2.14. Digital pre-distortion system

Suppose the output of a memoryless non-linear amplifier may be modeled as follows:

$$y(t) = g(x(t)) \quad (2.9)$$

where  $g(\cdot)$  is a generalized complex gain mapping as shown in Figure 2.15.

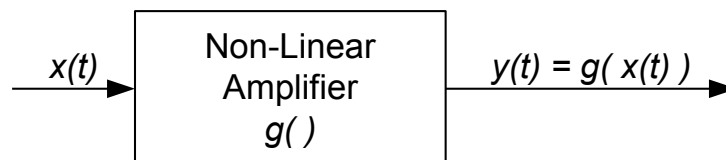


Figure 2.15: Amplifier model

Assuming that the desired response,  $h(\cdot)$ , of the ideal amplifier is a constant gain,  $G_d$ , such that

$$g_{ideal}(x) = h(x) = G_d x . \quad (2.10)$$

However, in reality, the amplifier gain is not constant, but rather varies as a function of the input signal. Hence, a simpler model based on the assumption that device gain changes only as a function of the magnitude of the input signal is assumed. Under this assumption,  $g(\cdot)$  may be decomposed into magnitude-dependent magnitude and phase products:

$$g(x) = x \cdot g_A(|x|) e^{jg_\theta(|x|)}, \quad (2.11)$$

where the functions  $g_A(\cdot)$  and  $g_\theta(\cdot)$  are referred to respectively in the literature as AM-AM and AM-PM characteristics.

Amplitude distortion occurs when the output amplitude is not a linear function of the input signal. As a result of the weakly nonlinear amplifier, gain expansion or compression at the fundamental frequency, as well as harmonic and intermodulation distortions, occurs. Harmonic distortion is the creation of harmonics of the fundamental frequency at the output. Intermodulation distortion occurs when multi-tone signals are present at the input. Due to the mixing of the input frequencies and the harmonic distortion, the creation of other frequency components is present at the output. Unlike harmonic frequencies, intermodulation products can fall in-band and near the

fundamental frequency, making it very difficult to filter out. However, digital pre-distortion can be used to cancel these distortion products near the signal of interest.

In addition to AM-AM distortion, an amplifier also exhibits phase (AM-PM) distortion. AM-PM distortion represents the change in phase of the transfer characteristics as the drive level increases towards compression. In the frequency spectrum, AM-PM distortion can often attribute to an asymmetric spectral regrowth.

To determine the pre-distorted input signal, the inverse function of the AM-AM and AM-PM distortion was determined using a polynomial fit based on evenly-spaced amplitudes of 2000 points. Using this behavioral model, a signal with memory-less pre-distortion can be generated to produce a linear output signal at the output of the power amplifier.

## **2.4 Envelope Tracking Power Amplifier Performance**

The Mark II broadband test-bench is capable of a wide range of tunable carriers and great spectral flatness over the entire instantaneous bandwidth and to demonstrate its performance over the wide range of frequency, measurements of envelope tracking power amplifiers implemented at UHF (~300 MHz), at 780 MHz, 2.14 GHz, and at mm-wave (44 GHz) have been demonstrated and will be discussed in the following sub-sections. Excellent efficiency has been demonstrated at UHF, S-band, and Q-band using the same VDD amplifier. One of the advantages of using the envelope tracking technique for high efficiency broadband power amplifiers is that, in concept, envelope tracking is not

sensitive to the carrier frequency and can be applied over a broad range of carrier frequencies due to the fact that the envelope of the RF signal remains independent of the carrier frequency.

### **2.4.1 UHF Envelope Tracking Power Amplifier**

At UHF, high efficiency power amplifiers for military systems such as the Mobile User Objective System (MUOS), an UHF geosynchronous satellite communications system based on the commercial WCDMA system), are highly desired. With next generation radio technology, the warfighters can transmit an abundance of high quality data from the front line to the commander by MUOS. In order to increase mobility of the warfighter, the MUOS handset weight and form factor needs to be minimized. By decreasing the power consumption, fewer batteries will be needed, reducing the weight carried by the warfighters in the battlefield and improving combat agility directly.

A Si-LDMOS push-pull power amplifier, whose fixture was tuned to 295 MHz and biased in Class AB, was placed under envelope tracking, as depicted in Figure 2.16. Figure 2.17 illustrates the instantaneous measurements of the drain current, drain voltage, UHF input and UHF output signals. Observing the drain current and drain voltage, the shape of the waveforms is almost identical with no significant slope difference. This is due to the fact that the UHF power amplifier appears like a resistive load to the drain modulator. The agreement between the envelope of the UHF output signal and the dynamic supply voltage show that time alignment between the RF signal path and the dynamic envelope supply path was achieved.

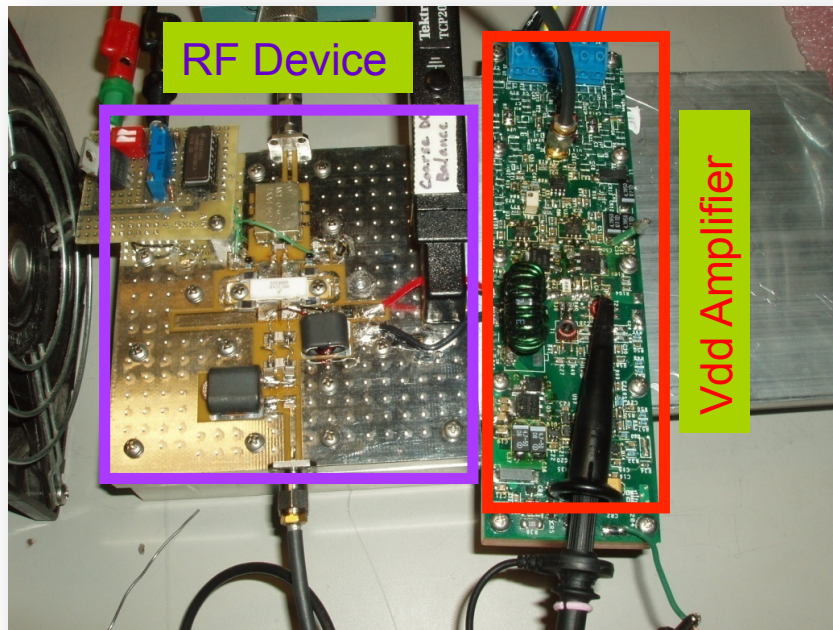


Figure 2.16: Single-ended Si-LDMOS UHF PA fixture tuned to 295 MHz, placed under envelope tracking with a high power dynamic supply modulator

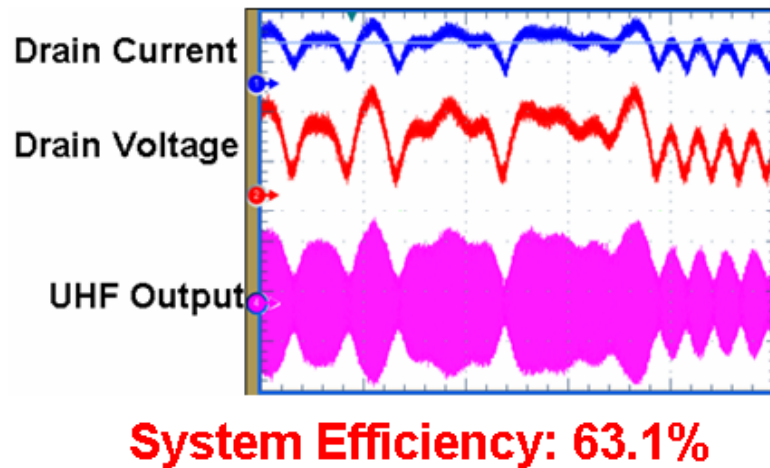


Figure 2.17. Instantaneous measurement of the drain current, drain voltage, and RF output for instantaneous drain efficiency

To demonstrate high efficiency under high output power, two sets of measurements were performed (one with a single push-pull PA and another with a balanced push-pull PA). An overall ET system efficiency of 63% was achieved with



85W output power at 23 dB gain using a signal carrier 3.5 dB PAPR WCDMA signal. With the ability to measure the instantaneous dynamic supply power and RF output power, the ET system efficiency could be separated to evaluate the individual efficiency of the two components, the UHF power amplifier and the dynamic supply modulator. The RF device demonstrated 79% average efficiency and the supply modulator demonstrated 77% efficiency. Contrast to the constant drain power amplifier configuration, an efficiency enhancement of 2.25 times (from 28% to 63%) was observed.

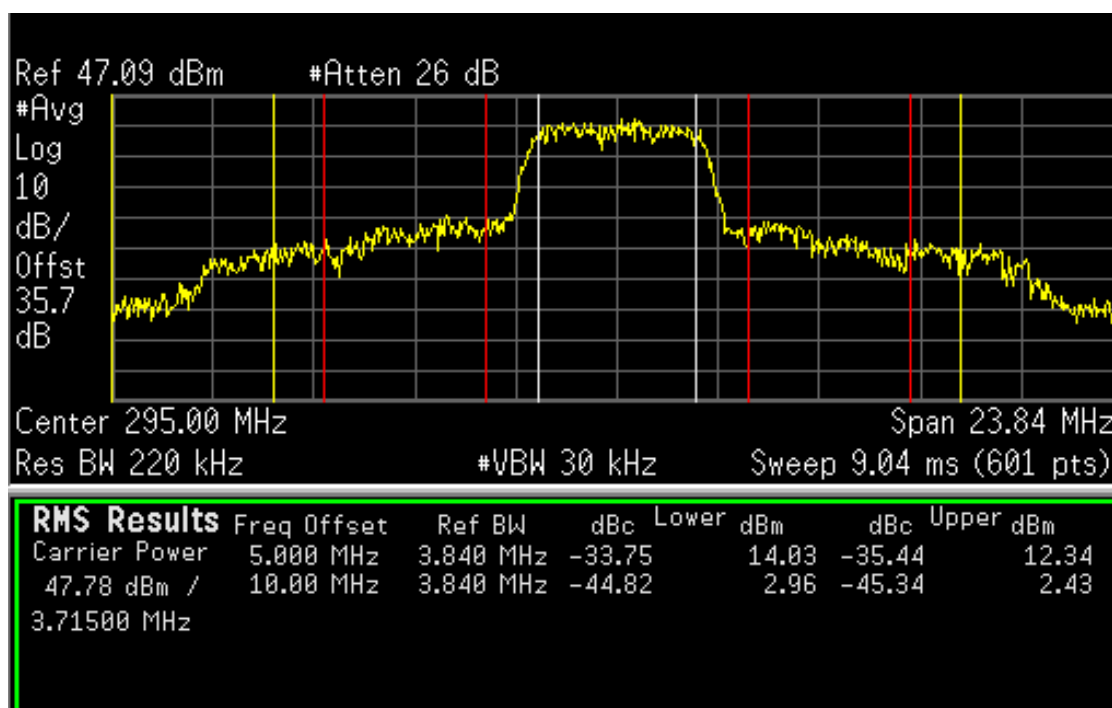


Figure 2.18: Output spectral response of the single push-pull UHF power amplifier (Specifications: -33 dBc / -43 dBc).

Figure 2.18 shows the spectral response at the output of the power amplifier. In this experiment, linearization techniques were not necessary to meet the linearity standards and, hence, were not applied. It was found that the output satisfied ACPR

requirements with a slight margin. At 5 MHz offset, the lower and upper ACPR were -33.75 dBc and -35.44 dBc, respectively. At 10 MHz offset, the lower and upper ACPR were -44.82 dBc and -45.34 dBc, respectively.

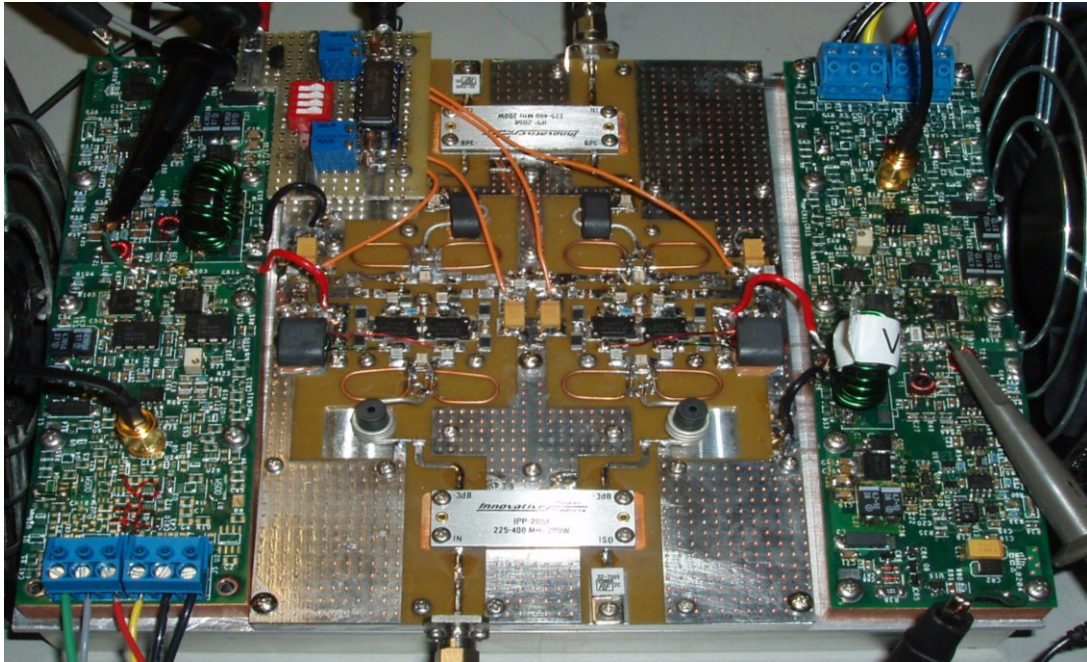


Figure 2.19: Dual modulator balance push-pull ET power amplifier, fed with a single signal generator.

In some applications, even high powers of greater than 100 W are necessary. However, because the design of the supply modulator is limited to 100 W output power, in such scenarios, it is necessary to use two supply modulators side-by-side. Depicted in Figure 2.19 is the dual modulator configuration. The power amplifier consists of two transistors operated in push pull and then combined in a balanced configuration. The balanced push-pull power amplifier is supplied by two modulators, one on each side. In order to ensure that the envelope supply waveforms on each side arrive at the drain of the transistors at the same time, identical phase-matched cables were used to feed the envelope into the modulators and identical feedlines were used for

biasing the drain. At 150 W output power, the efficiency was measured to be 60.2% with 20 dB of gain using the same WCDMA signal. One reason for the slight gain and efficiency drop is due to the use of the transformers and quadrature hybrids at the input and output of the balanced push-pull PA which introduced some additional losses.

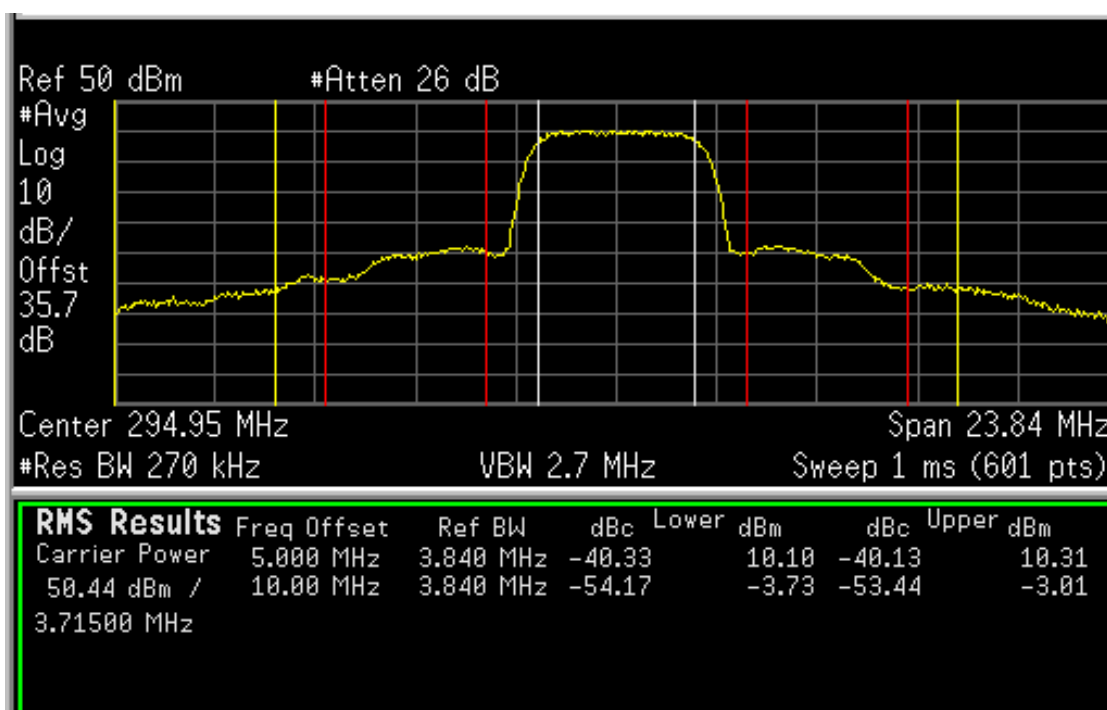


Figure 2.20: Output spectral response of the balanced single push-pull UHF power amplifier. (Specifications: -33 dBc / -43 dBc).

Figure 2.20 shows the output spectral response of the balanced push-pull UHF power amplifier with dual modulator configuration. At 5 MHz offset, the lower and upper ACPR were -40.33 dBc and -40.13 dBc, respectively, leading to at least 7 dB of margin. At 10 MHz offset, the lower and upper ACPR were -54.17 dBc and -53.44 dBc, respectively, giving at least 10 dB of margin. The significant improvements in the ACPR levels were due to the balanced configuration that was adopted in this design.

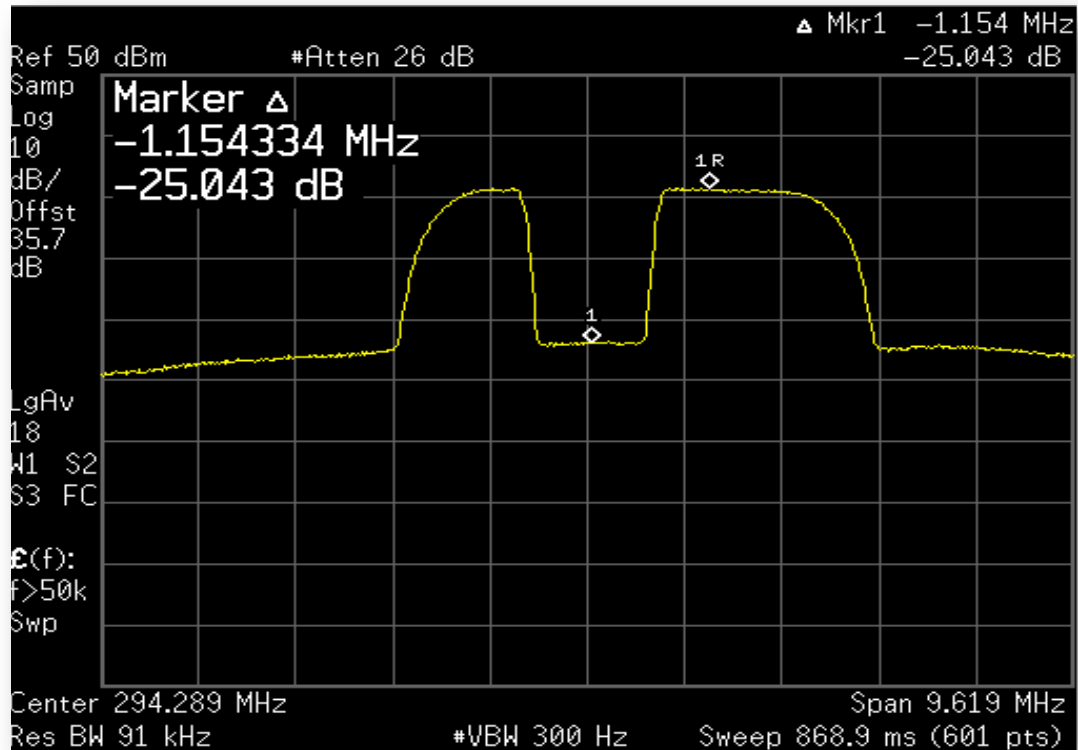


Figure 2.21: Output spectral response of the balanced single push-pull UHF power amplifier with a 1.2 MHz notch placed in the middle of the SA-WCDMA signal.

In addition to the traditional 3.5 dB PAPR WCDMA signal, the MUOS system also requires the amplification of a frequency ‘notched’ spectrum adaptation WCDMA (SA-WCDMA) signal to allow for simultaneous usage with legacy users. Under the worst-case scenario, in which a 1.2-MHz notch placed in the middle of the band, the ‘notched’ SA-WCDMA MUOS signal imposes a higher PAPR (~5-7 dB). Shown in Figure 2.21 is the measured output spectral response of the SD-WCDMA signal, demonstrating the dual-modulator ET UHF PA’s ability to achieve 1.2 MHz notch with -25 dBc suppression without the use of digital pre-distortion or other linearization techniques, meeting the system’s linearity specification of -24 dBc.

## 2.4.2 Band 14 - 780 MHz Envelope Tracking Power Amplifier

In next generation wireless systems such as LTE, as the demand from consumers for various multimedia services increases, it becomes increasingly important to develop high spectrum efficiency communication signals. With the television bands (698-806 MHz) becoming available for mobile communications due to the switch to digital television, increasing attention is being given to the design of power amplifiers that can operate with high efficiency over these bands.

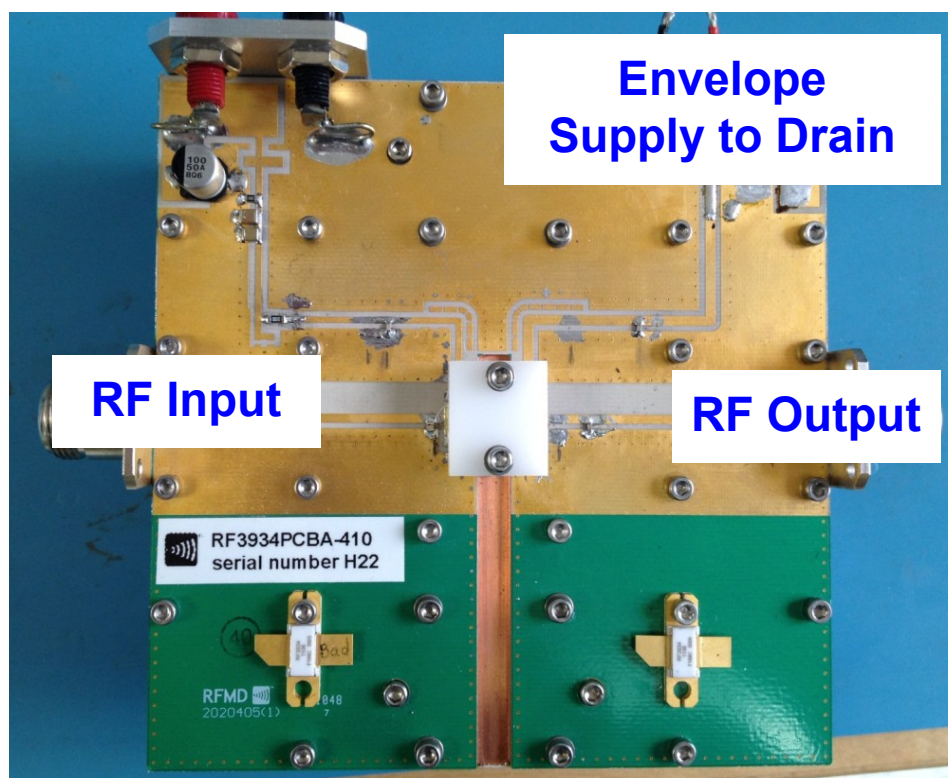


Figure 2.22: RF3934 RF power amplifier fixture tuned to 780 MHz operation.

The power amplifier used in this work, depicted in Figure 2.22, is the RFMD 120W RF3934 GaN HEMT device, based on RFMD GaN1C high breakdown voltage GaN technology. The gate length of the device was 0.5  $\mu\text{m}$  with a  $f_t$  of 11 GHz. The

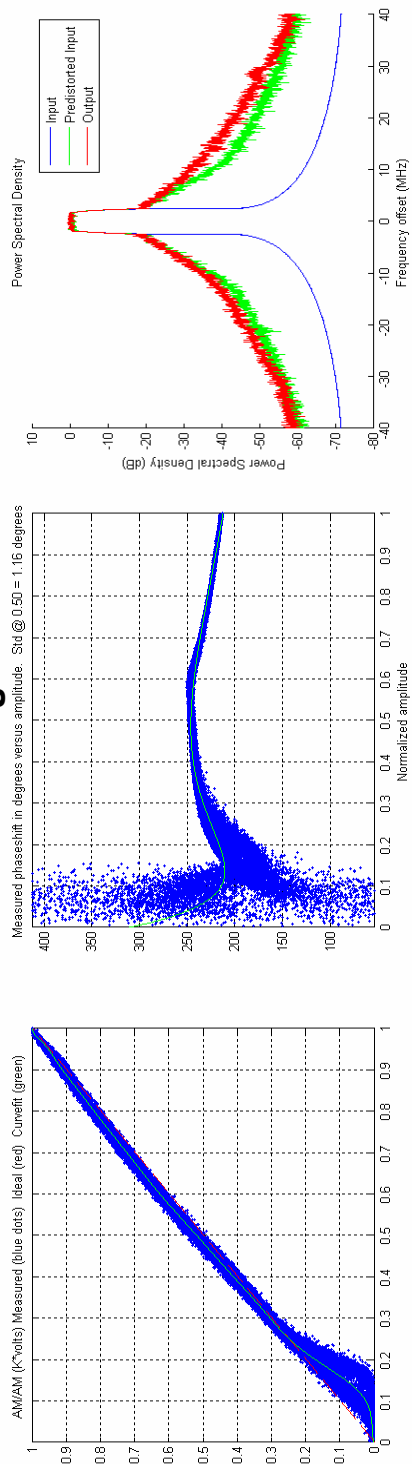
input and output matching networks were tuned for optimal operation at 780 MHz, corresponding to LTE Band Class 14. The RFPA was biased in Class AB at a gate voltage bias of -3.42V with 32.5V peak envelope voltage and a quiescent current of ~320 mA. The knee voltage of the device was ~5V.

Table 2.1 summaries the measurement results achieved for the two signals under test: 1) single carrier WCDMA signal with 6.6 dB PAPR and 2) 16-QAM 10 MHz LTE signal with 7.5 dB PAPR. Using the WCDMA signal, measured drain efficiencies of 70.3% and 69.4% are reported before and after memory DPD, respectively. A gain of ~13.5 dB was maintained before and after DPD, with a slight increase in the average output power to 28.6 W after DPD. For the 10 MHz 16-QAM LTE signal, measured drain efficiencies of 59.2% and 60% was reported before and after memory DPD, respectively. Similar to the WCDMA case, the gain of the envelope tracking power amplifier remained the same at about ~13.6 dB with about 23 W of average output power.

Table 2.1: Summary of results for 780 MHz ET power amplifier

	Drain Efficiency (%)	Gain (dB)	Output Power ( $W_{avg}$ )	NRMSE/EVM (%)	ACPR (dBc)
WCDMA before DPD	70.3	13.46	27	19.12	-22/-31
WCDMA after Memory DPD	69.4	13.53	28.6	1.51	-45/-51
10MHz LTE before DPD	59.2	13.57	23	20.93/12.24	-22/-32
10Mhz LTE after Memory DPD	59.9	13.57	22.8	3.34/3.03	-45/-46

### 1C WCDMA Before Digital PreDistortion



### 1C WCDMA After Digital PreDistortion

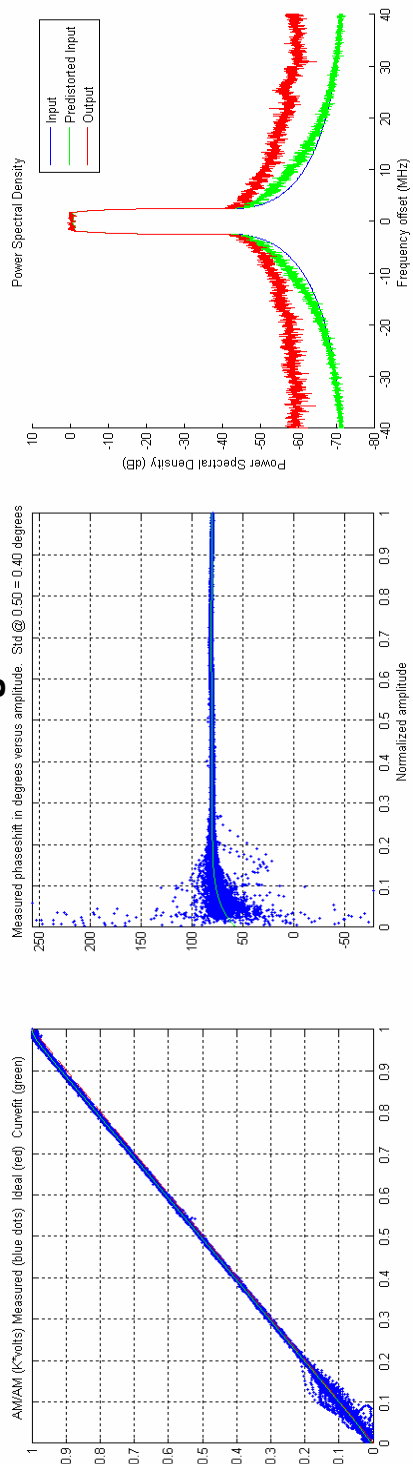
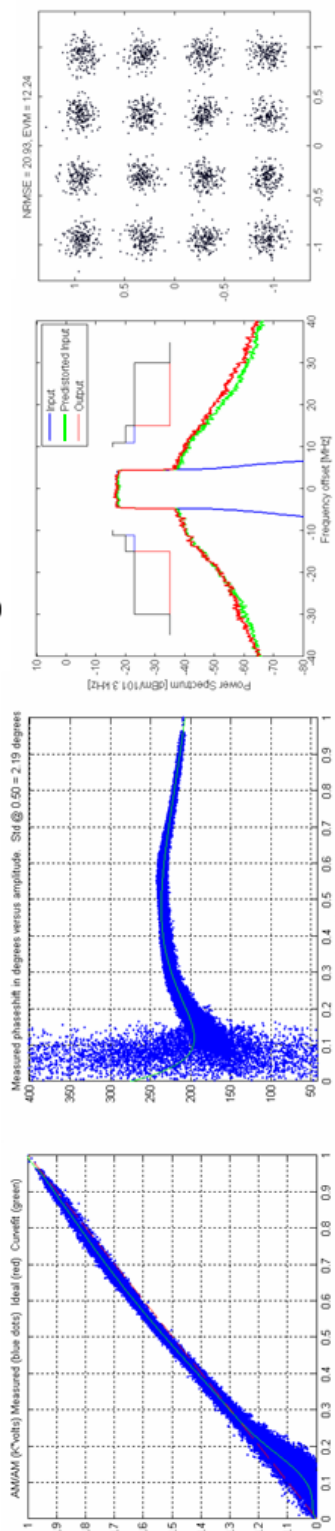


Figure 2.23: Measured AM-AM, AM-PM, and spectrum with a single carrier WCDMA signal, centered at 780 MHz before and after memory compensated digital pre-distortion.

### 16 QAM 10 MHz LTE Before Digital PreDistortion



### 16 QAM 10 MHz LTE After Digital PreDistortion

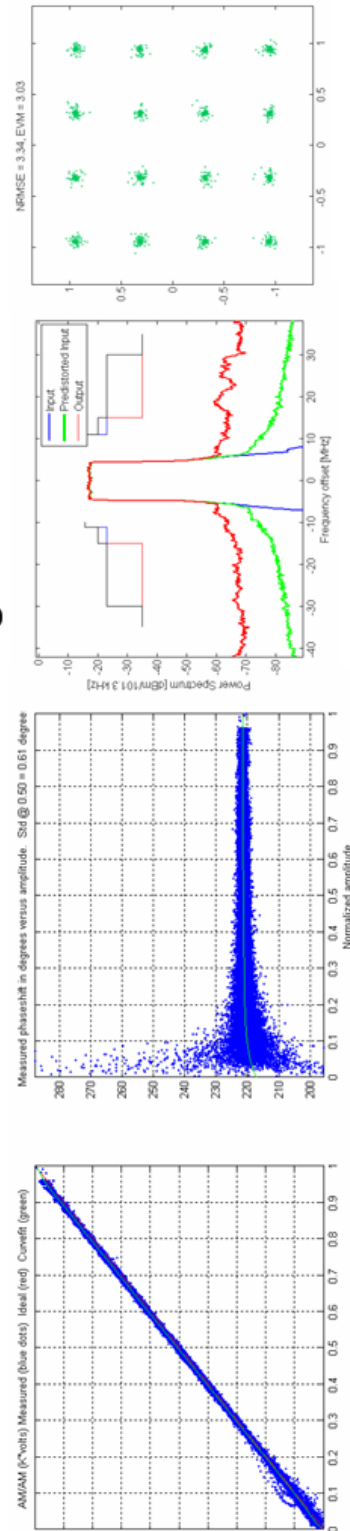


Figure 2.24: Measured AM-AM, AM-PM, spectrum, and constellation diagram with a 16 QAM 10 MHz LTE signal, centered at 780 MHz before and after memory compensated digital pre-distortion.



Figure 2.23 illustrates the measurement results using a single carrier WCDMA signal centered at 780 MHz before (top) and after (bottom) memory DPD. The left side of the figure shows the AM-AM (left) and the AM-PM (middle) of the measured output. A small amount of gain change was observed at low voltages, commonly seen in ET where de-troughing has occurred. A significant amount of phase distortion ( $\sim 40^\circ$ ), resulting in the spectral regrowth seen in the spectrum (right), was observed in the AM-PM plot (middle) before DPD. The amount of scatter in the AM-AM and AM-PM plots can be attributed to memory effects in the ETPA. At low amplitudes, a larger spread as well as gain collapse is observed, most visibly in the AM-AM plot (left). This is due to the higher knee voltages  $V_{knee}$  (as compared to GaAs HVHBTs and Si-LDMOS FETs) of these high breakdown GaN devices, resulting in some gain collapse at those voltages as we approach supply voltages close to  $V_{knee}$ . After memory compensated digital pre-distortion using successive approximation (bottom plots), a linear gain and a flat phase were achieved. In addition, the amount of scatter has been significantly reduced. The normalized RMS error (NRMSE) improved from 19.12% to 1.5%. Greater than -45 dBc and -50 dBc for ACPR1 and ACPR2, respectively, were achieved after memory DPD, meeting the WCDMA specifications.

Figure 2.24 shows the measured results before and after memory compensated digital pre-distortion for a 10-MHz 16-QAM LTE signal. In a similar fashion, a significant amount of memory effect is observed before digital pre-distortion as evident by the scatter in the AM-AM and AM-PM plots. The EVM before DPD was measured to be 12.24%. After memory DPD using successive approximation, the EVM was measured to be 3%. As a result of de-cresting the signal to a PAPR of 7.5 dB (for high

average efficiency), the inherent EVM of the de-crested signal was 2.91%. This quantifies the EVM floor to which memory compensated DPD can be used to improve EVM. Hence, the PAPR of the signal provides the system designer a tuning knob in which the EVM (while still meeting linearity specifications) can be traded-off for high efficiency through use of techniques such as de-cresting. After DPD, the ACPR was measured to be better than -45 dBc, meeting specifications for 10 MHz LTE signal.

### **2.4.3 2.14 GHz Envelope Tracking Power Amplifier**

In next generation commercial wireless and mobile military applications, the necessity for supporting smaller, lighter weight radios with low unit cost, high reliability communication capabilities has led to the demand higher efficiency solutions. Full-scale “net-centricity” of the military combat forces as well as consumer-based systems and public safety can only be achieved when size, power consumption, and bandwidth constraints can all be met. Power amplifiers represent one of the most expensive component sub-assemblies in modern wireless infrastructure equipment, and both their performance and cost are important drivers in system design and are an integral part of all base-station radio systems.

Table 2.2: Summary of results for the 2140 MHz Envelope Tracking power amplifier with a 5 MHz WCDMA signal.

	Gain [dB]	Pout [W]	Drain Eff. [%]	PAE [%]	$\eta_{PA}$ [%]	$\eta_{EA}$ [%]	EVM [%]	ACPR1 [dBc]	ACPR2 [dBc]	Notch Depth [dBc]
No Notch	Before	3.82	49.61	44.7	76.59	64.85	5.54	-45.87	-56.82	-
	After	9.54	4.14	51.01	45.9	78.41	65.06	-60.38	-61.45	-
Notched	Before	8.13	2.27	45.77	38.63	73	62.7	-35.89	-45.88	-32.7
	After	8.16	2.39	47.44	40.28	73.15	64.85	-47.75	-54.99	-45.68

Nitronex GaN HEMT NPTB00025 was used for the high efficiency RF power amplifier. Measurement results shown here are of an envelope tracking power amplifier operated at 2140 MHz, demonstrating high efficiency performance can be achieved at RF frequencies using the same modulator design as in the previous sub-sections. Under the excitation of a MUOS signal, peak powers greater than 10W was measured. Table 2.2 summaries the results achieved under a 3.5 dB PAPR WCDMA signal and a 6.75 dB PAPR ‘notched’ SA-WCDMA MUOS signal, both with 5 MHz modulation bandwidth centered at 2140 MHz. With the 3.5-dB PAPR WCDMA signal, the measured drain efficiency was 49.6% with a gain of 9.5 dB at 3.8 W output power. Without applying pre-distortion, the measured out-of-band nonlinearities quoted by the ACPR at 5 MHz and 10 MHz offset were -45.87 dBc and -56.82 dBc, respectively, satisfying the linearity requirement with more than 10 dB of margin. After applying digital pre-distortion (DPD), the linearity was dramatically improved to better than -60 dBc while the gain, output power, and drain efficiency remained relatively the same at 9.54 dB, 4.14 W, and 51%, respectively.

Figure 2.25 plots the measured ‘output amplitude vs. input amplitude’ (AM-AM) and ‘output phase vs. input amplitude’ (AM-PM) of the power amplifier under envelope tracking. As depicted by the mostly linear behavior of the AM-AM and small phase lead of  $7.5^\circ$  in the AM-PM, very little nonlinear distortion was observed prior to applying any form of pre-distortion. To understand the performance of the ET system under more severe dynamic ranges, measurements were performed with a 6.75 dB SA-WCDMA MUOS signal with a 1.2 MHz notched in the middle of its frequency band (most severe signal requirements – worst case for the MUOS system). The measured efficiency with

the ‘notched’ SA-WCDMA MUOS signal before applying pre-distortion was 45.8% at a gain of 8.13 dB and output power of 2.3 W. Without applying pre-distortion, the measured ACPR at 5 MHz and 10 MHz offset were -35.89 dBc and -45.88 dBc, respectively, passing linearity requirements with more than 2 dB of margin. After applying digital pre-distortion (DPD), the linearity was improved by more than 10 dB to -47.8 dBc and -55 dBc at 5 MHz and 10 MHz offset, respectively. The measured gain, output power, and drain efficiency remained relatively the same. The in-band linearity in the MUOS system is quantified by measuring the notch depth of the output signal using the SA-WCDMA signal. Measured results indicated that the notch depth was -32.7 dBc and -45.68 dBc before and after applying digital pre-distortion, respectively, meeting specification in both cases with more than 8 dB margin (spec: -24 dBc). Figure 2.26 illustrates the measured spectrum under the four described scenarios above. Based on our measured results, linearity requirements were met even without the use of digital pre-distortion while simultaneously achieving high efficiency, demonstrating great potential for improving today’s military handheld and man-pack units. In addition, given the significant margin provided with the use of DPD, this implies that trade-offs in linearity can be made to achieve high efficiency and better PA performance in the ETPA by driving the PA harder into compression and retuning the input/output matching networks.

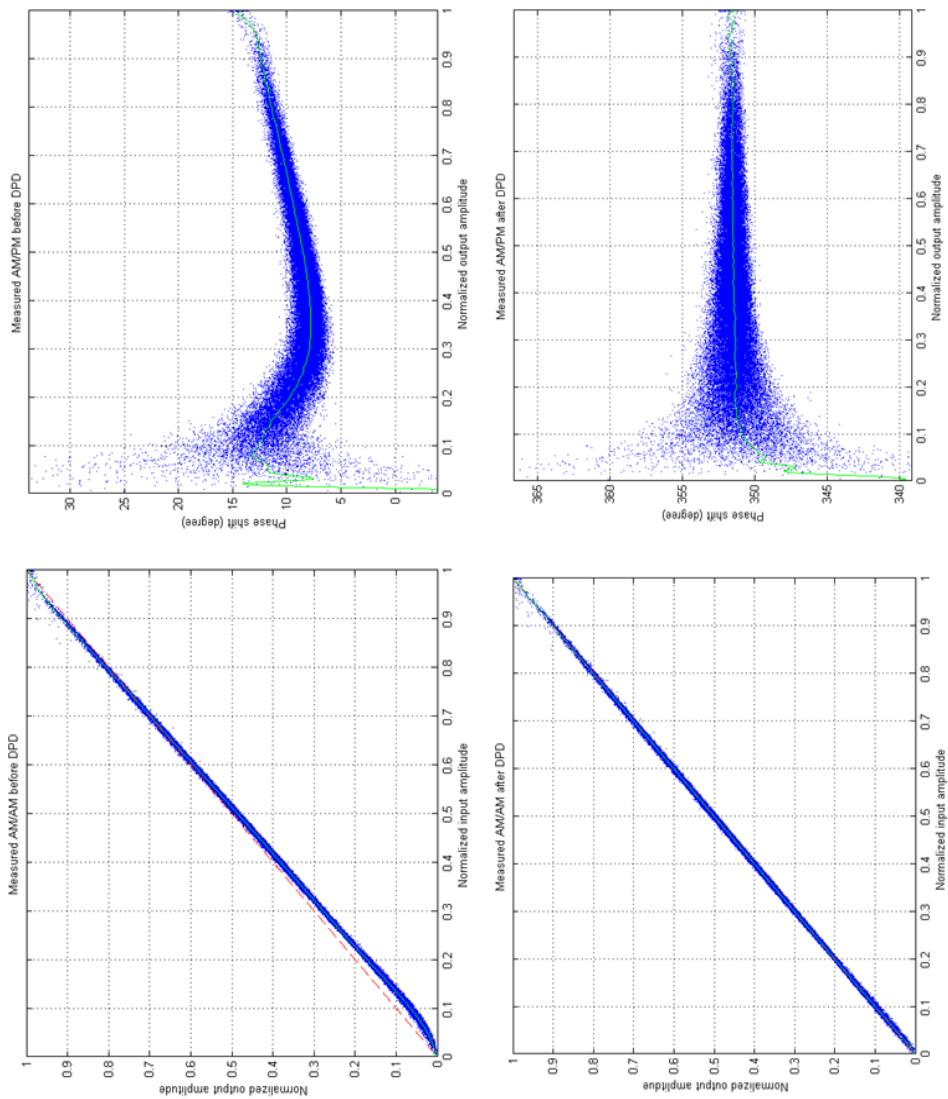


Figure 2.25: Measured instantaneous output amplitude and phase (normalized) vs. input amplitude, prior to pre-distortion (up) and after pre-distortion (down).

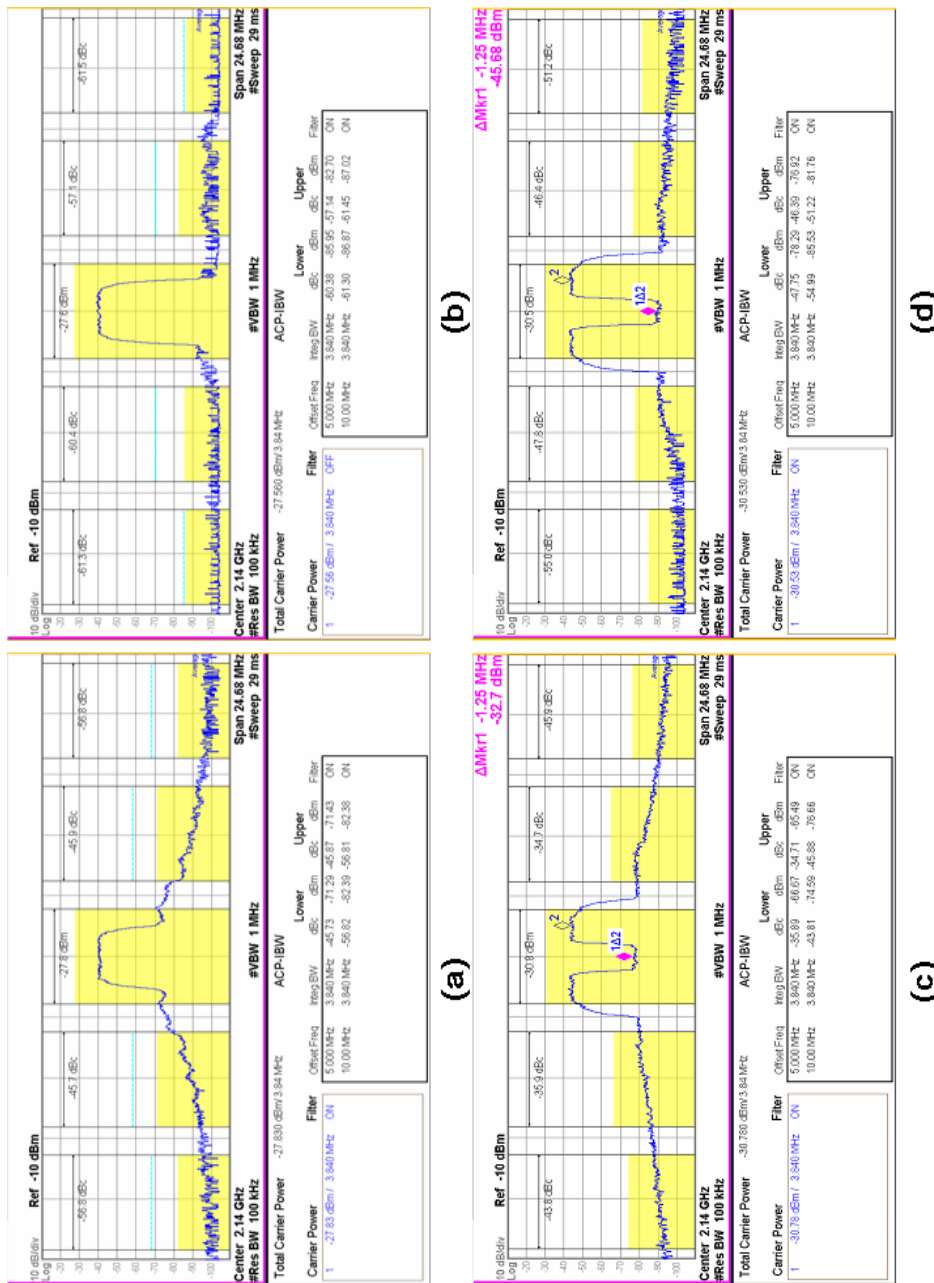


Figure 2.26: Top: Measured spectrum of the 5 MHz bandwidth 3.5-dB PAPR WCDMA signal before digital pre-distortion (a) and after DPD (b). Bottom: Measured spectrum of the 5-MHz 3.5-dB PAPR SA-WCDMA signal before DPD (c) and after DPD (d).

## 2.4.4 Envelope Tracking Power Amplifiers for Mm-wave

Emerging millimeter wave applications such as satellite services, automotive radars, point-to-point digital radios, and military systems, have led to an increasing interest in high frequency power amplifier design. Recent developments in GaN have enabled the design of high power amplifier MMICs in the mm-wave regime. However, in wireless communication systems, which employ signals with time-varying envelope with high peak-to-average power ratio (PAPR), the average efficiency degrades in a constant drain implementation, leading to the need for alternative solutions. In principle, the envelope tracking (ET) architecture offers a straightforward solution for efficiency enhancement for power amplifiers in the Q-band since the envelope of the fully modulated signal is independent of the RF frequency. The same drain modulator used for low frequency wireless systems can, theoretically, be directly applied to Q-band power amplifiers.

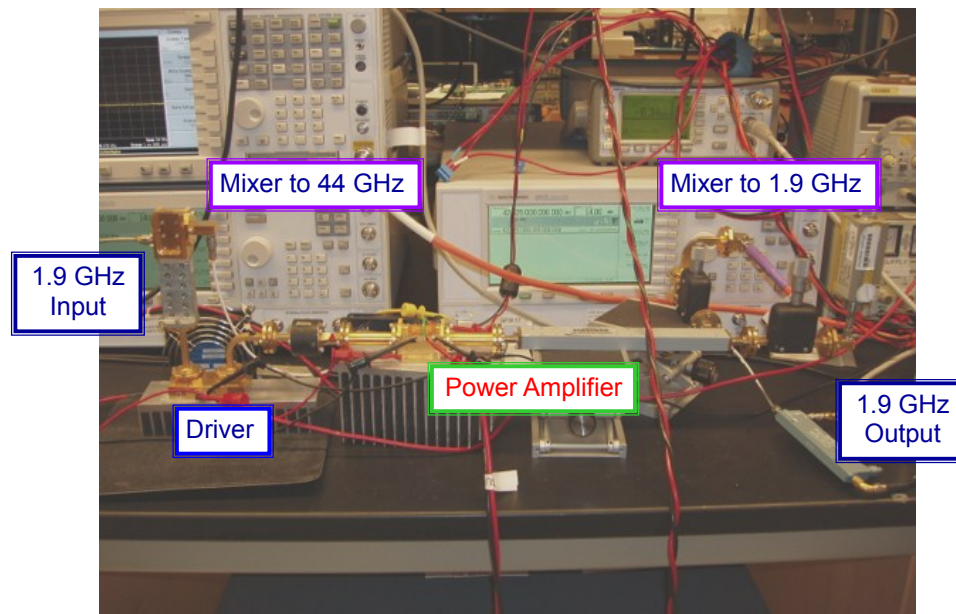


Figure 2.27: Mm-wave ET power amplifier system.



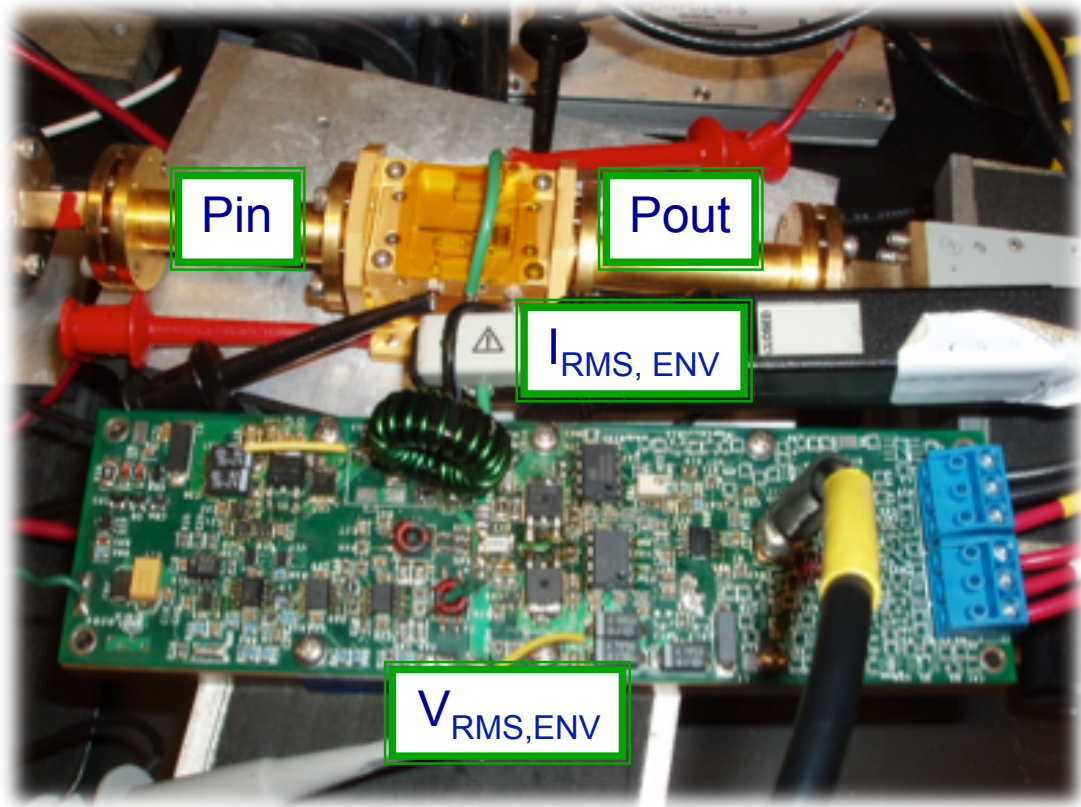


Figure 2.28: Q-band MMIC power amplifier under envelope tracking.

In the ET configuration for mm-wave PA, the power amplifier is fed with a fully modulated RF signal at the input and supplied with a modulated drain bias in accordance with the envelope of the modulated signal. As a result, the power amplifier at all times is kept near saturation where the efficiency is highest. Figure 2.27 depicts the system for the 44-GHz ET system. The modulated signal is generated in digital baseband using MATLAB and its phase and magnitude components are sent to a pair of DACs, sampling at 207.36 MS/s, via a logic analyzer. The envelope supply waveform is fed to the drain modulator for amplification. The fully modulated RF signal is then up-converted to an intermediate frequency of 1.9 GHz before a final up-conversion to 44 GHz is performed. A pre-driver was used at 1.9 GHz (IF2) to provide adequate power levels into

the mm-wave mixers to drive the driver and the MMIC PA. At the output of the PA, a power meter and a spectrum analyzer were used to evaluate the output power level and spectral response. Linearization of the system is performed via digital pre-distortion (DPD) in which the output is sampled and down-converted to baseband, after undergoing an initial down-conversion to 1.9 GHz. Time alignment between the PA output and the desired signal is executed and the nonlinear behavior of the power amplifier is extracted. Using the inverse of the PA behavior model, a pre-distorted signal is generated and sent to the PA to achieve a linear output and clean spectral response at the output.

The Triquint TGA4046 chip, a 3-stage Q-band MMIC power amplifier, was used for both ET and fixed drain bias testing as shown in Figure 2.28. The chip was designed with a  $P_{1dB}$  of 32 dBm (and a  $P_{sat}$  of 33 dBm) with a gain of 16 dB. At 44 GHz, a peak PAE of approximately 10% at a fixed drain bias of 6 V was attained under CW excitation (and the average PAE drops to near 3% with a high PAPR signal of 7.6 dB).

Table 2.3: Summary of results of the Q-band Envelope Tracking power amplifier.

Method	Before Digital Pre-distortion				After Memoryless DPD				After Memory Compensation			
	Pout (dBm)	Drain Eff (%)	EVM (%)	ACPR1 (dBc)	Pout (dBm)	Drain Eff (%)	EVM (%)	ACPR1 (dBc)	Pout (dBm)	Drain Eff (%)	EVM (%)	ACPR1 (dBc)
Constant Drain	25.6	3.03	8.9	-28.07	21.65	1.22	1.54	-38.14	-	-	-	-
Envelope Tracking	24.77	8.4	3.5	-24.87	23.3	6.12	2.9	-32.63	23.78	7	2	-40

Measurements were done with the same power amplifier under both constant drain and modulated drain biasing. The measured results are summarized in Table 2.3. The signal used for measurements was a 20-MHz 7.6-dB PAPR 64-QAM waveform. When operated under a fixed drain bias of 6 V and gate bias of -0.7 V, the

MMIC PA achieved 3.0% efficiency at an average output power of 25.6 dBm with an EVM of 8.9%. Under ET with the same gate bias, the MMIC PA achieved 8.4% drain efficiency (more than 2.8 times improvement) at an average output power of 24.8 dBm before DPD. This efficiency improvement can be attributed to the operation of the MMIC PA near saturation at most times; lower consumption results from reducing the supply voltage at the lower powers. Additionally, with ET, the self-heating of the MMIC and dissipated power were dramatically reduced, (from 12.1W to 3.6W), leading to higher performance and potentially greater reliability.

Further enhancement of efficiency of the PA MMIC relative to the constant drain case was observed after DPD, up to a factor of 5.7 times improvement. This further improvement stems from the higher peak gain of the MMIC attainable with reduced self-heating. The overall ET system efficiency, including the drain modulator, assuming that the drain modulation efficiency could reach 65%, would be approximately 4.55% with a factor of 3.7 times in efficiency enhancement compared to the fixed drain bias scenario after DPD while meeting ACPR requirements.

Figure 2.29 shows the AM-AM and AM-PM characteristics of the MMIC PA under ET. Compared to the fixed drain bias case, the AM-AM characteristics appear more linear. At the lower and medium power levels where the envelope supply waveform is de-toughed, the MMIC PA is operating linearly with a small amount of gain expansion. The nonlinearity in AM-PM characteristics under ET was observed to follow a quadratic dependence with a small phase lead at the lower power levels and a phase lag at higher power levels ( $\sim 7.5^\circ$  phase variation under ET compared to  $\sim 20^\circ$  phase variation under constant bias). In addition, compared to the fixed drain bias operation, a

modest amount of memory effects was seen from the spread in the plots (spread of  $10^\circ$ ), due to the drain modulator. The EVM was measured to be 3.5% and the lower and upper ACPR at 20 MHz offset were -24.87 dBc and -24.06 dBc, respectively. The lower in-band nonlinearity in ET can be attributed to the softer compression at high power levels seen in the AM-AM plot in ET since the MMIC PA was maintained under a constant compression as the drain supply was varied; while under fixed drain bias, the MMIC PA exhibits strong compression.

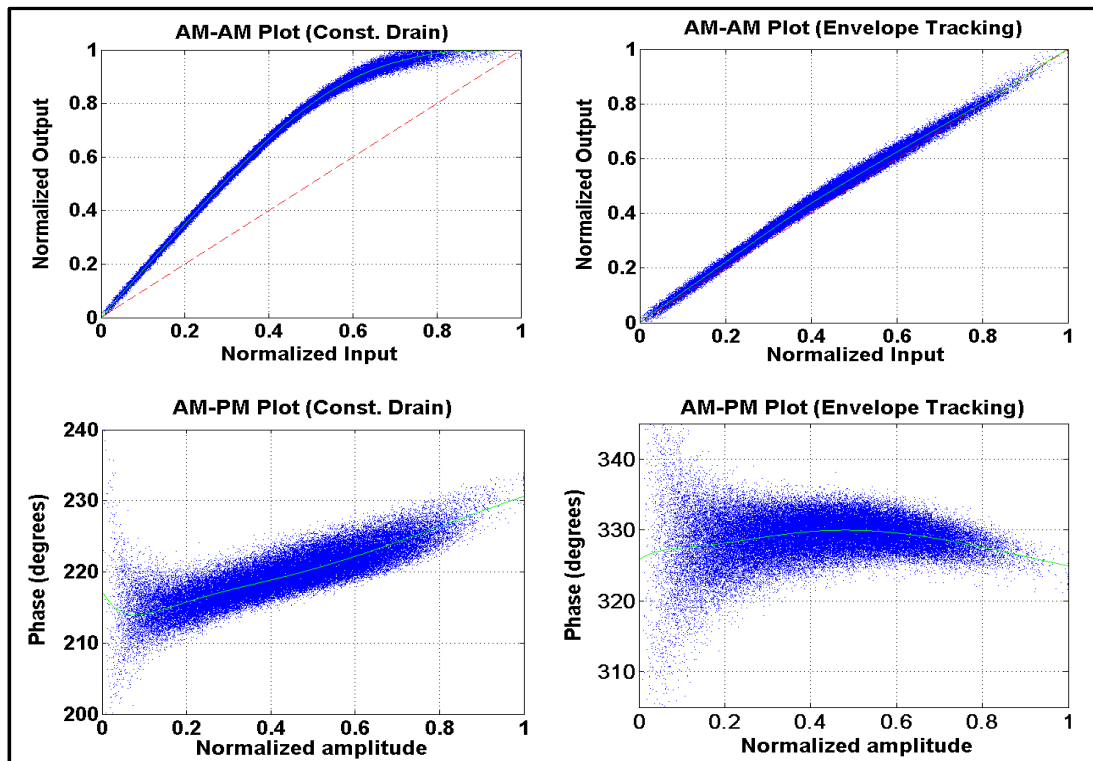


Figure 2.29: AM-AM and AM-PM characteristics before digital pre-distortion under both constant drain and envelope tracking conditions.

Digital pre-distortion (DPD) was applied to linearize the MMIC PA. The pre-distorted input was generated in digital baseband based on the down-converted, sampled, distorted output. Figure 2.30 shows output power spectrum before DPD, after

memoryless DPD, and after memory compensated DPD. After memoryless DPD (2.9% EVM), gain compression was corrected for and the output of the MMIC PA follows a linear behavior. However, a small amount of memory effect was observed, represented by the uneven skirts in the spectral response. After memory compensated DPD (2.0% EVM), using an algorithm described in [2], the amount of spread is reduced; hence, the memory effects were lowered and -40 dBc ACPR at 20 MHz offset was achieved.

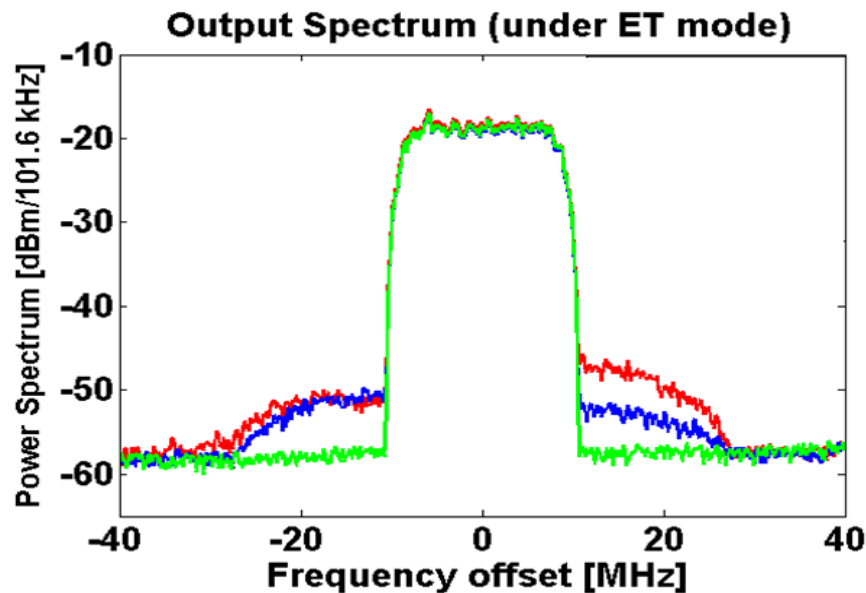


Figure 2.30: Output power spectrum before digital pre-distortion (red), after memoryless DPD (blue), and after memory compensation (green).

## 2.5 Summary

In this chapter, the overall envelope tracking power amplifier architecture was discussed. The overall efficiency is dependent on the efficiencies of both the dynamic supply modulator and the RF power amplifier efficiency. Loss mechanism in the modulator were discussed. In addition, RF PA performance under envelope tracking based on constant supply measurements was analyzed. A broadband test-bench for

evaluating envelope tracking power amplifiers as well as linearization techniques was implemented. The system has a tunable bandwidth from 100 MHz to 3.5 GHz with data vector patterns for up to 220 samples ( $\sim 5$  us) in depth and utilizes two 210-MSps 14-bit DACs and one 12-bit ADC with 100 MHz of pre-distortion bandwidth. In order to achieve flat spectral response over the entire bandwidth of the test-bench, a pre-equalization calibration filter was implemented. Measurement results demonstrated an improvement from 8% EVM to 1% EVM with a 40 MHz signal as a result of utilizing a pre-equalization FIR filter. To demonstrate the test-bench ability to perform envelope tracking over a wide range of carrier frequencies, measurements on ETPAs from UHF to mm-wave frequencies were performed.

One of the advantages of using the envelope tracking technique for high efficiency broadband power amplifiers is that, in concept, envelope tracking is not theoretically sensitive to the carrier frequency and can be applied over a broad range of carrier frequencies due to the fact that the envelope of the RF signal remains the same as the carrier is changed. To demonstrate this, using the same modulator design, high efficiency has been demonstrated at UHF, S-band, and Q-band.

At UHF, better than 63% drain efficiency was measured at 85W output power using a single push-pull amplifier. In addition, the implementation of a dual modulator approach for extremely high output powers was shown to provide better than 60% efficiency at 150 W. At the 700 MHz band, a GaN envelope tracking power amplifier was presented, demonstrating high record average efficiency of  $\sim 70\%$  (while meeting linearity specifications under the excitation of a WCDMA signal) with an average output power of 28.6 W and a gain of 13.5 dB, thus illustrating the potential of GaN FETs, in

combination with an dynamic modulator, for next generation LTE power amplifiers. For the 2140 MHz range, high efficiencies of greater than 50% was demonstrated for the standard 3.5-dB PAPR WCDMA signal and greater than 45% for the ‘notched’ SA-WCDMA MUOS signal under its worst case scenario of 6.5-dB PAPR with a 1.2 MHz notch. Measurement results have demonstrated that the system can be designed to satisfy the stringent MUOS requirements without the use of digital pre-distortion with high margins. In addition, from observing the excellent linearity performance after applying DPD, a design space exists such that the PA can be placed into even deeper compression for high efficiency performance while allowing DPD to compensate for its linearity. The application of ET to millimeter wave power amplifiers for efficiency enhancement was also demonstrated. An increase of more than 5.7 times in MMIC PA efficiency under ET, when compared to a fixed drain bias, was measured for a 20-MHz 7.6-dB PAPR 64-QAM signal after DPD. These results indicate that ET offers a promising solution for the design of high efficiency power amplifiers in the millimeter-wave regime.

## **2.6 Acknowledgments**

The author is very grateful to MaXentric Technologies and Nokia Siemens Network for the contributions to the development of the broadband power amplifier test-bench and QuinStar Technologies, RF Micro Devices, Freescale and Nitronex for the power amplifier fixtures, without which this work would not have been possible. The author also thank to Donald Kimball, Paul Theilmann, Chin Hsia, Young-pyo Hong,

James Schellenberg, and Professor Peter Asbeck for their valuable collaborations, discussions and suggestions.

Some of the materials in Chapter 2 are as they appear in “A High Efficiency 780 MHz GaN Envelope Tracking Power Amplifier”, Jonmei J. Yan, Paul Theilmann, and Donald F. Kimball, published in IEEE Compound Semiconductor Integrated Circuit Symposium 2012, in “Efficiency Enhancement of mm-Wave Power Amplifiers Using Envelope Tracking”, Jonmei J. Yan, Calogero D. Presti, Donald F. Kimball, Young-pyo Hong, Chin Hsai, Peter M. Asbeck, and James Schellenberg, published in IEEE Microwave and Wireless Components Letters, Vol. 21 No. 3, and in “High-efficiency, high-linearity envelope tracking power amplifier for mobile UHF applications”, Jonmei J. Yan, Donald F. Kimball, Chin Hsia, Hsuan-yu Pan, Scott Ricketts, and Houman Ghajari, published in IEEE MILCOM 2010. The contributions from the co-authors are appreciated. The author of this dissertation was the primary investigator and primary author for these publications.



# **Chapter 3**

## **Envelope Tracking Power Amplifiers Under Average Power Back-off**

### **3.1 Introduction**

As a result of the need for spectral efficiency, modern communication systems use signals with high peak-to-average power ratio (PAPR) resulting in average efficiency degradation in conventional constant supply power amplifiers. Efficiency enhancement techniques, such as the Doherty power amplifier [11]-[12] and envelope tracking power amplifier [13]-[14], have been demonstrated to improve efficiency in the presence of these high PAPR signals. In the previous chapter, the performance of envelope tracking power amplifiers at maximum average power was discussed in more depth. However, in practical communication systems, the average power transmitted the base-station can fluctuate, as a result of the varying number of users and data transmission demands occurring throughout different times of the day or seasonally. For example, shown in

Figure 3.1 is a representative loading profile. During the nighttime, the power transmitted can be backed-off by 8.55 dB from its peak operation power for this specific profile. Since pilot channels of a base-station use 5-10% of the base-station maximum power, the power transmitted can fluctuate by as much as 10 dB. As a result, the power amplifier may not always be operating at the maximum average output power, where the average efficiency is generally specified. Consequently, opportunities for system energy savings arise from the ability to back-off on the average output power while maintaining high efficiency under these power varying conditions. Shown in Figure 3.2 is the efficiency performance as a function of instantaneous output power for various power amplifier architectures. As the average output power is backed-off, significant efficiency degradation can be seen in the other architectures, particularly the constant bias PAs. On the other hand, envelope tracking offers much less efficiency degradation compared to other architectures with the same peak efficiency, making it a promising candidate for average back-off operation.

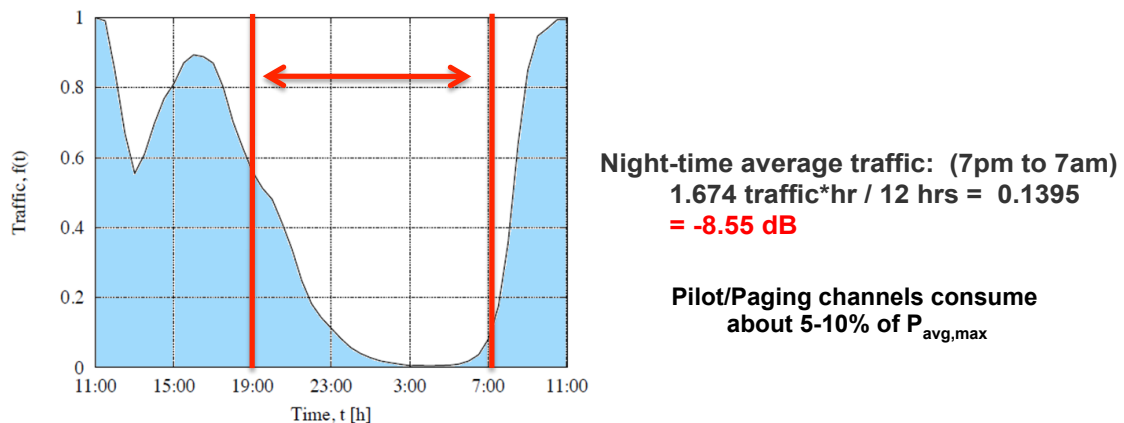


Figure 3.1: Normalized traffic profile as a function of time over a 24-hour period.

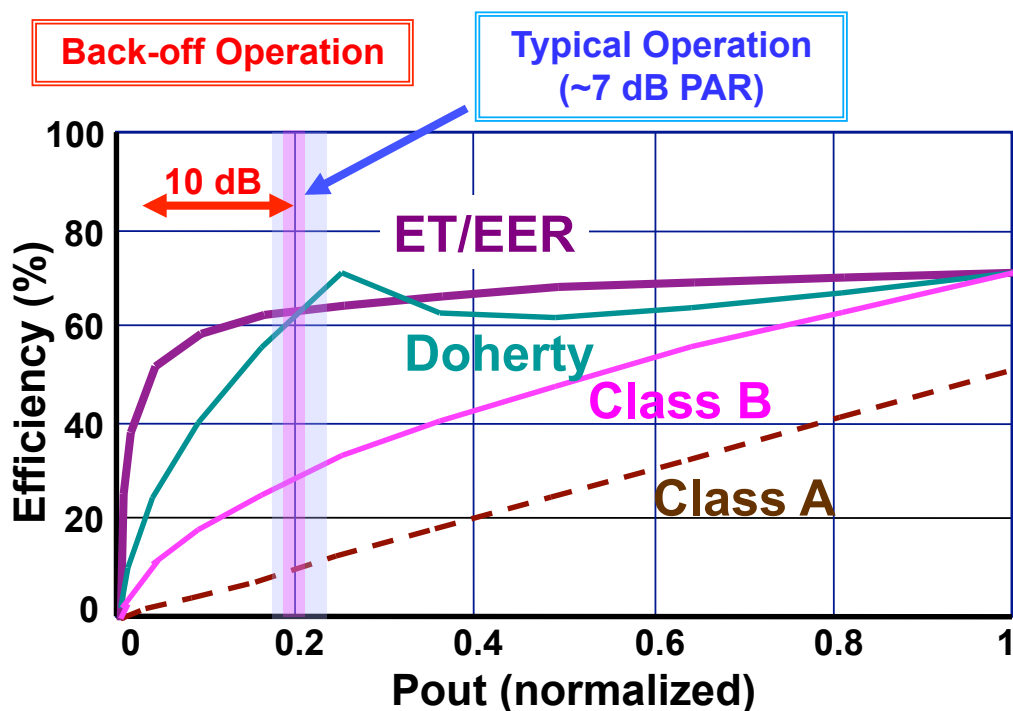


Figure 3.2: Efficiency performance of power amplifiers as a function of output power.

In this chapter, the performance of envelope tracking power amplifiers under average power back-off will be analyzed and compared with measured results. In order to maintain envelope tracking operation, the dynamic supply and the RF signal are simultaneously backed-off in power to allow the power amplifier to maintain operation in saturation at most times where the efficiency is highest for that power level. Under envelope tracking, less than a factor of 2 in efficiency reduction was achieved at 10 dB average power back-off. In addition, long-term efficiencies of Class B, Doherty, and envelope tracking power amplifiers are estimated and compared using Monte-Carlo simulations based on a projected time-varying power profile. For the specific power profile investigated, ET power amplifiers demonstrated more than 40% improvement in long-term efficiency (averaged over a period of more than 24 hours) as compared to Doherty amplifiers with the same peak efficiency.

## 3.2 Envelope Tracking Operation in Back-off

Envelope tracking employs a dynamic power supply that tracks the envelope of the RF signal. High efficiency for high PAPR signals can be achieved as a result of keeping the power amplifier close to saturation at most times where the efficiency is highest. Under average power back-off operation, in order to keep the RF power amplifier close to saturation and maintain envelope tracking operation, the RF input and the envelope dynamic supply were scaled simultaneously as shown in the block diagram in Figure 3.3. The signal power levels were adjusted for back-off operation in the digital domain.

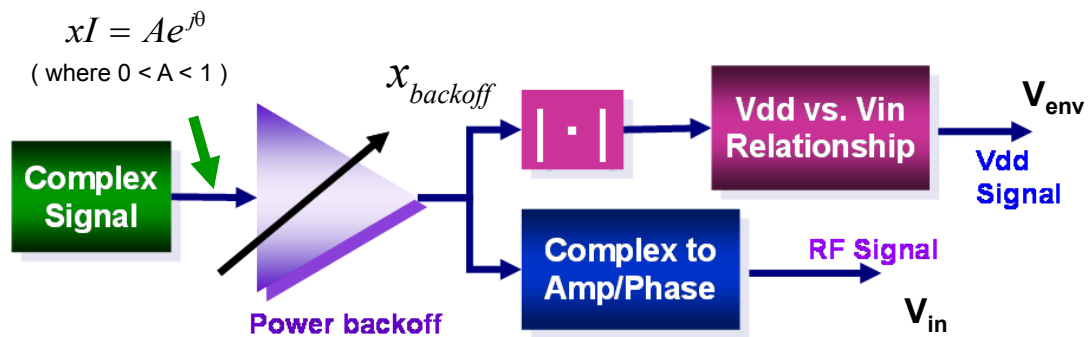


Figure 3.3: Back-off implementation algorithm.

As described in Chapter 2, the supply envelope is “de-trouged” with respect to the true envelope of the RF signal in order to prevent gain collapse and minimize sensitivity to time misalignment between the two paths. Since this is still desirable under average power back-off, the ‘de-trouging’ relationship, normalized to the peak supply voltage at full average power, was maintained. As a result, the envelope tracking power amplifier is operated over a single supply trajectory as the output power is varied between full power and back-off. Figure 3.3 illustrates the algorithmic implementation of the

power back-off in the digital domain. The normalized complex signal in voltage  $\hat{x}_{input}$ , corresponding to full power operation, is backed-off by the desired amount, specified by the attenuation factor  $\alpha_{back-off}$  (ie. for -5 dB back-off,  $\alpha_{back-off} = -5$ ), giving the following expression of the backed-off input signal:

$$x_{back-off} = \hat{x}_{input} 10^{\frac{\alpha_{back-off}}{20}} \text{ where } \hat{x}_{input} = A \cdot e^{j\theta} \quad (3.1)$$

where  $x_{back-off}$  is the complex backed-off voltage signal.

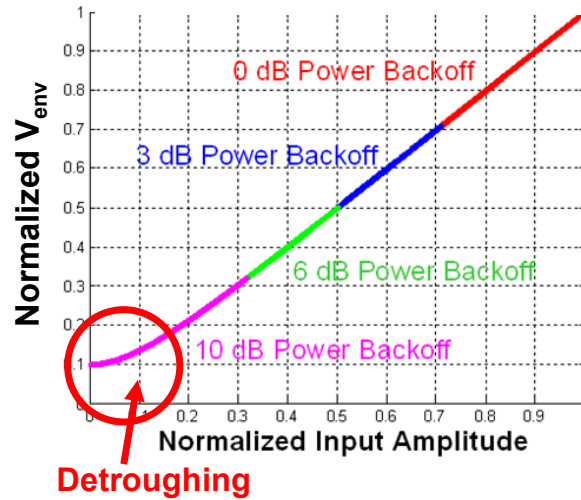


Figure 3.4: Normalized  $V_{env}$  versus normalized  $V_{in}$  at the different back-off levels.

The envelope voltage signal for the dynamic power supply is generated by massaging the magnitude of  $x_{back-off}$  through an envelope shaping (or “de-trounging”) function given by:

$$V_{env}(t) = V_{DD,max} \left( |x_{back-off}| + b \cdot e^{-\frac{|x_{back-off}|}{b}} \right), \quad (3.2)$$

where  $V_{DD,max}$  is the maximum supply voltage corresponding to operation at full average power. The fully modulated RF signal is up-converted to a digital IF, containing both the amplitude and phase components and is expressed as:

$$\begin{aligned}
 V_{in}(t) &= AP_{max} \cdot Re[x_{back-off}] \\
 &= AP_{max} \cdot Re \left[ \hat{x}_{input} 10^{\frac{\alpha_{back-off}}{20}} \right] \\
 &= AP_{max} \cdot Re \left[ |\hat{x}_{input}| \cdot 10^{\frac{\alpha_{back-off}}{20}} e^{j\theta} \right] \\
 &= AP_{max} \cdot \left[ A \cdot 10^{\frac{\alpha_{back-off}}{20}} \cos(\omega_{IF}t + \theta) \right].
 \end{aligned}
 \tag{3.3}$$

Figure 3.4 illustrates the normalized supply voltage as a function of the true envelope of the normalized input signal ( $V_{env}$  vs.  $V_{in}$ ) at different power back-off levels. The supply voltage ( $V_{env}$ ) was chosen to track linearly with the envelope of the RF input signal. At low input voltage values, however,  $V_{env}$  was “de-troughed” in order to avoid gain collapse in the RFPA, as well as reduce sensitivity to time misalignment. Figure 3.5 illustrates the time domain representation of the envelope supply voltage as the average output power is backed-off at various back-off factors. As shown, the troughs of the supply envelope remain the same as a result of maintaining the “de-troughing” relationship.

Calibration between the digital bits in the MALAB code and the actual analog values is crucial to ensure we operate the ETPA efficiently as the average power is backed-off. Based on the DAC calibration and envelope amplifier gain, the expected values for the maximum, minimum, mean and RMS (root-mean-square) of the envelope

signal can be calculated from the digital bits in MATLAB. These values are compared to experimental results where the corresponding values are measured at the output of the supply modulator using an oscilloscope, as shown in the block diagram in Figure 3.6. Figure 3.7 plots the corresponding dynamic supply voltages as a function of average power back-off for both the calculated and measured cases. Similarly for the RF path, a power meter was used to measure the average output power at the various power back-off values, as dictated in MATLAB, to validate this implementation.

Table 3.1 tabulates the measured power amplifier output power at different back-off levels, confirming the accuracy of the digital power control and system consistency. In this work, we consider the power amplifier performance at 0, -3, -6, and -10 dB average power back-off.

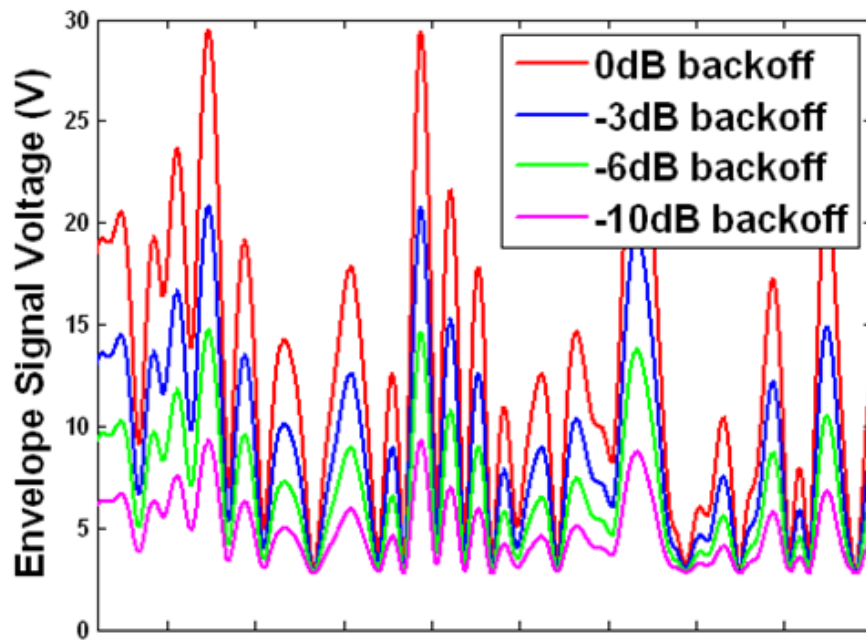


Figure 3.5: Supply envelope voltage for different back-off power levels as a function of time, while maintaining the ET de-toughing relationship

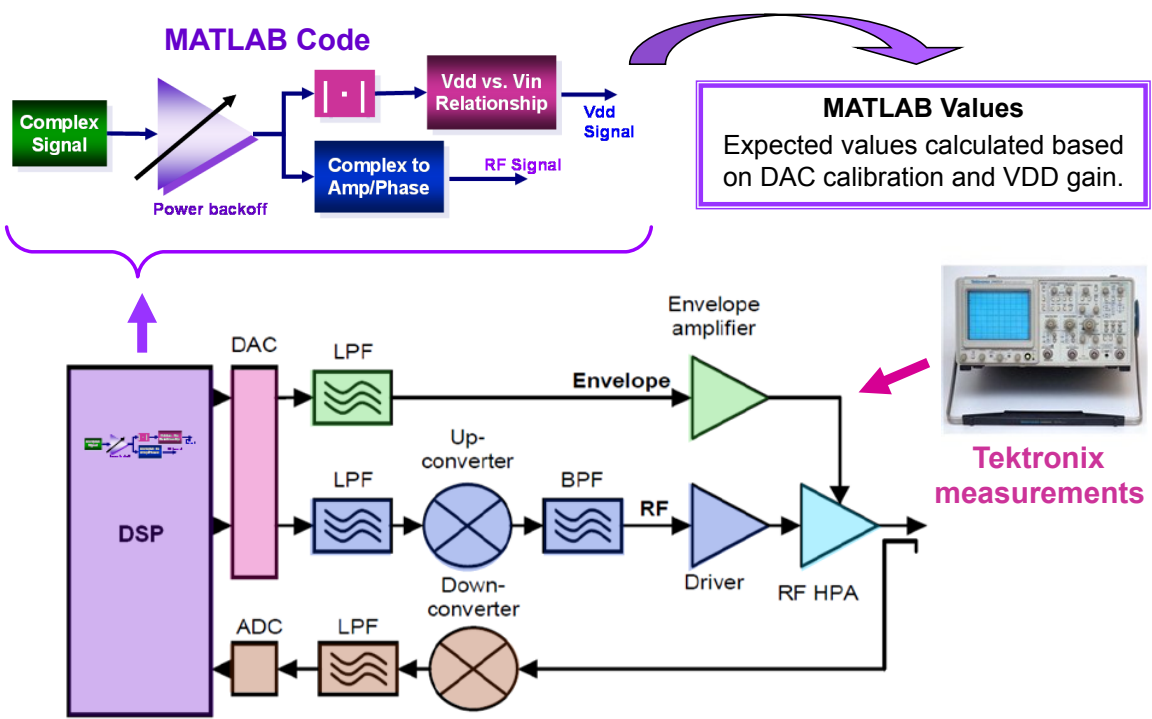


Figure 3.6: Measurement setup for calibration for power back-off

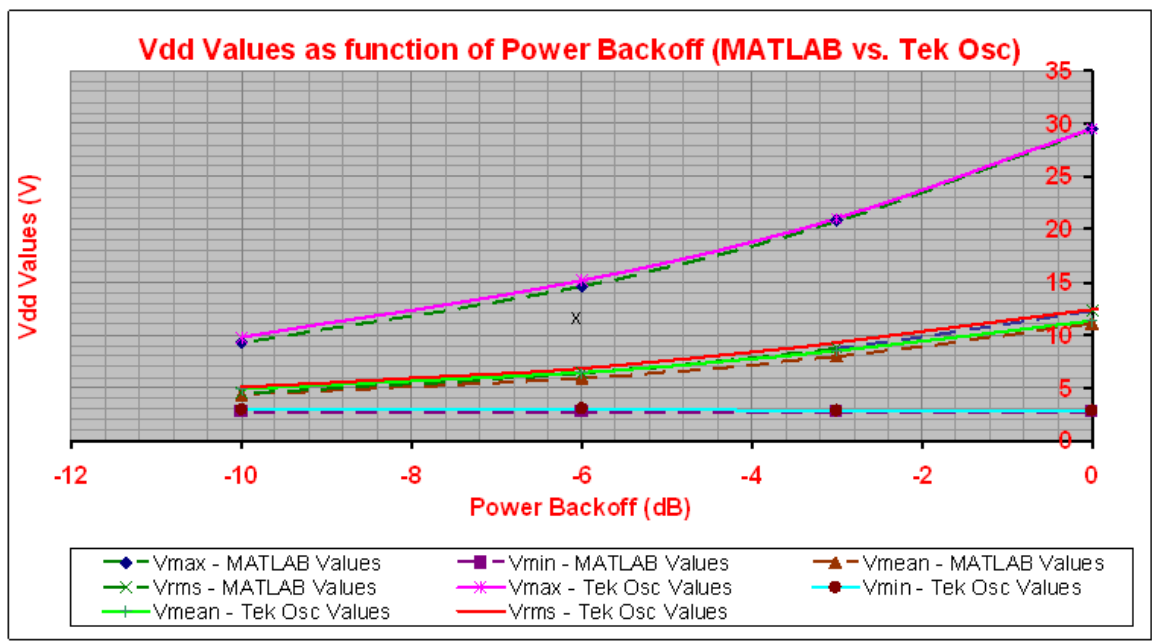


Figure 3.7: Measured versus calculated envelope supply voltages



Table 3.1: Measured power back-off at the output of the RF PA demonstrates the precision of the digital control, performed digitally in DSP.

Envelope Tracking Power Control		
Output Power (W)	Expt Backoff (dB)	Ideal Backoff (dB)
19.49	0.00	0
9.9	-2.94	-3
4.99	-5.92	-6
1.95	-10.00	-10

### 3.3 Average Power Efficiency in Back-off

Efficiency measurements were made on the ETPA under back-off conditions. At full power (35W), the measured ET-HPA efficiency was 59.7%. Backing off the average output power by -3, -6, and -10dB, the ET-HPA efficiency was measured to be 52.6%, 45%, and 35.4%, respectively. In the following we consider the factors influencing this efficiency, and we compare the results with the performance expected from other amplifier configurations. The measured results along with the comparisons discussed below are shown in Figure 3.8.

#### 3.3.1 Power Amplifier Efficiency at Various Output Powers

Under envelope tracking operation, the overall ET system efficiency can be defined as the product of the RF amplifier efficiency ( $\eta_{RF}$ ) and the supply modulator efficiency ( $\eta_{Env}$ ), expressed as:

$$\eta_{ET} = \frac{P_{out}}{P_{DC}} = \frac{P_{out}}{P_{env}} * \frac{P_{env}}{P_{DC}} = \eta_{RF} * \eta_{Env}, \quad (3.4)$$

where  $P_{out}$  is the RF output power,  $P_{env}$  is the modulated envelope supply power, and  $P_{DC}$  is the DC power into the supply modulator.

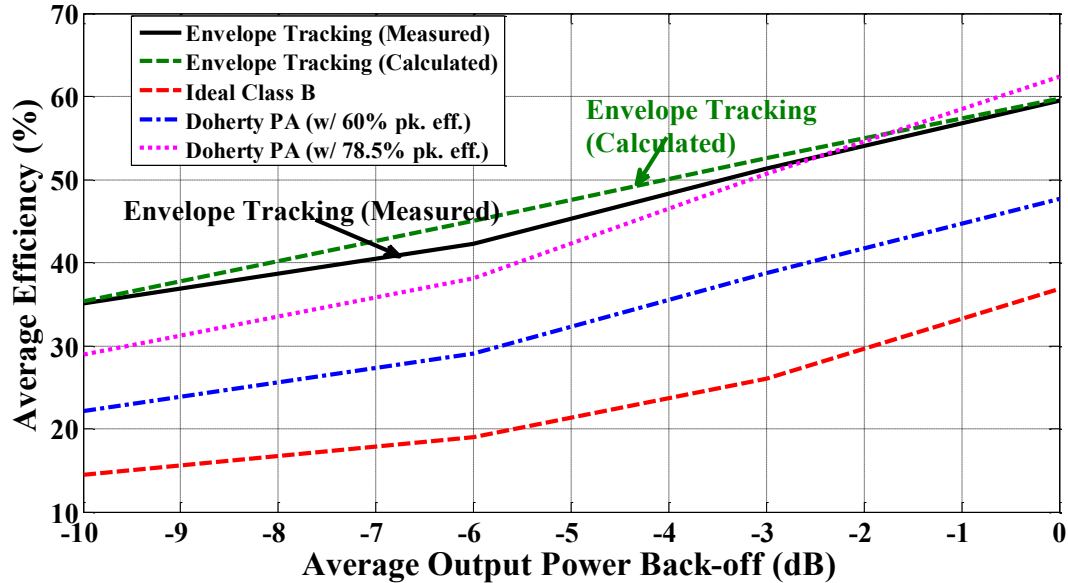


Figure 3.8: Average efficiency using a single carrier 7.54 dB PAPR WCDMA signal as the average output power was backed-off up to -10 dB for an ideal Class B, ideal Doherty (with 78.5% peak eff.), Doherty (with 60% peak eff.) and measured ET results.

The envelope tracking (ET) system was implemented using a GaAs High Voltage HBT as the RF power amplifier. Measurements were done with a 7.54 dB PAPR WCDMA input signal centered at 2.14 GHz. The GaAs HVHBT was operated at a peak envelope voltage of 29.5V. The "instantaneous collector efficiency" of the GaAs HVHBT was measured to be 85% over a 12.5 dB output power range before the efficiency begins to roll off. Here, the "instantaneous efficiency" corresponds to the expected result for single tone signals as the output varies at the modulation rate between the different power levels. The supply modulator efficiency was approximately 70% in our experiments. The instantaneous output power and instantaneous efficiency of the ET power amplifier can be approximately analyzed by the quasi-static relationship between

the instantaneous input power and instantaneous supply voltage, using the simplifying assumption that  $\eta_{Env}$  is constant. Figure 3.9 illustrates the instantaneous efficiency of the ET amplifier as a function of the instantaneous output power. For comparison, the results expected for an ideal Class B, ideal Doherty amplifier with a peak efficiency of 78.5%, and a Doherty amplifier with a peak efficiency of 60% are shown. Additional architectures (such as Doherty amplifiers or envelope tracking amplifiers with adjustable power supply voltages) are possible, but are not considered here, for simplicity.

The instantaneous efficiency of a Class B power amplifier with an ideal maximum efficiency of 78.5%, expressed as a function of RF output power ( $P_{RF}$ ), is given by [4]:

$$\eta_{D,classB} = \frac{\pi}{4} \sqrt{\frac{P_{RF}}{P_{RF,max}}} \quad (3.5)$$

where  $P_{RF,max}$  is the maximum output power of the power amplifier. Also shown is the instantaneous efficiency of a Doherty amplifier (assumed to be a 2-way symmetric Doherty amplifier, in which the peak efficiency is achieved at -6 dB back-off and at full power), which can be expressed as [4]:

$$\eta_{D,Doherty} = \begin{cases} \eta_{Doherty,max} \sqrt{\frac{P_{RF}}{\frac{P_{RF,max}}{4}}}, & P_{RF} \leq \frac{P_{RF,max}}{4} \\ \eta_{Doherty,max} \frac{2 \cdot \frac{P_{RF,max}}{P_{RF}}}{3 \sqrt{\frac{P_{RF,max}}{P_{RF}} - 1}}, & P_{RF} \geq \frac{P_{RF,max}}{4} \end{cases}, \quad (3.6)$$

where  $\eta_{Doherty,max}$  is the peak efficiency of the Doherty amplifier. Since experimental Doherty amplifiers do not reach the ideal efficiency, we also show a curve that is scaled to correspond to a 60% peak efficiency (still greater than many reported experimental results [11]-[12]).

### 3.3.2 Average Efficiency with Modulated Signals

The average output power using a modulated signal can be determined by averaging the instantaneous output power ( $P_{out}$ ) weighted by the probability distribution function (PDF) of the signal  $p(P_{out})$ , as given by:

$$\langle P_{out} \rangle = \int P_{out} * p(P_{out}) dP_{out} \quad (3.7)$$

The average DC power can be calculated as the weighted average of the instantaneous output power divided by the instantaneous RFPA efficiency, expressed as:

$$\langle P_{out} \rangle = \int \frac{P_{out}}{\eta_{RF}(P_{out})} * p(P_{out}) dP_{out} \quad (3.8)$$

where  $\eta_{RF}(P_{out})$  is the "instantaneous" RFPA efficiency. Hence, the average efficiency of the RF amplifier under the excitation of a modulated signal at a particular average output power can be calculated as:

$$\langle \eta_{ET} \rangle = \frac{\langle P_{out} \rangle}{\langle P_{DC} \rangle} \quad (3.9)$$

In the calculations that follow, the probability density functions of a 7.54 dB PAPR WCDMA signal under various back-off conditions were used. Figure 3.9 shows the signal PDFs for full power, -3dB, -6dB and -10dB back-off, as determined by calculation in MATLAB. Integrations, according to equations (6)-(8), of the instantaneous efficiencies of the power amplifiers shown in Figure 3.9 was carried out with the PDF of the modulated signal at various power back-offs to determine a corresponding average efficiency curve as a function of average output power for the different power amplifiers. Results are shown in Figure 3.8. Calculated values of the ET power amplifier efficiency were in very good agreement with the measurements, as shown in Figure 3.8. At full power (35W), the measured ET system efficiency was 59.7%. As the average output power of the WCDMA signal was backed-off to -3, -6, and -10dB, the ET system efficiency was measured to be 52.6%, 45%, and 35.4%, respectively.

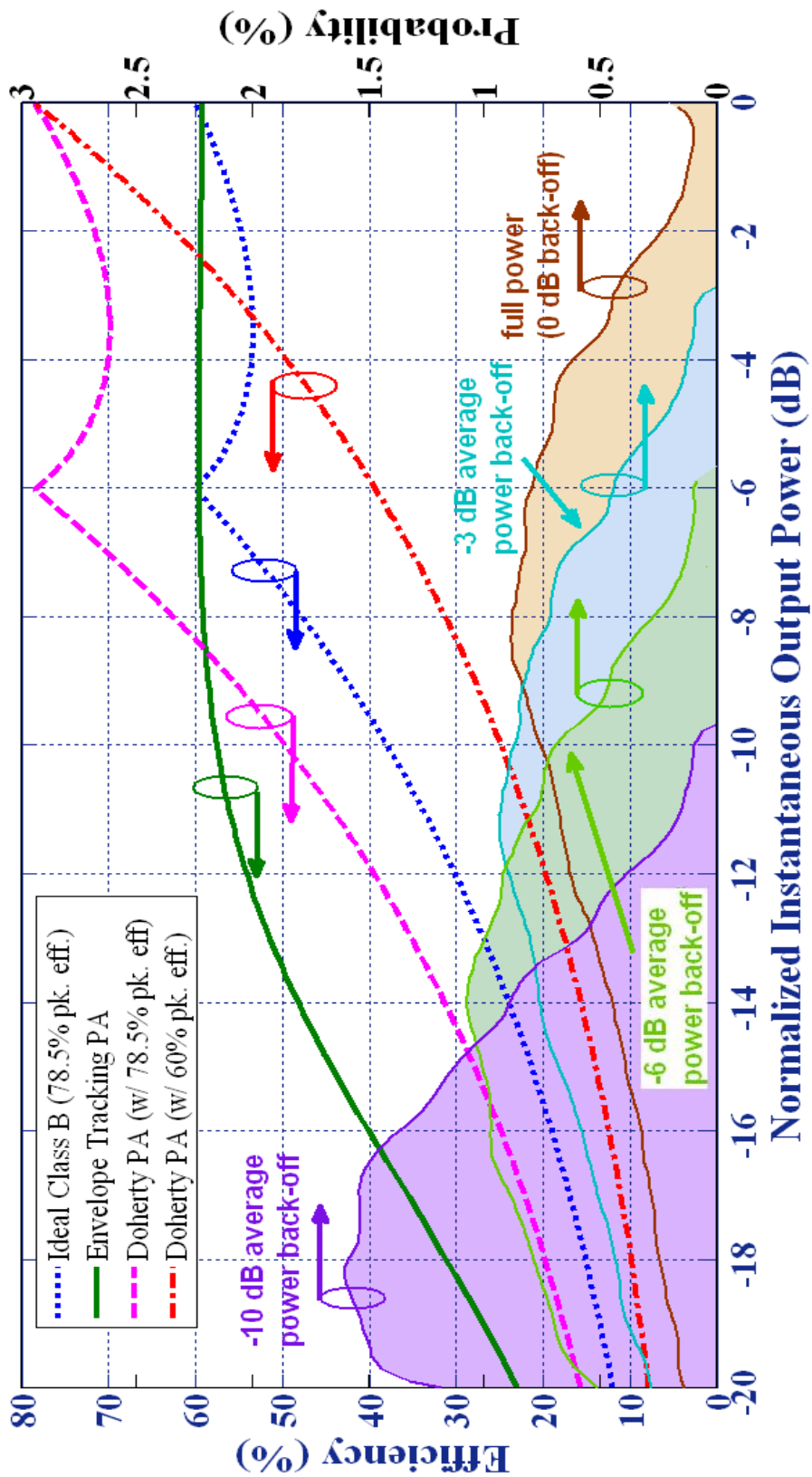


Figure 3.9: Left axis: "Instantaneous" efficiency vs. output power of measured ET PA, normalized to peak power. Right axis: PDF of a 7.54 dB single carrier WCDMA signal at full power, -3 dB, -6 dB, and -10 dB average power back-off.

### 3.4 Scalable DPD Model for Average Power Back-off

Memoryless digital pre-distortion (DPD) was carried out by collecting the output data via the down-converter chain, synchronizing the output data with the corresponding input, and fitting the data with an appropriate polynomial. The pre-distorted signal was generated from the fitted polynomial to provide a linear input-output relationship. In this work, we studied how the linearity requirements change under power back-off operation, and developed a simple DPD model capable of being used at the different back-offs.

Figure 3.10 illustrates the relationship between the output power, input voltage, and supply voltage for the RFPA. The output power of a RFPA is a function of the input power and the supply voltage. In the case of the ET-HPA, where the supply voltage and the input voltage are strongly coupled by the expression given in (3.2), for a particular supply voltage relationship, the ET-HPA follows a single trajectory such that

$$P_{out} = f(x_{RF}, V_{DD}) = f[x_{RF}, g(|x_{RF}|)] \quad , \quad (3.10)$$

where  $x_{RF}$  is the RF input signal and  $V_{DD}$  is the supply voltage, as depicted by the solid blue line in Figure 3.10. This suggests that a single behavioral model can be extracted and scaled to generate the pre-distorted inputs for the other average power back-offs.

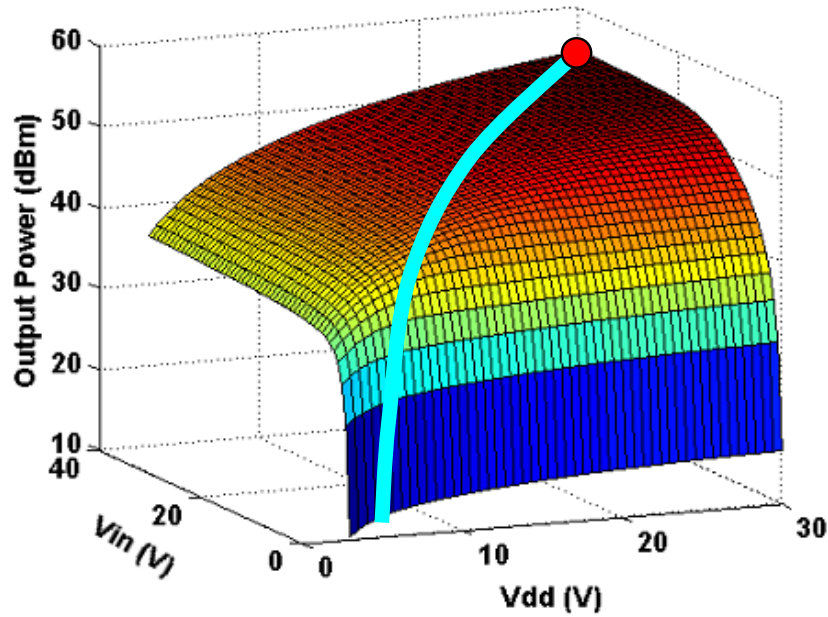


Figure 3.10: Relationship surface between output power, input voltage, and supply voltage of a RFPA. The ET-HPA follows a single trajectory as depicted by the blue line.

In order to perform DPD with up to 10 dB average power back-off, measurements at full power and 7 dB back-off, as depicted in Figure 3.11 were combined to develop the scalable look-up table (LUT). By combining these datasets, there is sufficient overlap to validate consistency while providing higher confidence in the LUT model in the low power regime, where relatively few points exist in the full power measurement, as depicted in Figure 3.12 by the PDF of the signal at full power and at 7 dB back-off. The AM-AM distortion was determined using a 16<sup>th</sup> order polynomial fit based on evenly-spaced amplitudes of 2000 points to model the gain expansion occurring at low input voltages that is characteristic of envelope tracking PAs. The AM-PM distortion was determined in a similar manner with a 4<sup>th</sup> order polynomial fit. Using this behavioral model, a signal with memory-less pre-distortion can be generated for various back-off levels without the need to regenerate a DPD model at each back-off level. Figure 3.13



illustrates the measured results at 0 dB and 7 dB back-off from which the behavioral model was extracted. A small amount of gain expansion and about 25 degrees of phase lead were observed before DPD. The overlap of the two sets of measurements demonstrates that the ET-HPA follows a single gain trajectory for which a scalable DPD model can be used.

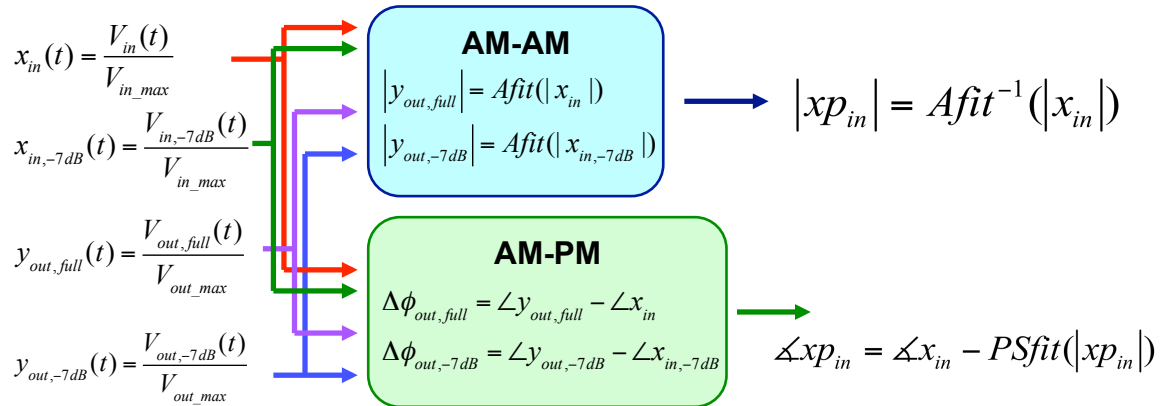


Figure 3.11: Implementation to determine the AM-AM and AM-PM characteristics by using two data sets (at full power and at -7 dB) concatenated together to generate a single LUT capable of scaling with average output power.

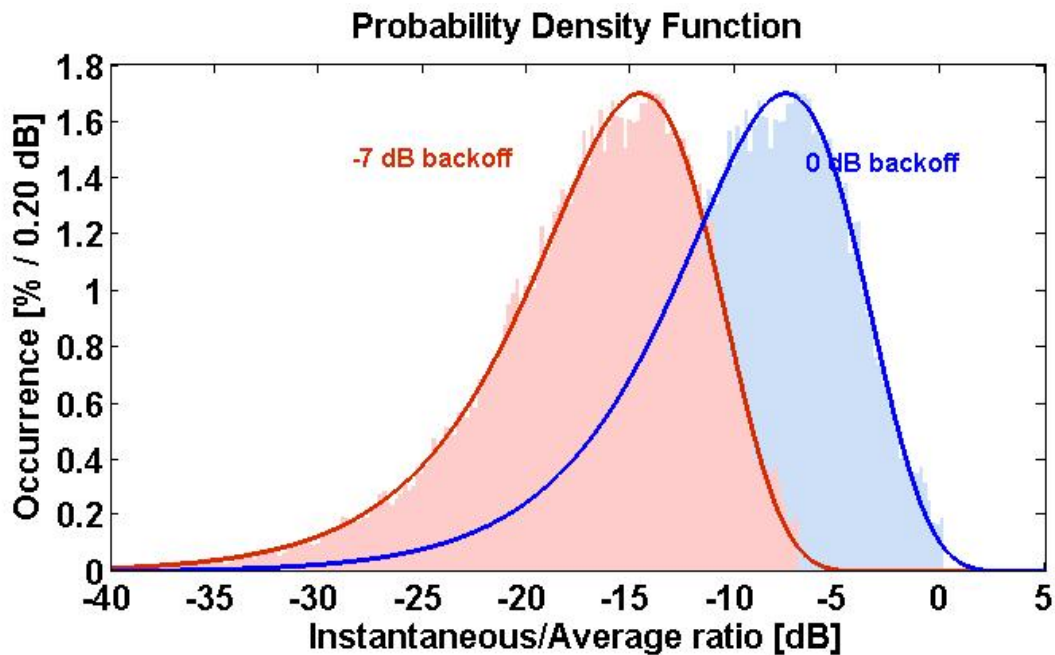


Figure 3.12: Probability density function of the modulated 7.54 dB PAPR WCDMA signal at 0 dB and at -7 dB back-off.

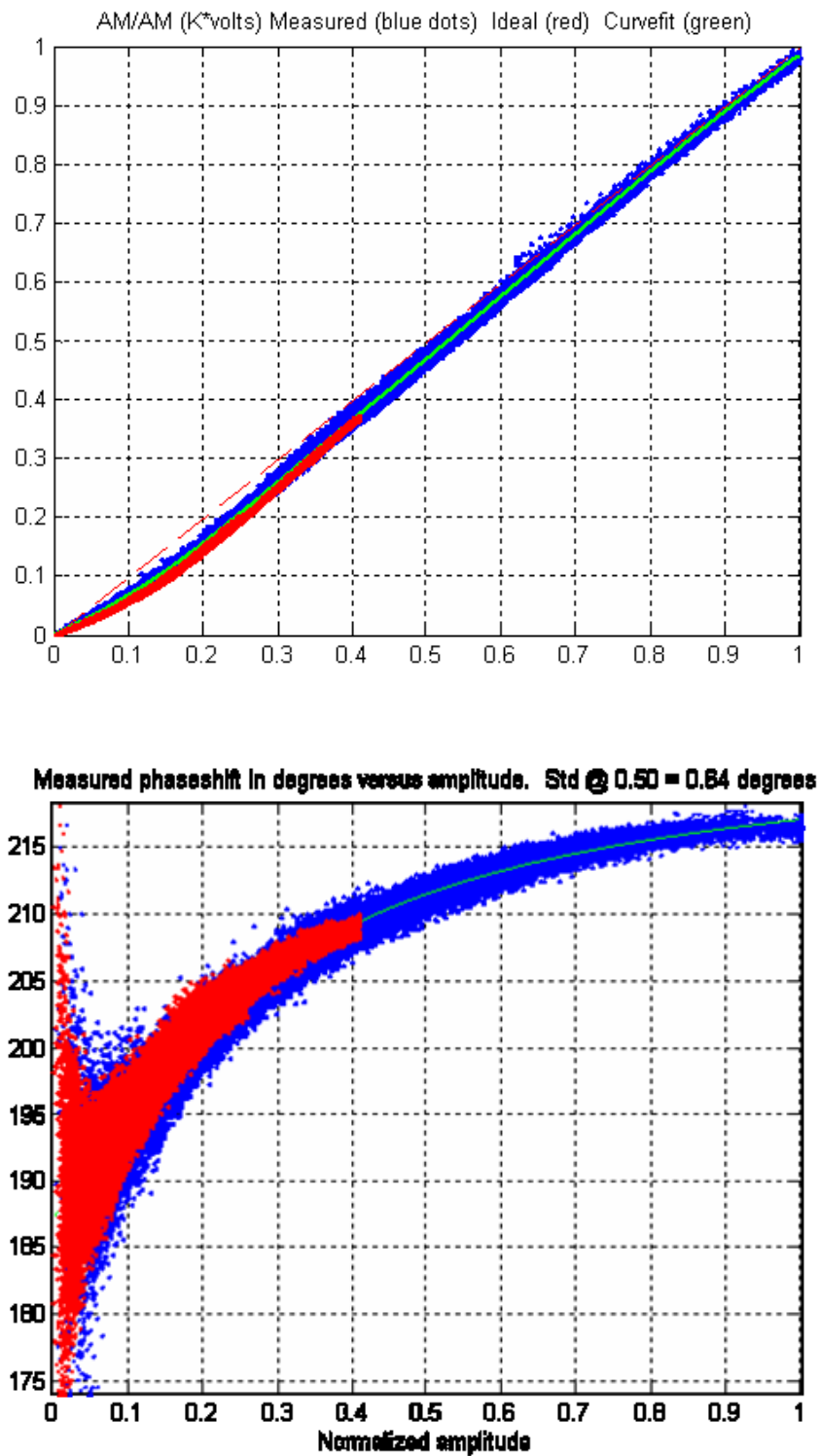


Figure 3.13: Normalized AM-AM (top) and AM-PM (bottom) measured at full power (blue) and at 7 dB back-off (red) used to generate a single scalable LUT.

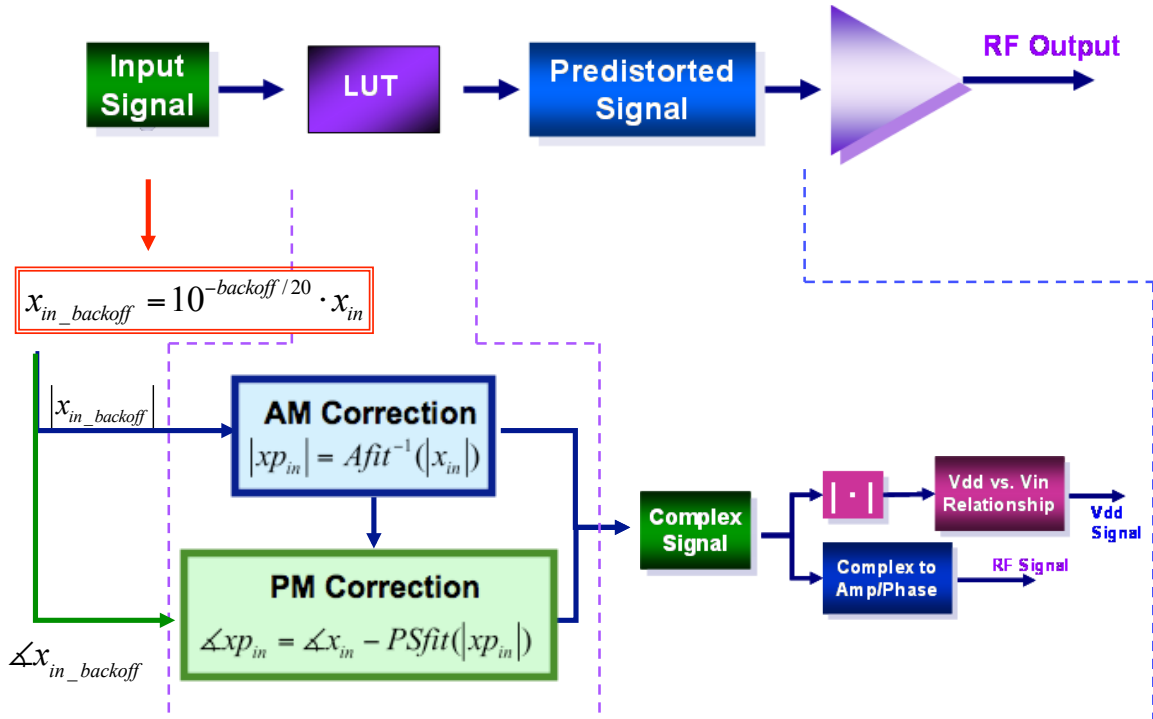


Figure 3.14: Implementation of the open loop pre-distorted signal for various power back-off levels.

To demonstrate linearization at back-off, two different power levels (2 dB and 9 dB back-off) were selected and the corresponding pre-distorted inputs were generated from the derived LUT, as shown in Figure 3.14. Figure 3.15 and Figure 3.16 shows the resulting AM-AM (amplitude-amplitude) and AM-PM (amplitude-phase) after DPD using the single scalable DPD model at 2 dB and 9 dB back-off, respectively. The linear behavior of the AM-AM and the flat response of the AM-PM at these various average power levels demonstrate that the GaAs HVHBT was successfully linearized using the single DPD model. In contrast, with a DPD model generated from only full average power data, successful linearization was achieved for only up to 3-4 dB average back-off, due to the lower accuracy in the DPD model at the lower powers. Table 3.2 summarizes the measured linearity at the different backed-off powers. The measured NRMSE was less than 2% over a 10 dB average power range and the ACPR (adjacent channel power

ratio) linearity specification of the WCDMA standard was satisfied. A small amount of history dependent memory effects were present in the ETPA, adding slightly to the spectral content; these can be observed by the spread in the AM-AM and AM-PM after memory-less DPD. Further reductions in ACPR could be done (if needed to provide greater margin relative to specifications) by including memory-related corrections.

Table 3.2: Summary of measured linearity results at various back-offs.

Power Back-off	NRMSE (%)	ACPR1 (dBc)	ACPR2 (dBc)
0 dB	2	-48.63	-51.69
-2 dB	1.88	-49.42	-51.8
-9 dB	1.93	-47.99	-52.67

## 3.5 Modeling of Long Term Envelope Tracking Power Amplifier Performance

The transmitted power from a base-station varies with time of day and seasonally, according to user requirements. The good performance of the ET amplifier in back-off can increase the long-term efficiency of a base-station, to an extent dependent on its usage profile. Such usage profiles are not available in the open literature. Here we develop an approximate model for the profile. The long term probability distribution for the base-station output power is estimated based on a known traffic profile.

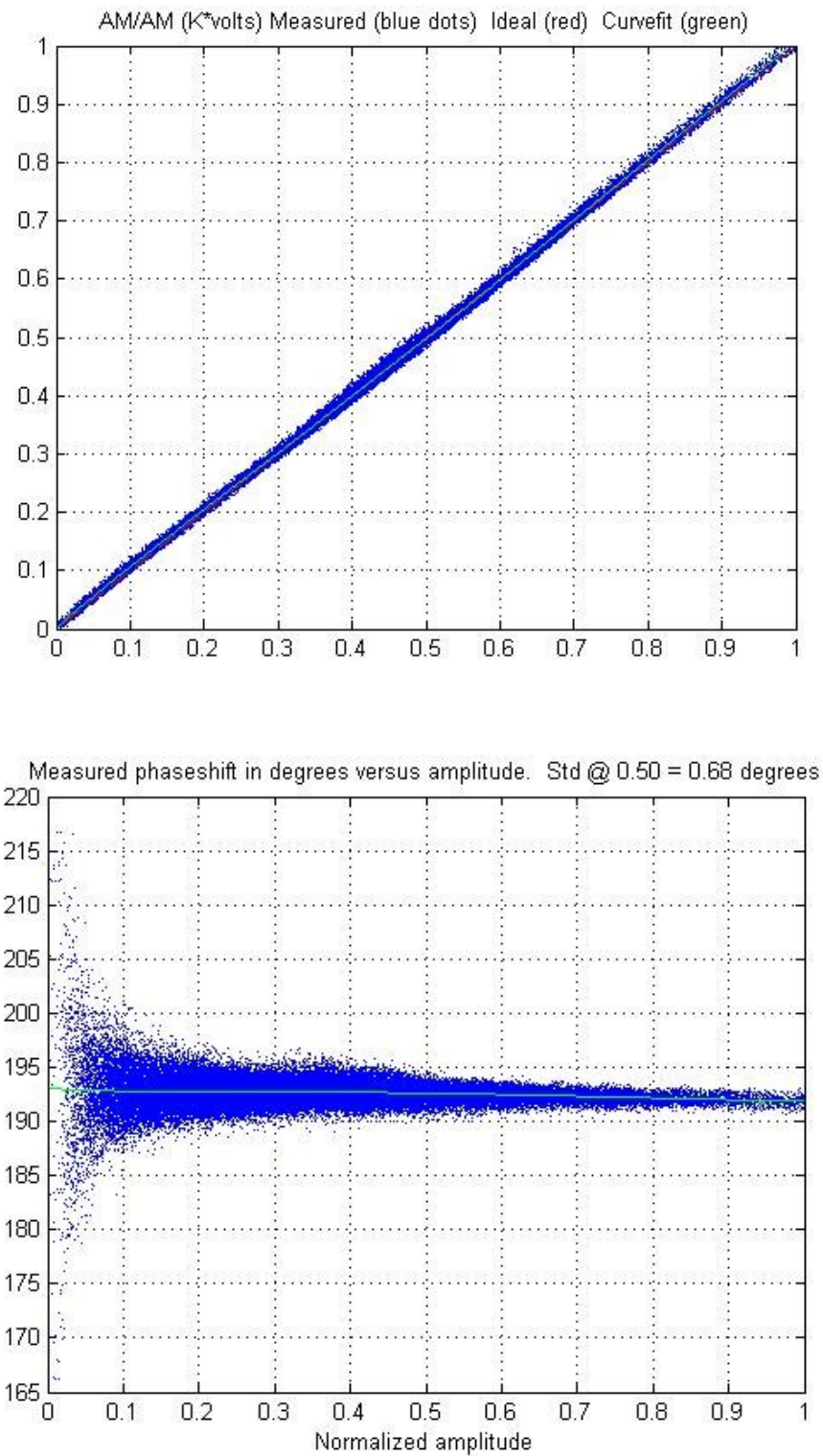


Figure 3.15: AM-AM (top) and AM-PM (bottom) at 2 dB back-off using the scalable open loop DPD.

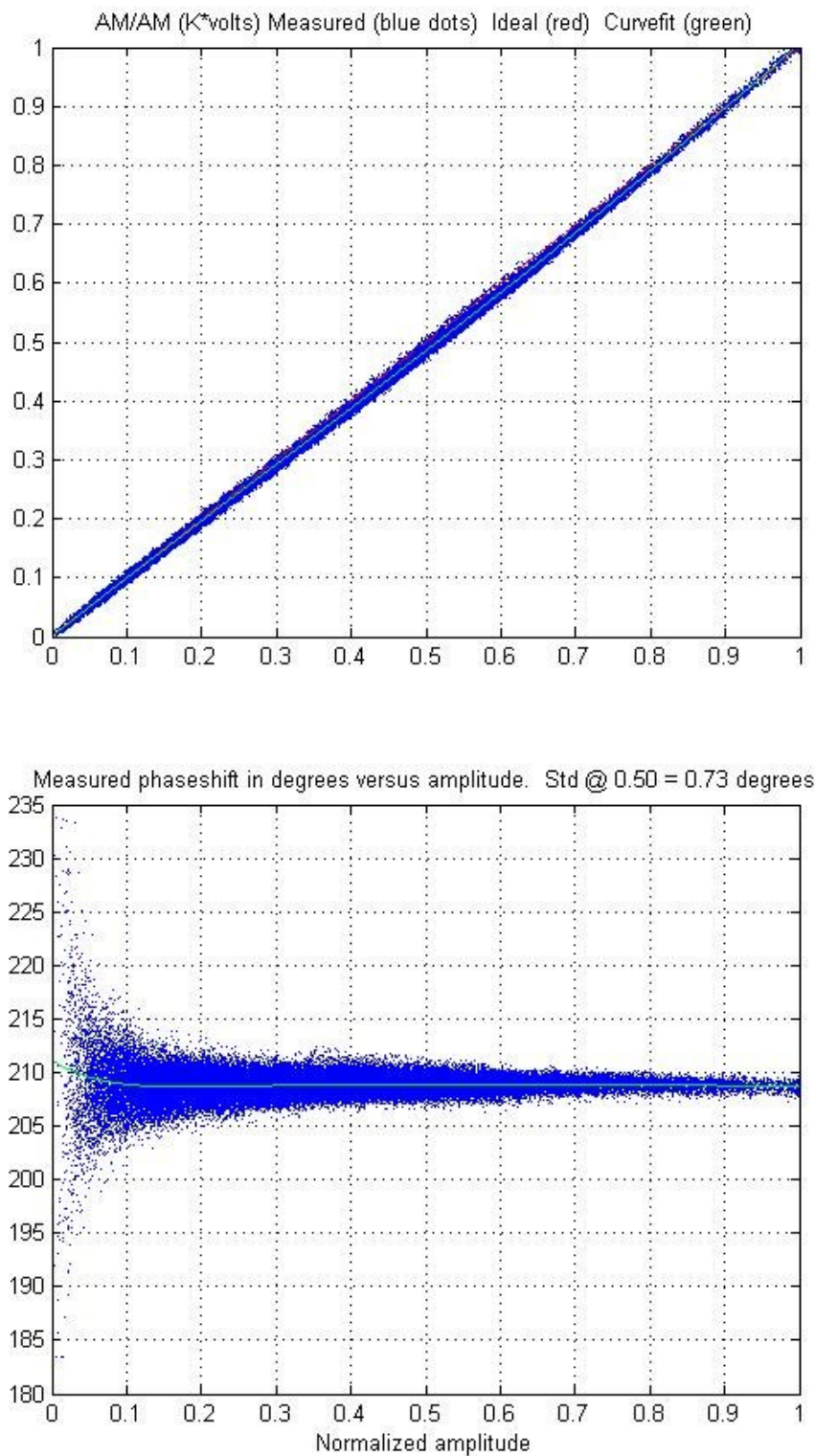


Figure 3.16: AM-AM (top) and AM-PM (bottom) at 9 dB back-off using the scalable open loop DPD.

### 3.5.1 Base-Station Average Output Power

The total transmitted power of a base-station ( $P_{BS}$ ) can be calculated as the sum of the overhead power for pilot, paging, and synchronization ( $P_{overhead}$ ) and the power transmitted to each user ( $P_{TX,n}$ ) in the cell. For  $n$  users, this leads to:

$$P_{BS} = P_{overhead} + \sum_n P_{TX,n} \quad (3.11)$$

In the calculations that follow, it is assumed that the power transmitted to each user is proportional (by a factor  $K$ ) to the power transmitted by each user back to the base-station. The user power typically fluctuates because of changing fading, path loss, shadowing, etc. In our simplified system model, the power transmitted to all the users in the cell is expressed as:

$$\sum_n P_{TX,n} = K \cdot \sum_n P_{user,n} \quad (3.12)$$

$K$  can be found in the limiting case where the transmit power is the greatest (the maximum number of users are present at the cell edge), giving:

$$K = \frac{P_{BS,max} - P_{overhead}}{N_{user,max} \cdot P_{user,max}} \quad (3.13)$$

The power transmitted by each mobile terminal can be estimated based on the long-term PDFs for the urban and suburban environments obtained from the CDG4 operational system performance test [15]. Further, a traffic profile can be used to

estimate the number of users in a cell site at any given time. Figure 3.17 shows the representative traffic profile assumed in this work (adapted from [16]). In general, this distribution may change as the usage mix changes from primarily voice to primarily data. The largest usage occurs during the day-time, with peak usage around 11am and a 2nd peak around 4pm. However, between 11pm and 7am, the usage is significantly reduced with a minimum around 4am. Within a cell in which the maximum number of users is 128, the PDF of the number of users at any given time, in 15 minute intervals is illustrated in Figure 3.18.

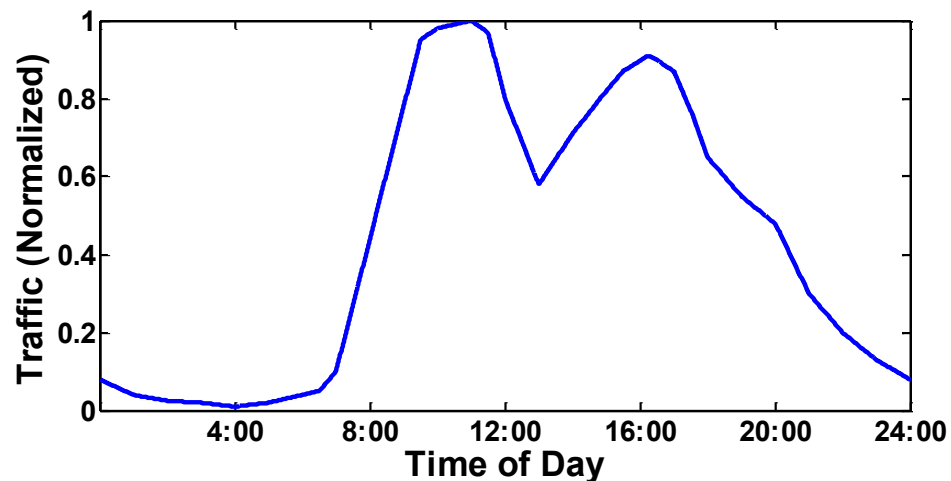


Figure 3.17: Normalized traffic as a function of the time in the day over 24 hours.

To determine the probability density function of a base-station average output power  $P_{BS}$ , Monte-Carlo simulations were performed based on the PDFs of the traffic profile and the CDG4 profiles. To provide suitable randomness, 100,000 trials were performed. The number of users present in the cell at any given time was generated using the acceptance-rejection method such that the random number of users generated  $X$  is bounded between



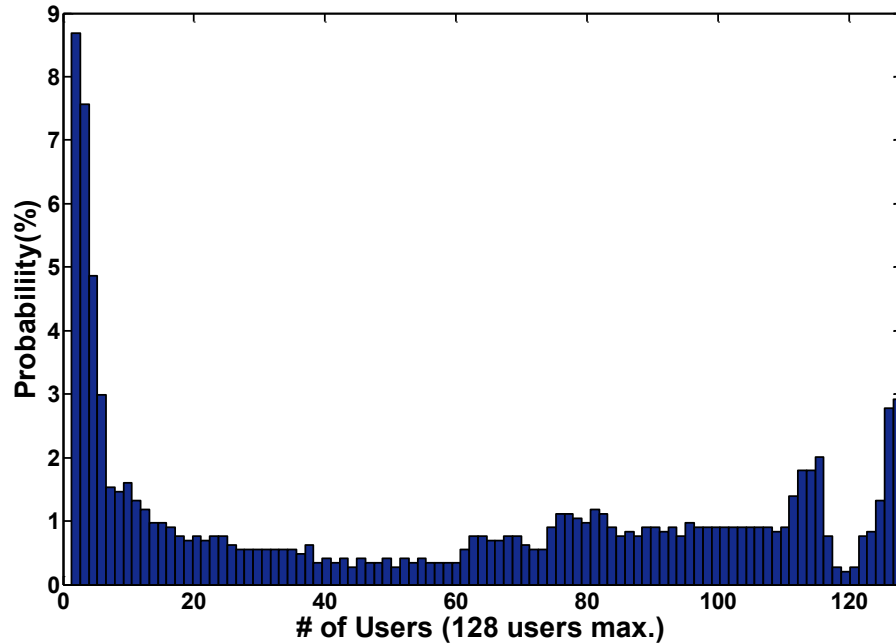


Figure 3.18: Probability density function of the number of users over a 24-hr period in a given cell in which the maximum number of users is 128.

$$0 < \frac{f(X)}{c \cdot g(X)} \leq 1, \quad (3.14)$$

where  $f(x)$  is the known PDF of the traffic profile,  $g(x)$  is PDF of random variables  $X$ , and  $c$  is chosen to be 1.1. Thus, we obtained a set of the number of users whose PDF is within 10% of the PDF of the traffic profile. For each trial,  $n$  number of users exists at a given 15 minute interval. For each user within the given 15 minute interval, a random output power  $P_{user,n}$ , scaled by a factor  $K$ , as expressed in (3.12), was generated based on the CDG4 profile using the acceptance-rejection method, similar to the procedure described earlier, for both the urban and suburban environment. The summation of the output power  $P_{user,n}$  contributed due to each user  $n$  and the overhead power  $P_{overhead}$  given the average output power  $P_{BS}$  of the base-station during the specific 15 minute intervals, as expressed in (3.11). Figure 3.19 shows the PDF of the average base-station power  $P_{BS}$ ,

as a result of 100,000 Monte-Carlo trials, for the specified traffic profile for the suburban and urban environment.

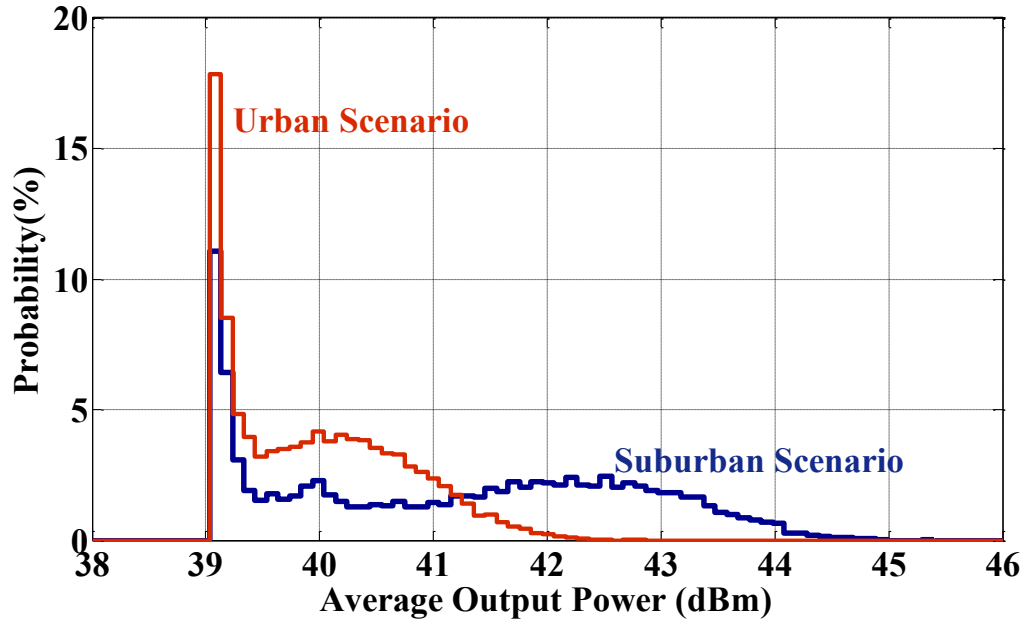


Figure 3.19: Probability density function of average output power in a 40W base-station based on the traffic profile described in Figure 3.17.

The average efficiency over a 24 hour time-scale, as defined by the traffic profile, can be calculated by dividing the average base-station output power over the 24 hour time-scale  $\langle P_{BS,out} \rangle$  by the average power consumption over the same time-scale  $\langle P_{BS,DC} \rangle$ , given by:

$$\langle \eta_{BS,avg} \rangle = \frac{\langle P_{BS,out} \rangle}{\langle P_{BS,DC} \rangle} = \frac{\int \langle P_{out} \rangle * p(\langle P_{out} \rangle) d\langle P_{out} \rangle}{\int \frac{\langle P_{out} \rangle}{\eta_{avg}(\langle P_{out} \rangle)} * p(\langle P_{out} \rangle) d\langle P_{out} \rangle} \quad (3.15)$$

Table 3.3 tabulates the average efficiency, energy consumption, and energy dissipation calculated for the specified traffic profile. The average RF energy output for this base-station is calculated to be 9.9 W\*hr for the urban case and 13.7 W\*hr for the suburban

case. For the specified traffic profile, the base-station overall output power was calculated to be 4.65 dB and 6.05 dB backed-off from the maximum average power, for the suburban and urban scenarios respectively, or approximately 13.5 dB backed-off from maximum peak efficiency. For the specific traffic profile, envelope tracking offers >45% efficiency. Its associated energy consumption is >1.4x lower than that of an ideal Doherty with 60% peak efficiency.

Table 3.3: Energy usage of a base-station over 24 hour period.

	$\langle \eta_{BS,avg} \rangle$ (%)		$\langle Energy_{consumption} \rangle$ (W*hr)		$\langle Energy_{dissipation} \rangle$ (W*hr)	
	Sub-Urban	Urban	Sub-Urban	Urban	Sub-Urban	Urban
Ideal Class B	22.22	19.06	61.64	52.10	47.94	42.17
Ideal Doherty	43.63	37.99	31.38	26.13	17.69	16.21
Doherty (60% eff)	33.51	28.60	40.86	34.72	27.16	24.79
Envelope Tracking	48.36	45.56	28.31	22.28	14.62	12.35

### 3.6 Summary

In this chapter, operation of an ET amplifier was considered for a base-station in which the usage profile varies over a period of hours to days. A simple scalable memoryless DPD model was demonstrated to successfully linearize the ET-HPA in representative back-off conditions. Estimates were also made of the long-term power efficiency of base-station amplifiers, taking into account fluctuating number of users. It is shown that long-term efficiency is lower than the commonly quoted value of efficiency at peak output power. For ET amplifiers, less than 2x reduction in efficiency was measured as average power was decreased over a 10 dB range. Calculations of long-term efficiency indicate that, compared to an ideal Doherty amplifier with the same peak

efficiency, ET amplifiers can provide more than 1.4x reduction in overall energy consumed. Thus, envelope tracking provides significant opportunities for system energy savings under realistic operation conditions. Further long-term efficiency improvement can potentially be obtained by using Doherty amplifiers in conjunction with envelope tracking [17].

### **3.7 Acknowledgments**

The author is very grateful to Triquint Semiconductors for providing GaAs HVHBT power amplifier used in this work, to Nokia-Siemens Networks for their valuable discussions, and to Mr. Paul Draxler, Mr. Don Kimball, Dr. Calogero Presti , and Dr. Peter Asbeck for their valuable discussions and suggestions.

Some of the materials in chapter 3 are as they appear in “Digital Pre-distortion of Envelope Tracking Power Amplifiers under Average Power Back-off and Long-Term Average Power Efficiency for Base-Station Applications”, Jonmei J. Yan, Paul Draxler, Calogero D. Presti, Donald F. Kimball and Peter M. Asbeck, published in the International Journal of Microwave and Wireless Technologies, 2013 Issue 2. The contributions from the co-authors are appreciated. The author of this dissertation was the primary investigator and primary author for this publication.

# **Chapter 4**

## **Broadband Envelope Tracking Power Amplifier**

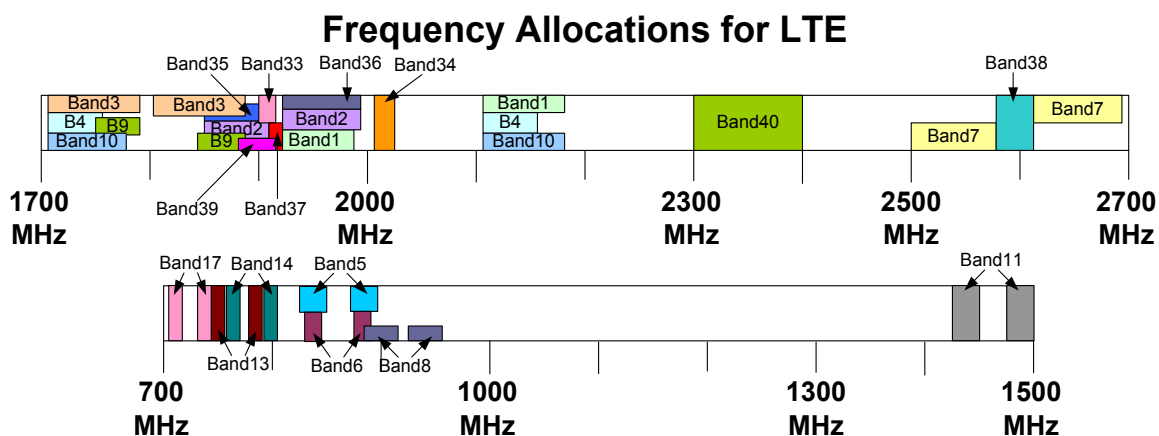
### **4.1 Introduction**

In the previous chapter, practical performance advantages of the envelope tracking power amplifier under fluctuating power conditions were discussed. However, the design of power amplifiers for next generation wireless systems is further complicated as a result of the wide range of carrier frequencies that is required for numerous emerging wireless systems, including software-defined radios, intelligent jammer systems, public safety radio services, and commercial wireless communication systems such as those planned for the next generation LTE-A as shown in the examples in Table 4.1. Broadband power amplifiers are desired in the commercial industry to provide multi-band transmission for operators of EDGE, GSM, WiMAX, LTE-A, etc systems. In the public safety sector, they can be used to synchronize communication between police, firemen, medical response and civil personnel in the event of an

emergency. In the military section, efforts to provide a network centric environment for cross communication within multiple platforms such as UAVs, HUMVEEs, ships, and software defined radios for soldiers have already began. Accordingly, multi-band wireless transmitters capable of seamless operation over very wide frequency ranges are being developed, and increasing attention has been placed on the design of high efficiency broadband power amplifiers.

Table 4.1: Examples of wideband wireless communication systems and frequency allocations for LTE systems.

Bandwidth	Applications
300 MHz – 1.8 GHz (UHF)	Intelligent Jammer Systems, Mobile User Objective System (MUOS), Joint Tactical Radio System (JTRS), UAV Communications
700 MHz – 1 GHz	Public Safety Radio Service
470 MHz – 860 MHz	TV Transposers, DTV, LPTV
1.7 GHz – 2.8 GHz	Next Generation Mobile Networks



In recent years, the availability of high performance gallium nitride (GaN) devices has resulted in significant advances in the design of power amplifiers. Characteristics of gallium nitride (GaN) transistors, such as high drain voltage operation, high power density, and high output impedance, make them uniquely suited for high efficiency, high

power broadband power amplifiers. In this chapter broadband power amplifiers are described that leverage the intrinsic benefits of gallium nitride transistors. The broadband power amplifiers are designed to have a load resistance equivalent to 50 ohms, thereby avoiding the need for a narrowband impedance transformation network and enabling broadband output match. To achieve broadband input match and flat gain response, a feedback network is used. The amplifiers demonstrate greater than 50% power added efficiency (PAE) at output powers greater than 12 W over a bandwidth greater than 3:1 (from 500 MHz to 1700 MHz). In addition, an improved push-pull design utilizing a low-loss broadband balun to provide even harmonic terminations is discussed. Measurement results demonstrated PAE greater than 47%, including the loss of the balun, with output powers between 12.5 W – 18.2 W and greater than 16 dB gain across the frequency band from 500 MHz to 2500 MHz. By virtue of its high gain as well as high drain efficiency, the present amplifier achieves state-of-the-art performance as well as providing smaller size. To overcome the challenges of high PAPR signals in modern wireless communication systems, an envelope tracking demonstration was done with one of the broadband amplifiers. Unlike some of the other power amplifier architectures designed to achieve high efficiency in the presence of signals with high PAPR, envelope tracking power amplifier is fundamentally immune to these limitations since the envelope of the RF signal remains the same as the carrier frequency varies. Hence, the same modulator can be used for signals at different carrier frequencies. The overall efficiency of the envelope tracking power amplifier, using a 6.6 dB PAPR single-carrier WCDMA, was 25% - 31% with 10.3 dB - 13.9 dB gain over a bandwidth of greater than 3:1, including the dissipation of the modulator. For the WCDMA signal,

more than 2 times improvement in average efficiency in the RFPA was observed as a result of operating in envelope tracking (as compared to constant drain mode), along with higher power density.

## 4.2 Broadband GaN Power Amplifier

The need to maintain a broadband input and output match as well as a flat gain response as a function of frequency makes the design of a broadband power amplifier challenging. Especially at low frequencies, the available gain of a power amplifier can be large. The high drain voltage operation, high power density, and high output impedance of GaN transistors make them uniquely suited for high efficiency, high power broadband power amplifiers (PA). Due to the high breakdown voltage of these devices, high VSWR tolerance and high voltage operation are possible. In addition, the high power density capable in GaN technology enables the design of smaller devices, resulting in lower capacitance. GaN devices also offer higher output impedance, a key benefit for broadband applications. High output impedance allows for lower impedance transformation ratio, thereby, increasing the bandwidth.

Using GaN transistors, high efficiency power amplifiers covering a wide range of frequencies with single-tone excitation have been described [19]-[20]. For example, tapered line distributed architecture or multi-stage matching networks have been used to achieve broadband operation [21]. Push-pull amplifiers can also be used; although, they require the design of a low-loss broadband balun [22]. In this work, an alternate approach to broadband operation is employed.



### 4.2.1 Stacked Power Amplifier Design

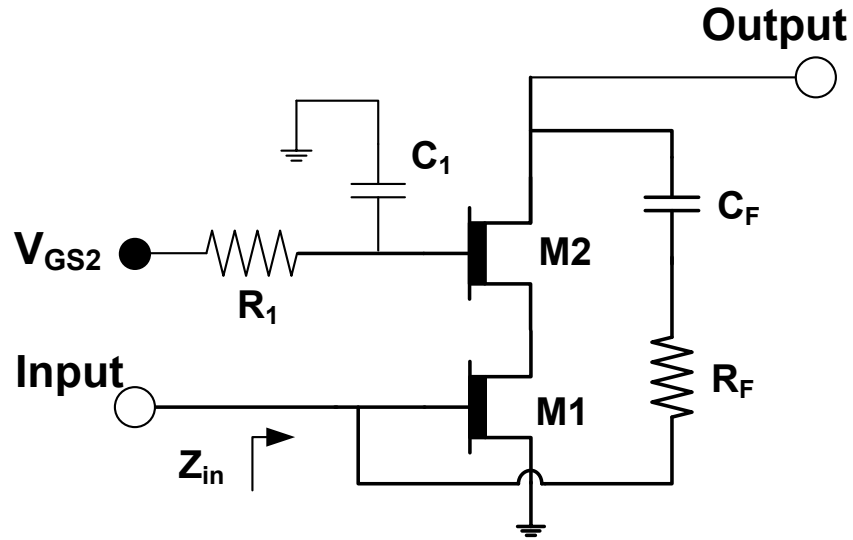


Figure 4.1: Schematic of the proposed stacked GaN power amplifier with RC feedback.

The intrinsic high breakdown voltage and high output impedance of GaN devices are leveraged to increase the output impedance of the power amplifier such that the optimal load impedance is 50 ohms, thereby avoiding the need for an output matching network, whose Q often limits the maximum achievable bandwidth. The amplifier circuit is shown in Figure 4.1. A stack of two transistors is used to further increase the load impedance and to attain higher voltage gain. The two identically sized stacked transistors have widths chosen such that the optimal load impedance at peak power is 50 ohms with a Class AB bias. In the stacked configuration, the input and output capacitances are reduced for a given output power, as desired for envelope tracking and broadband power amplifier designs. An appropriately sized capacitor was inserted at the gate of the top FET to allow a desired amount of voltage swing at the gate, leading to better output voltage handling capability without increasing the drain-to-gate voltage of the top FET

excessively [23]. A large resistor was placed at the gate of the top FET as a DC bias feed resistance.

Another consideration for broadband power amplifier design is the gain variation as a function of frequency. Using a simplified model of a stacked transistor structure in which  $C_{gd}$  is neglected, the transducer gain can be expressed analytically as:

$$Gain_T = \left| \frac{P_{out}}{P_{avail}} \right| = \left| \frac{I_{out}}{I_{in}} \right|^2 \cdot \frac{4R_L R_S}{|R_S + Z_{in}|^2} \quad (4.1)$$

where  $R_L$  is the load resistance,  $R_S$  is the source impedance,  $Z_{in}$  is the input impedance of the stacked PA structure,  $P_{avail}$  is the power available from the source, and  $I_{out}/I_{in}$  is the current gain. For the basic stacked structure, we have

$$Z_{in} = Z_{in0} = R_{g1} + \frac{1}{j\omega C_{gs1}} \quad (4.2)$$

$$\frac{I_{out}}{I_{in}} = -g_{m1} Z_{in0} \quad (4.3)$$

where  $Z_{in0}$  is the input impedance of the basic stacked structure,  $R_{g1}$  is the gate resistance,  $C_{gs1}$  is the gate-to-source capacitance, and  $g_{m1}$  is the transconductance of the bottom FET. Especially at low frequencies, the available gain can be rather large and the input impedance is capacitive, which is poorly matched to 50-ohm sources and is frequency dependent. From equation (4.3), we see that the output current of the stacked PA is governed by the operating point of the bottom FET.

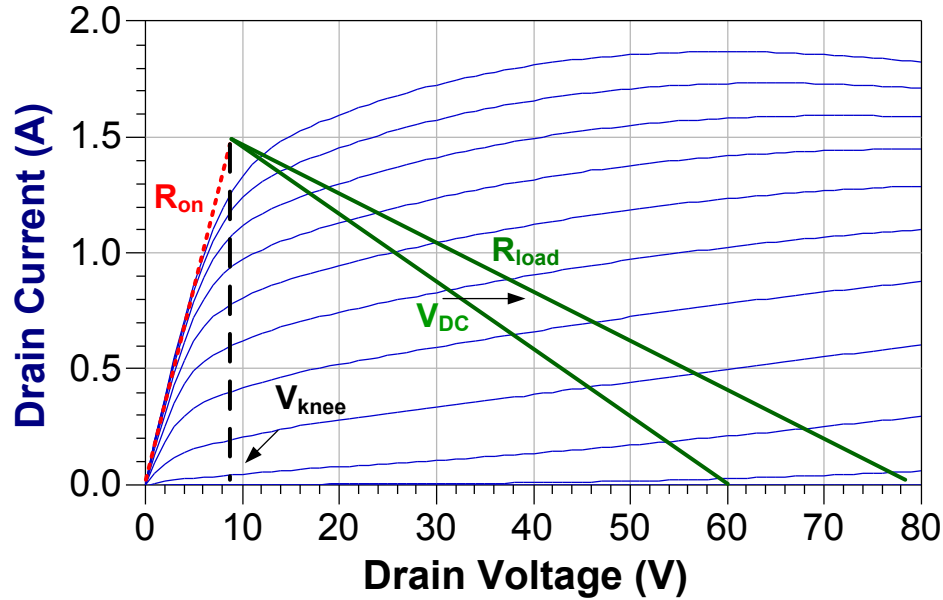


Figure 4.2: Simulated DC IV curve of a stacked GaN FET structure.

As a result of stacking two FETs, the knee voltage  $V_{knee}$  and on-resistance  $R_{on}$  of the composite structure increase over values for a single device, as shown in the modeled  $I_d$ - $V_{ds}$  characteristics in Figure 4.2. This increase in  $R_{on}$  affects the maximum achievable efficiency of the power amplifier [24]. Depending on the class of operation and its corresponding voltage and current waveforms, the effect of  $R_{on}$  on drain efficiency of the RF power amplifier varies [24]. The efficiency degradation factor  $F_{eff}$  due to  $R_{on}$  can be expressed as

$$F_{eff} = \frac{1}{1 + \gamma \frac{R_{on}}{R_{load}}} \quad (4.4)$$

where  $\gamma$  is a coefficient that is dependent on the class of operation. Since the power amplifier is designed such that  $R_{load} \gg R_{on}$ , equation (4.4) can be approximated as

$$F_{eff} \approx 1 - \gamma \frac{R_{on}}{R_{load}} \rightarrow \eta_{RF} \propto 1 - \frac{V_{knee}}{V_{DC}} \quad (4.5)$$

The drain efficiency of the RFPA, reduced by the factor shown in equation (4.5), is affected by the knee voltage  $V_{knee}$  of the power amplifier and the DC bias voltage,  $V_{DC}$ , applied to the drain of the PA. Hence, for a given  $R_{on}$ , to improve the drain efficiency, it is necessary to design for higher load impedance by applying a higher  $V_{DC}$  bias on the drain. For this stacked structure, a constant drain bias of greater than 40 V is desired.

### 4.2.2 RC Feedback Implementation

An RC (resistor-capacitor) feedback network from the drain of the top FET to the gate of the bottom FET is used in this work, as shown in Figure 4.1, to reduce the gain variation over frequency and provide a better input match to 50 ohms. By applying a RC feedback network around the stacked FETs, the input impedance and the current gain are reduced by a factor equal to  $1 + \alpha$ , where  $\alpha$  is the loop gain:

$$\frac{I_{out}}{I_{in}} = \frac{g_{m1}Z_{in0}}{1 + g_{m1}Z_{in0}\beta} \quad (4.6)$$

$$Z_{in} = \frac{Z_{in0}}{1 + g_{m1}Z_{in0}\beta} \quad (4.7)$$

where the feedback factor  $\beta = \frac{R_L}{R_L + Z_{fb}} = \frac{R_L}{R_L + R_F + \frac{1}{j\omega C_F}}$ . In the limit where the feedback resistor is much larger than the load resistance ( $R_F \gg R_L$ ) and the loop gain is large, we can approximate the input impedance and current gain to be:

$$\frac{I_{out}}{I_{in}} \approx \frac{R_F}{R_L} \quad (4.8)$$

$$Z_{in} \approx \frac{R_F}{g_{m1}R_L} \quad (4.9)$$

At high frequencies, the GaN PA IC is limited by the available gain as a result of the finite transition frequency  $f_t$  of the device technology. The feedback behavior is determined by the feedback resistor  $R_F$  (since  $R_F$  dominates over  $C_F$  at high frequencies). To ensure that  $Z_{in}$  is close to 50 ohms even at high frequencies, a value of  $R_F \sim 550$  ohms is calculated from equation (4.9) with  $g_{m1} \sim 220$  mS and  $R_L = 50$  ohms. The input return loss and the gain of the stacked PA can be calculated as:

$$|\Gamma_{in}| = \left| \frac{Z_{in} - R_S}{Z_{in} + R_S} \right| \quad (4.10)$$

$$Gain = \left( \frac{g_{m1}Z_{in}}{Z_{in} + R_S} \right)^2 4 R_L R_S \quad (4.11)$$

The calculated results based on equations (4.10) and (4.11) are shown in Figure 4.3 and Figure 4.4 for the input return loss and gain, respectively, with and without the feedback network, using the extracted input gate resistance and capacitance of  $R_{g1} = 1 \Omega$  and  $C_{gs1} = 2.6$  pF. For comparison, measured results for the fabricated amplifier and simulated results are also shown on the same plot. In the simplified analytical model,  $R_{out}$ ,  $C_{ds}$ , and  $C_{gs}$  are neglected. The simulation results used complete models of the transistors, passives, and bondpads provided through the foundry PDK. Bondwire

inductances and bias tee impedances were also included. Both the simplified analytical model and the detailed simulations are in good agreement with the experimental results. The source and load impedances are terminated to 50 ohms. Without the feedback network, the input return loss is higher than -2 dB while the gain varied more than 8 dB across the frequency range of interest. With the addition of the RC feedback network, the input return loss is reduced to below -5 dB and the gain is flattened. The calculations presented here are based on small signal models. Simulations with large signals ( $\sim P_{-1dB}$ ) show that at high frequencies, model parameters were similar. At low frequencies, discrepancies between the large signal model and small signal model were observed, contributing to larger differences at low frequencies between the simulated and measured results.

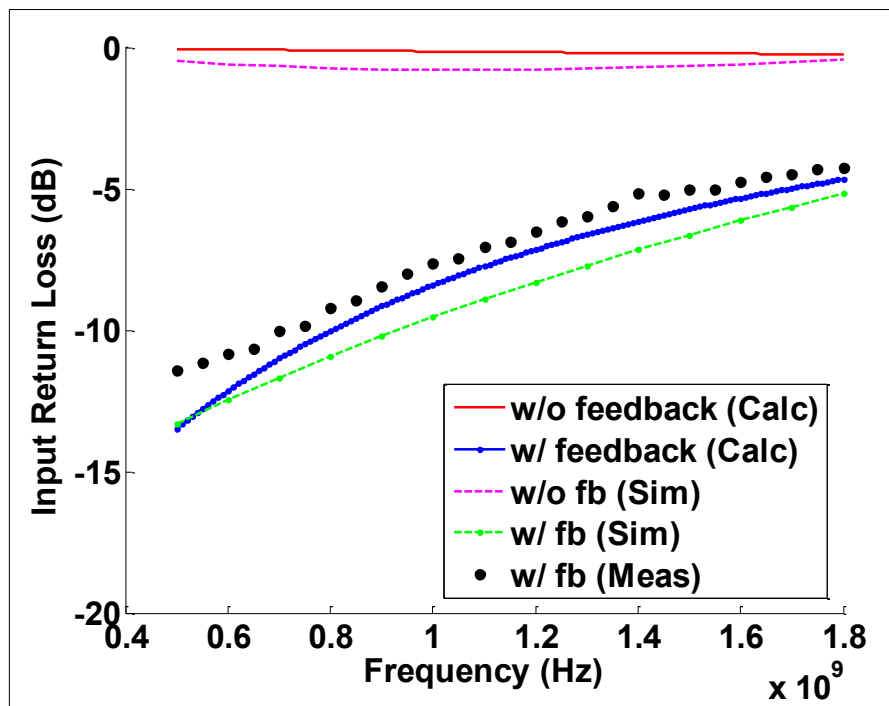


Figure 4.3: Comparison of the input return loss of the conventional stacked PA without RC feedback and with RC feedback.

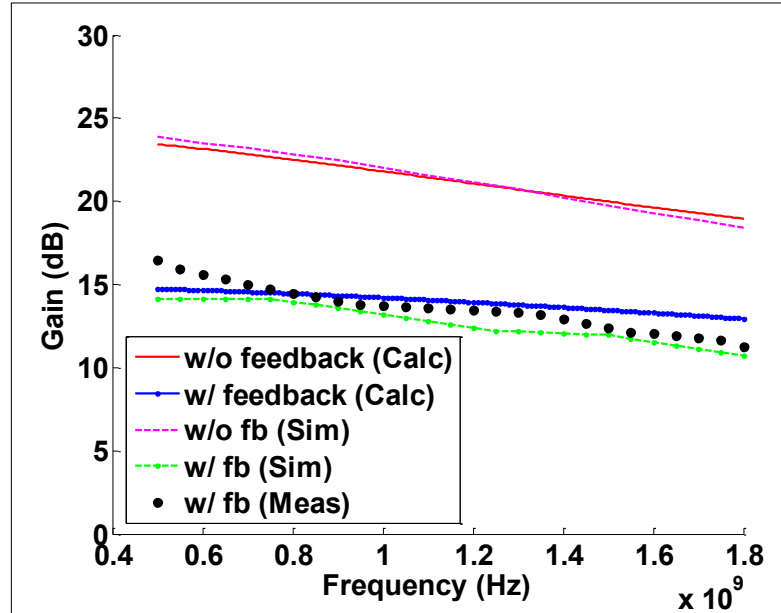


Figure 4.4: Comparison of the gain of the conventional stacked PA without RC feedback and with RC feedback.

### 4.2.3 GaN Stacked Power Amplifier with RC Feedback Performance Results

The AlGaIn/GaN HEMTs were fabricated on a semi-insulating SiC substrate. The amplifier consisted of two equally sized transistors with 2.22-mm gate periphery and gate length of 0.5  $\mu\text{m}$ . These devices had a maximum drain current of 900  $\text{mA}/\text{mm}$ , a typical peak  $g_m$  of 225  $\text{mS}/\text{mm}$ , and  $f_t$  of 11 GHz. The GaN PA IC was biased in Class AB and was designed for input and output impedances of 50 ohms. The feedback resistance was chosen to be 500 ohms, in rough accord with the value calculated in equation (4.9). Using this value, the feedback network does not degrade the drain efficiency significantly. The intent of the feedback capacitor is to block DC while allowing a small amount of RF feedback for better input return loss and lower gain variation. With consideration of the occupied area, the capacitor was chosen to be 23 pF, a large value in order to extend the operation range to very low frequency. The capacitor at the gate of the

FET was used to maximize the voltage handling capability of the FET stack. It was found that a value of 1 pF provided equal voltage swing across each of the two transistors. Figure 4.5 shows a micrograph of the fabricated power amplifier IC. The chip area was  $2.05 \text{ mm}^2$  including the pads.

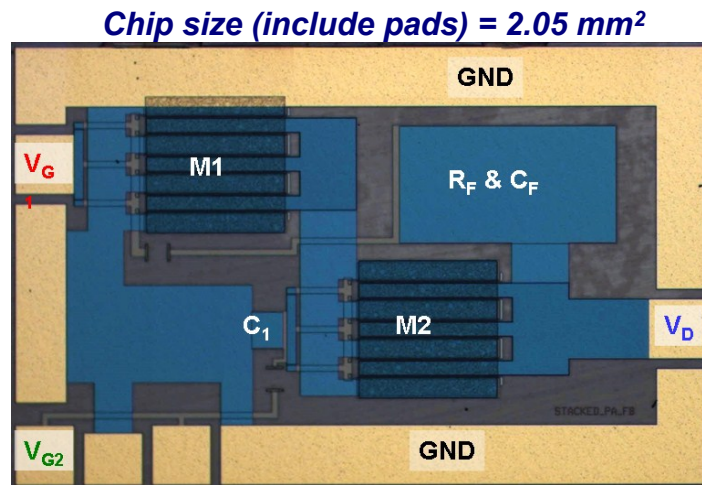


Figure 4.5: Micrograph of the fabricated GaN power amplifier IC.

The RFPA, consisting of the single chip GaN power amplifier, was measured to have greater than 50% drain efficiency when operated between 500 MHz to 1750 MHz under a Class AB bias (using a gate bias of  $-3.72 \text{ V}$ , while the threshold voltage was  $-4 \text{ V}$ ). For the single-tone measurements, the gate and drain bias were provided with the use of external bias tees (Picosecond 5589). The gate bias of the top FET was provided directly to the  $V_{G2}$  pad via a bondwire. The bias value was determined with an external on-board voltage divider to allow for maximum voltage handling capability. The PA IC was mounted directly onto copper to maximize thermal performance, as depicted in Figure 4.6.



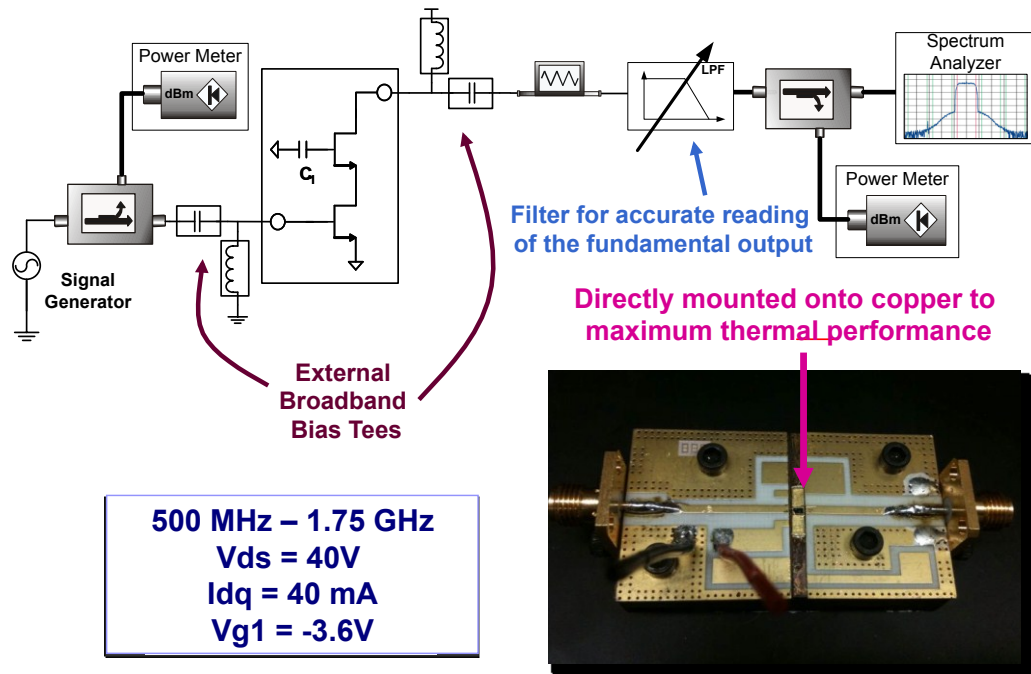


Figure 4.6 Measurement setup and implemented GaN broadband PA.

To test that the power amplifier was unconditionally stable, S-parameters biased at the desired quiescent point was measured and the Rollett's stability factor,  $K$ , and the stability measure,  $b$ , was extracted from these S-parameter measurements, given by, respectively:

$$K = \frac{1 - |S_{11}|^2 - |S_{22}|^2 + |\Delta|^2}{2|S_{21}S_{12}|} \quad (4.12)$$

$$b = 1 + |S_{11}|^2 - |S_{22}|^2 - |S_{11}S_{22} - S_{12}S_{21}|^2 \quad (4.13)$$

where  $\Delta = S_{11}S_{22} - S_{12}S_{21}$ . As shown in Figure 4.7, the power amplifier was unconditionally stable.

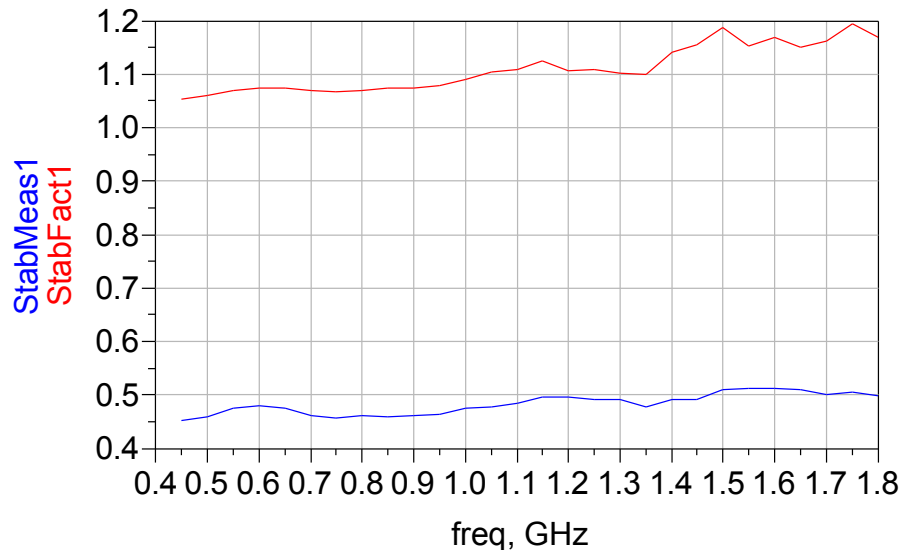


Figure 4.7: Extracted stability factor and stability measure based on measured S-parameters

Power sweeps at the different frequencies from 500 MHz to 1750 MHz were performed while keeping other conditions constant. The measured drain efficiency, gain, and output power under single-tone excitation at a constant drain bias of 40 V across the frequency range of interest are shown in Figure 4.8. Efficiencies greater than 50% across the frequency range from 500 MHz to 1750 MHz was measured when terminated directly to 50 ohms at both the input and the output. The output power reaches more than 12 W at a constant drain bias of 40 V at its maximum PAE point with corresponding gain greater than 10 dB across the frequency band. At around 750 MHz, the peak efficiency was 64.3% with a gain of 14.7 dB. The output power measured at maximum PAE ( $\sim 2.5$  dB in compression) was observed to be flat across the band, corresponding to high power densities of  $\sim 3.7$  W/mm<sup>2</sup>. One of the challenges in the GaN PA design is the ability to extract the heat from the chip. As a result of temperature rises at the transistor junctions, the amplifier was thermally limited to operate at 40 V with 12 W of output power. At

high frequencies, the gain begins to roll-off as a result of the  $f_t$  of the device. The effect of the feedback network diminishes at low frequencies as evident by the higher gain. As the carrier frequency decreases, the impedance of the feedback capacitor increases, reducing the amount of signal fed back to the input of the RFPA. For comparison, Figure 4.8 also shows simulated results for the RFPA biased at the same quiescent current as for the measurements; good agreement was found. Figure 4.9 illustrates the average drain efficiency, average output power, and average gain of the GaN PA IC placed under a constant drain bias while using a 6.6 dB PAPR representative WCDMA input signal. The peak average efficiency of 26.4% was achieved at 752 MHz with a gain of 16.7 dB. A flat average output power of 2.5 W was measured across the band. The peak power reached 12 W, which is in accord with the single-tone measurements. Across the frequency band, the average drain efficiency, when excited with the WCDMA signal, was 18.4% - 26.4%, measured at maximum PAE. The results depicted in Figure 4.9 show that, with high PAPR modulated signals, the drain efficiency of the RFPA degrades significantly.

### **4.3 Push-pull Broadband GaN Power Amplifier**

Push-pull power amplifiers inherently offer broadband even harmonic terminations and can be tuned for high efficiency. However, they require the design of a broadband low loss balun, which is frequently challenging. Coaxial baluns provide a convenient solution, but they typically are large and not suitable for higher frequencies. In this work, we demonstrate GaN integrated circuits, which individually provide high

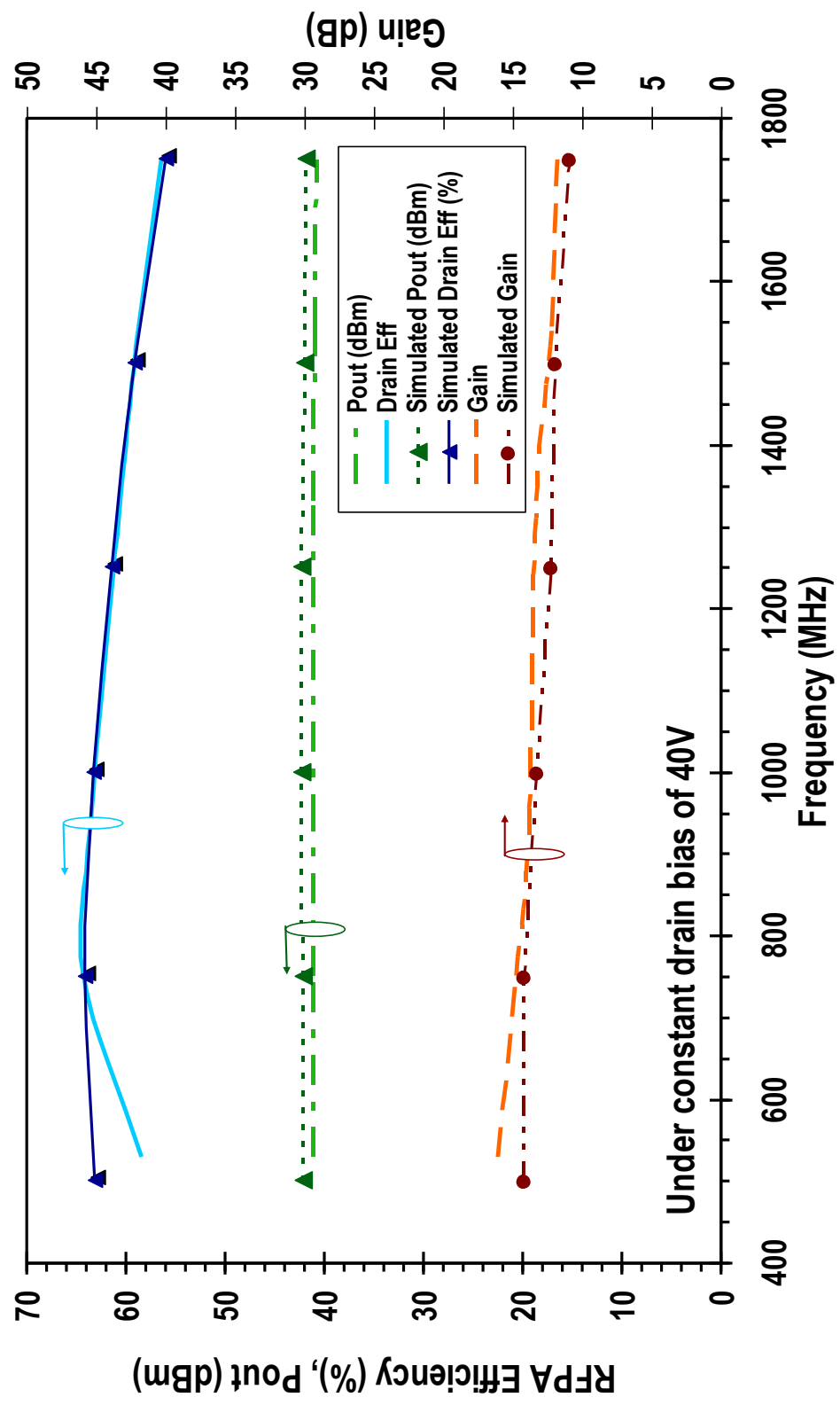


Figure 4.8: CW Measurements of the GaN PA IC under a constant drain bias of 40V, biased in Class AB, illustrating the drain efficiency, gain, and output power across the frequency band of interest.

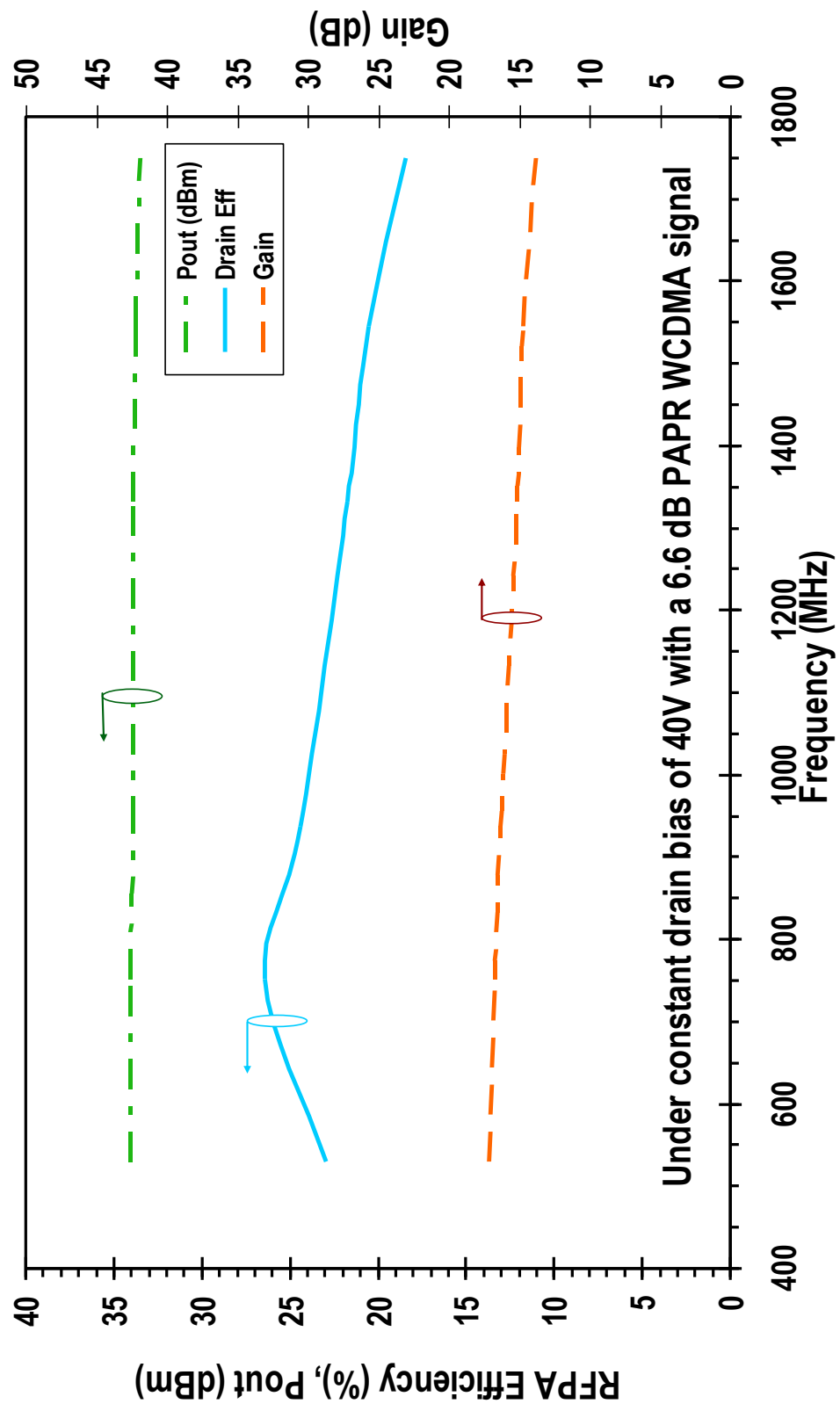


Figure 4.9: Measured drain efficiency, gain, and output power of the GaN PA IC under a constant drain bias of 40V, biased in Class AB, using a 6.6 dB PAPR WCDMA signal, across the frequency band of interest.

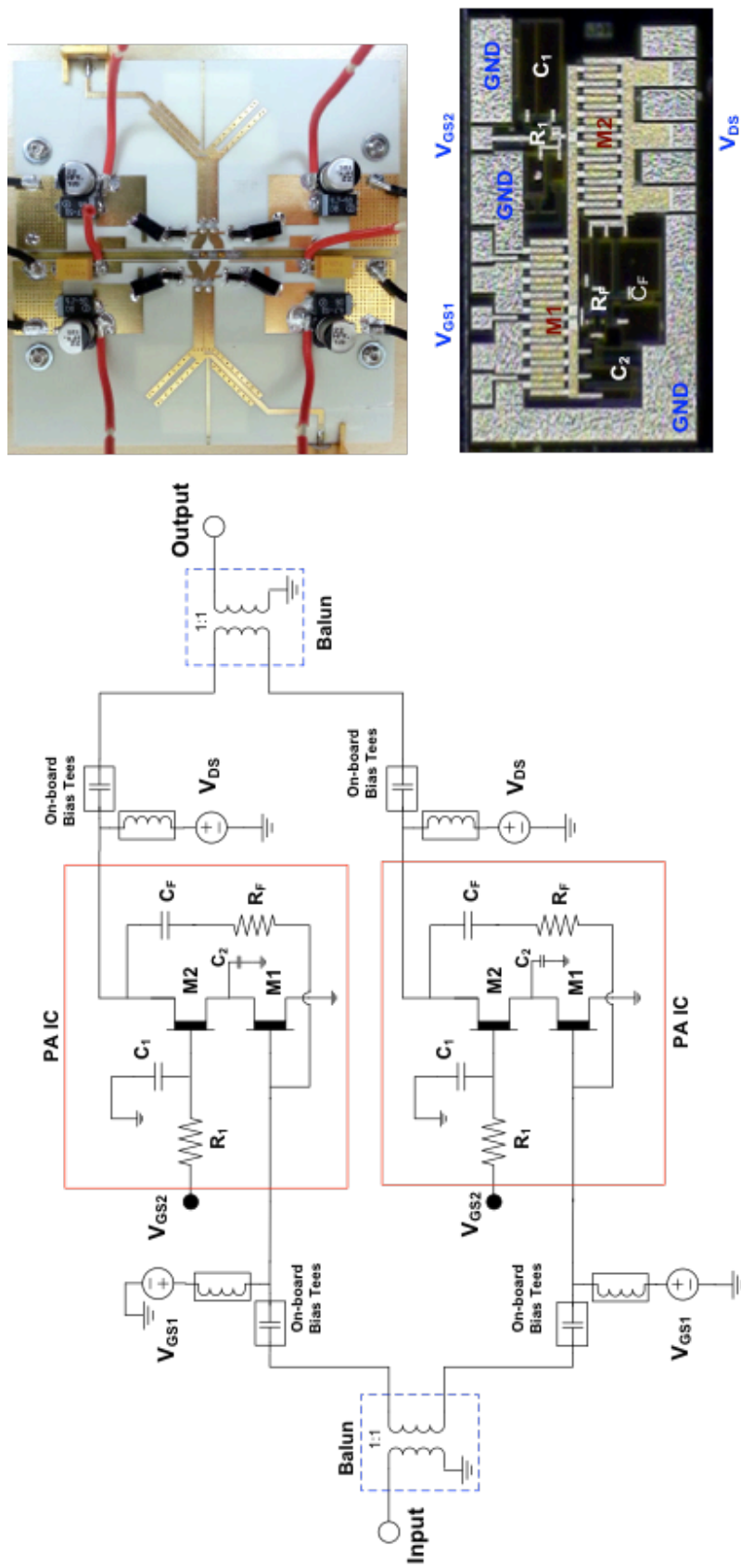


Figure 4.10: Schematic and photo of the push-pull power amplifier. The amplifier measures to be 80 mm x 80 mm.

power (up to 10W), and are combined together in a push-pull amplifier using a low-loss, broadband, and compact PCB-based balun to provide a broadband power amplifier. A balun with 1:1 impedance ratio is considered in this design in order to achieve broadband operation with low loss.

### 4.3.1 Stacked Feedback Design

The desired input and output impedance results in a  $50 \Omega$  differential impedance, or  $25 \Omega$  odd mode impedance. One approach to increase the output impedance of the power amplifier is by connecting two FETs in series [25]. In the design of the individual ICs, two transistors were series-connected (stacked) and sized such that the optimal load impedance was  $25 \Omega$  and input and output capacitances were reduced, relative to parallel-connected transistors. A RC feedback network,  $C_F$  and  $R_F$ , was used to provide a better input match to 25 ohms and to reduce gain variation over frequency. A capacitor,  $C_1$ , was placed at the gate of the top FET and sized to allow an appropriate voltage swing to prevent voltage breakdown of the FETs while achieving high efficiency. Additionally, a capacitor,  $C_2$ , at the drain of the bottom FET was used for better inter-stage matching. Figure 4.10 depicts the schematic and the micrograph, respectively, of the single IC with  $C_1 = 6 \text{ pF}$ ,  $C_2 = 1.5 \text{ pF}$ ,  $C_F = 10 \text{ pF}$ ,  $R_F = 700\Omega$ , and  $R_1 = 2000 \Omega$ .

The integrated circuits were fabricated with GaN HEMT MMIC technology with a transition frequency  $f_t$  in the order of 35 GHz, which provides high gain and enables RF feedback to be used to provide broadband matching and still maintain high overall gain ( $> 16 \text{ dB}$ ). The overall power supply voltage of 30V was partitioned in a way that

maintains approximately 15V bias across each device. The gate width for the FETs was chosen to be 3 mm.

### 4.3.2 Broadband Balun Design

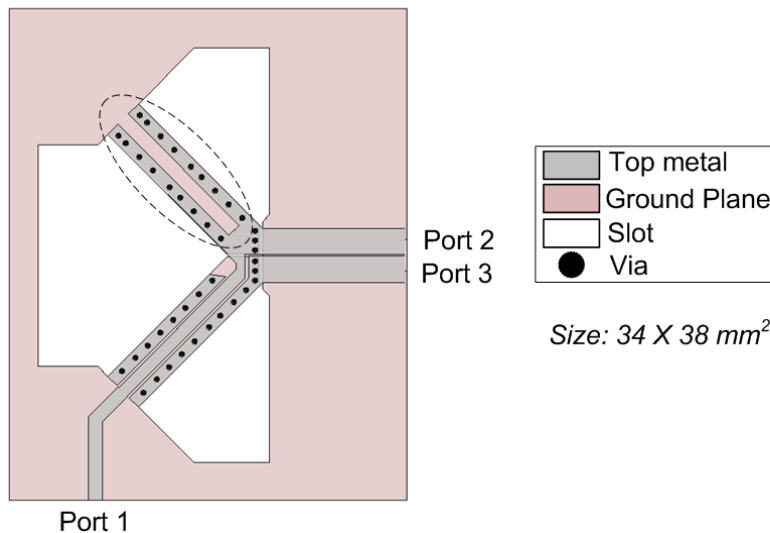


Figure 4.11: Geometry of the balun.

The broadband low-loss balun is based on the Marchand architecture [26]. Figure 4.11 shows a balun consisting of CPW-to-slotline transformation, quarter-wavelength slotline, impedance matching L-section (the dotted circle region in Figure 4.11), and via holes. The balun has  $50 \Omega$  impedance at the input port (port 1) and  $25 \Omega$  impedance at the output ports (ports 2 and 3). The balun was designed and fabricated on a 0.508 mm-thick RO4003C substrate with dielectric constant of 3.38. Measured results are compared with simulations, performed using Ansoft's High Frequency Structure Simulator (HFSS). Figure 4.12 shows the simulated and measured return and insertion losses of the balun in back-to-back configuration. Measured and simulated results agree well in the range from 500 MHz to 5 GHz, and the measured insertion loss for the balun is less than 1.5 dB



(0.75 dB for single balun) from 640 MHz to 5 GHz. For the single balun in HFSS simulation, the amplitude imbalance is less than 0.7 dB and the phase imbalance is less than  $1.5^\circ$  from 500 MHz to 5 GHz.

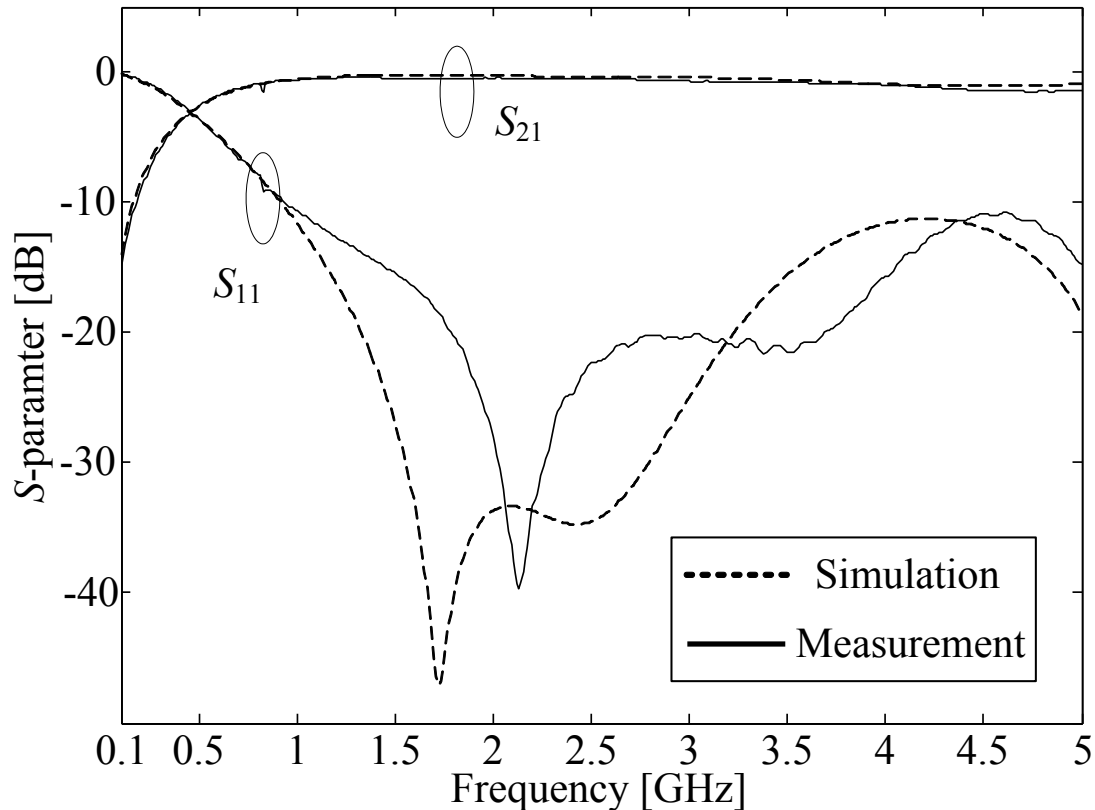


Figure 4.12: Simulated and measured result of back-to-back configuration.

### 4.3.3 Push-pull Power Amplifier Implementation and Performance Results

The implemented push-pull power amplifier, with on-board bias-tees, is depicted in Figure 4.10. The transistor was biased to have a quiescent current of 200 mA, corresponding to a gate voltage of -2.12 V under a Class AB operation and a drain bias of 30 V. The ICs were directly mounted onto brass for optimal thermal performance. Comparison of the simulation and on-wafer small signal measurements of

the single IC is shown in Figure 4.13, renormalized to  $25 \Omega$  source and load impedance. Better than 6 dB of input return loss and better than 5 dB of output return loss was measured across the band. Calculated stability factor shows that the IC was unconditionally stable.

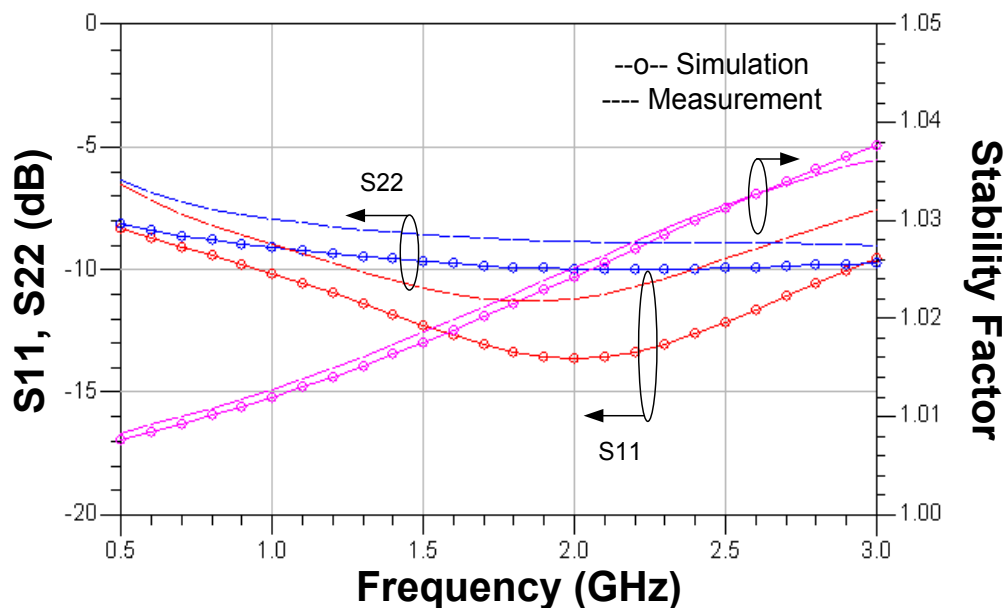


Figure 4.13: Simulated and measured S-parameter of the single IC and measured and simulated stability factor of the single IC.

Large signal measurements were performed using CW excitation. Power sweeps at various frequencies from 500 MHz to 2.5 GHz were performed while keeping all other conditions on the fixture constant. No additional matching at the input or the output was used during the measurement. Figure 4.14 depicts the output power, gain, and drain efficiency at 1500 MHz as the input power is swept. At the point of maximum PAE, the drain efficiency was measured to be 63.2% with 42.7 dBm of output power and gain of 17.2 dB. Similar measurements were performed over frequency. Figure 4.15 shows the measured gain, output power and drain efficiency, corresponding to the maximum PAE

point, over the frequency range of interest. Greater than 5:1 bandwidth with better than 16 dB gain, 47% power added efficiency (PAE) at output powers in the range of 12.5-18.2 W was measured on the push-pull power amplifier. Table 4.2 compares the performance of the present amplifier with other recently reported broadband power amplifiers. By virtue of its high gain as well as high drain efficiency, the present amplifier achieves better PAE than another reported push-pull amplifier [1] as well as providing significantly smaller size.

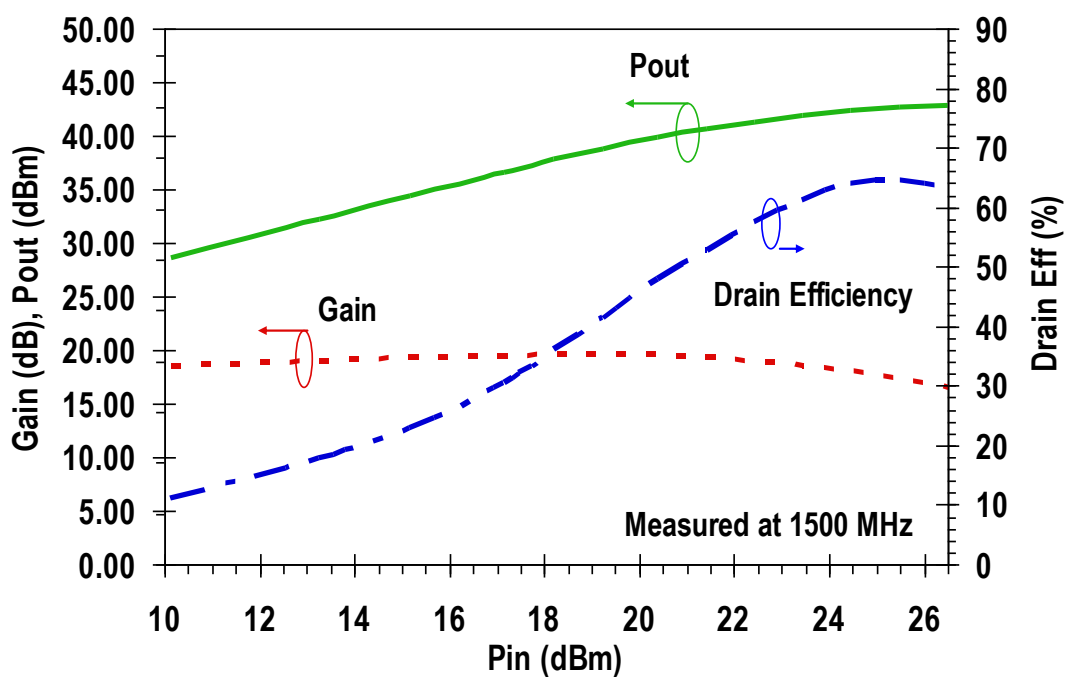


Figure 4.14: Measured output power, gain, and drain efficiency as a function of input power at 1500 MHz.

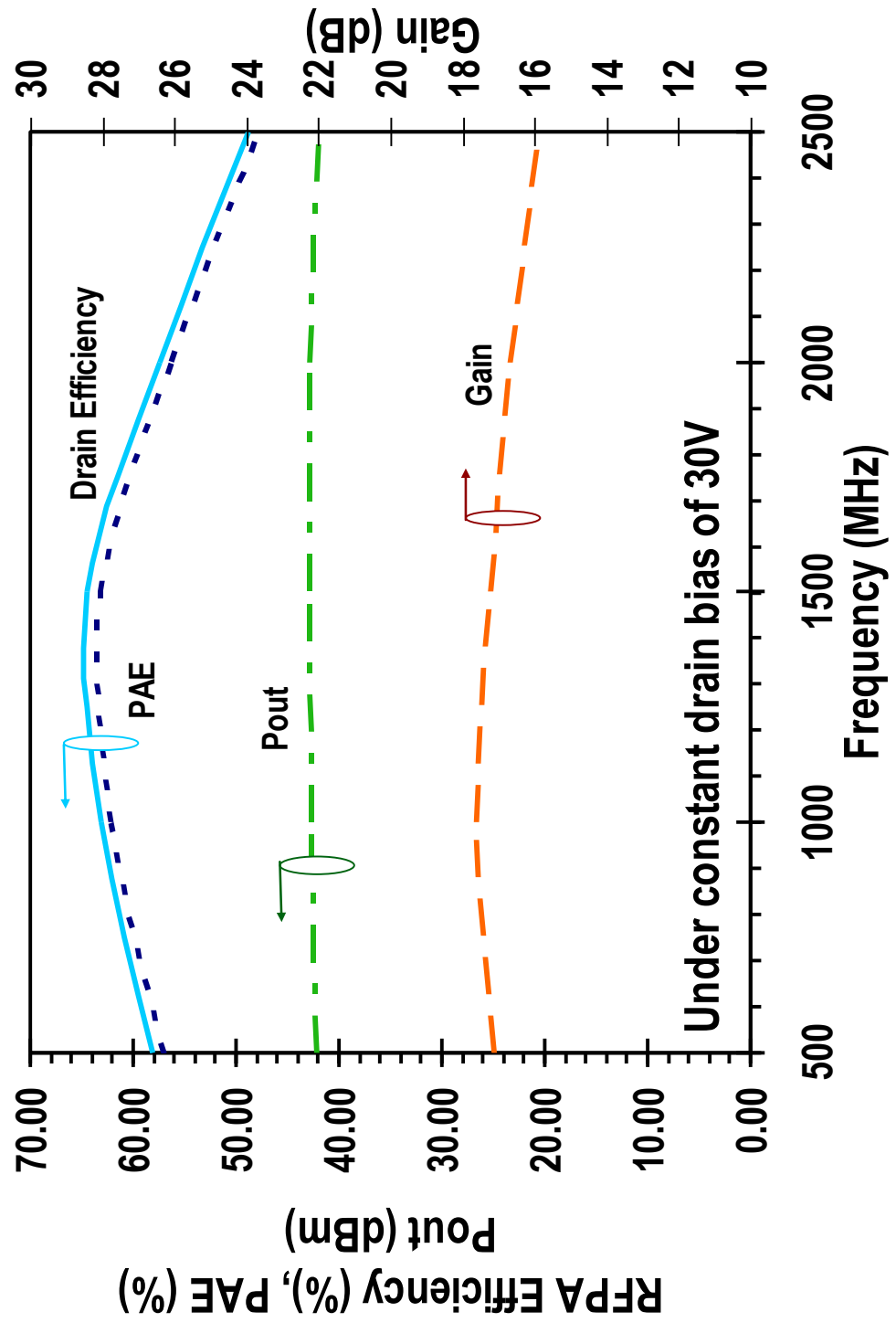


Figure 4.15: Measured output power, gain, and drain efficiency as a function of frequency, corresponding to maximum PAE point.

Table 4.2: Comparison of broadband RF power amplifiers

	Frequency (MHz)	Fractional BW (%)	Pout (dBm)	PAE (%)	Gain (dB)	Output Match
[1]	250-3100	170	40-46	16-65	7-20	Wideband Push-pull
[2]	20-2000	196	40	27-63	10-15	Distributed
[22]	2000-4000	67	40-42	50-62	9-11	Wideband Distributed
[23]	500-2500	133	42-44	33-40	9-11	Wideband Distributed
<b>This work</b>	<b>500-2500</b>	<b>134</b>	<b>41-43</b>	<b>47-63</b>	<b>16-18</b>	<b>Wideband Push-pull</b>

## 4.4 Multi-Octave Envelope Tracking Power Amplifier Design

Among the various high efficiency power amplifier architectures for signals with high PAPR are the Doherty [26]-[29], outphasing [30]-[31], and envelope tracking architectures [32]-[34]. Due to the frequency dependence of the quarter-wave impedance inverter, the conventional Doherty architecture does not lend itself to multi-octave use. Outphasing power combiners also have a limited bandwidth. On the other hand, the ET architecture is fundamentally immune to these limitations since its operation depends on the the envelope of the RF signal remains relatively unaffected as the carrier frequency is tuned. Hence, a single modulator, satisfying the required modulation bandwidth, can be used to provide a dynamically varying supply voltage as the carrier frequency is varied.

### 4.4.1 Broadband Envelope Tracking Power Amplifier Design

The RFPA used was a broadband GaN power amplifier, described in Section 4.2. To project the potential performance of the RFPA under envelope tracking, single-tone measurements at different constant drain supply voltages were performed while keeping the gate bias fixed. Shown in Figure 4.18 is the gain and drain efficiency of the GaN RF PA IC, plotted against the measured output power, taken at 752 MHz. Each curve represents the measured large signal characteristics at a different constant drain bias voltage. As the drain voltage varied from 10 V to 40 V, the GaN RF PA demonstrated greater than 10 dB gain and higher than 60% peak drain efficiency. Shown in Figure 4.18 are the drain efficiency trajectory, with the dotted blue line, and the gain desired for

maximum PAE, with the solid teal line, in the envelope-tracking mode. Due to the knee voltage of the stacked high voltage GaN structure, applying drain voltages below 10 V results in a reduction of the gain. Thus, at low RF powers, the drain supply was “de-troughed” to ensure that the drain supply voltage applied to the device did not fall below 10 V where the gain begins to collapse and also to reduce sensitivity to time misalignment; at medium to high powers, the drain supply voltage was chosen to track linearly with the envelope of the RF signal, keeping the RFPA in compression in these regions [24]. The choice of the envelope voltage  $V_{env}(t)$  can be expressed as:

$$V_{env}(t) = V_{DD,max} \cdot \left[ |x_{in}(t)| + b \cdot e^{-\frac{|x_{in}(t)|}{b}} \right] \quad (4.14)$$

where  $V_{DD,max}$  is the peak envelope voltage,  $|x_{in}(t)|$  is the normalized input RF signal amplitude, and  $b$  is the “de-troughing” ratio, given by  $\frac{V_{DD,min}}{V_{DD,max}}$  where  $V_{DD,min}$  was chosen to be close to 10 V. Figure 4.16 illustrates the normalized envelope voltage versus  $|x_{in}(t)|$  (AKA. “envelope supply shaping function”) expressed in equation (4.14). The envelope signal was shaped to obtain a peak voltage of 42 V and a trough voltage of 12 V. Figure 4.17 depicts the envelope signal of a 6.6 dB PAPR WCDMA signal in the time domain as applied to the drain of the RFPA. The gain and efficiency of the RFPA at the root-mean-square (RMS) of the modulated envelope supply voltage bias dominate the average performance of the RFPA. The RMS envelope voltage was measured to be ~23 V. Using the setup depicted in Figure 4.6 for constant drain measurements, the measured gain, output power, and RFPA drain efficiency is shown in Figure 4.19, corresponding to the maximum PAE point (at about 2.5 dB compression point) under a single-tone

excitation at a constant drain bias of 23 V at various frequencies across the band. The RFPA drain efficiency was measured to be between 55% and 62.8% with gain from 11.5 dB to 15 dB.

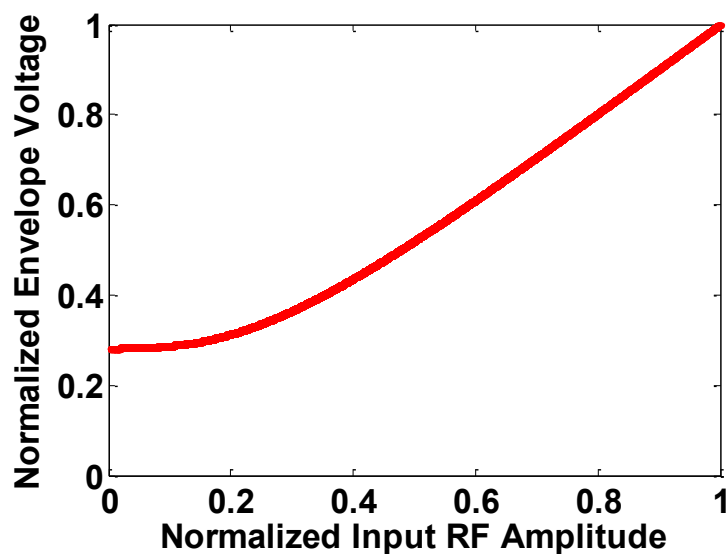


Figure 4.16: Normalized envelope shaping function, corresponding to 42 V peak and 12 V minimum envelope.

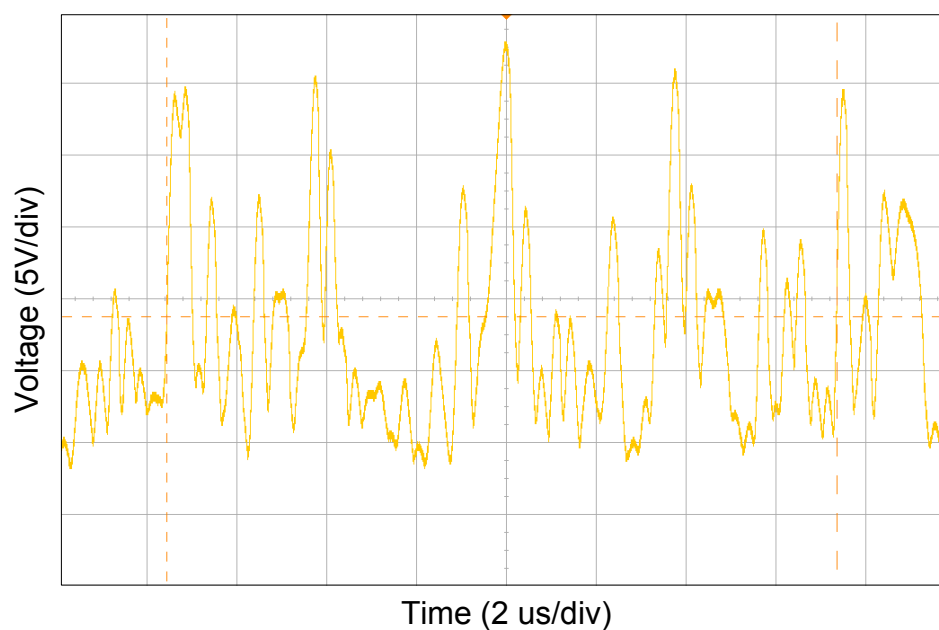


Figure 4.17: De-trothed envelope signal, with 42.3 V peak and 23.2 V rms, applied onto the drain of the RFPA in the time domain.



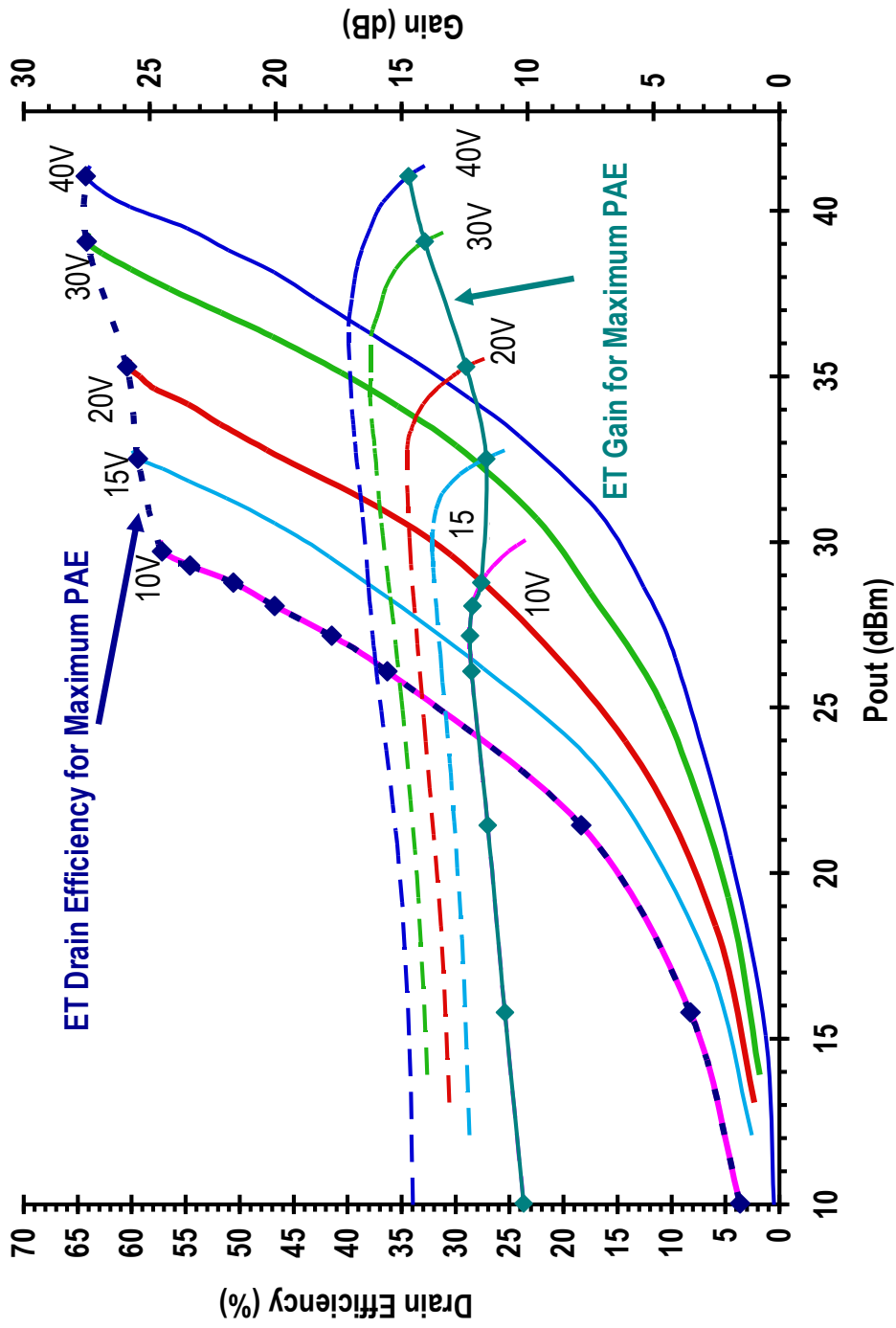


Figure 4.18: CW Measurements of the GaN PA under single-tone excitation at 752 MHz as a function of output input power for various drain biases.

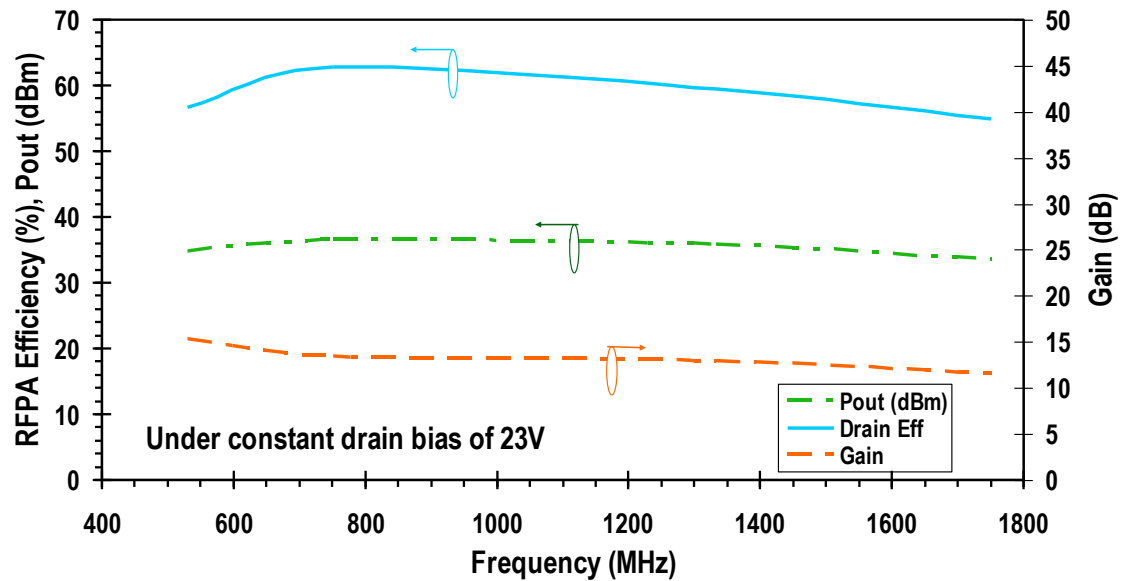


Figure 4.19: CW Measurements of the GaN PA under single-tone excitation as a function of frequency from 500 MHz to 1750 MHz at a drain bias of 23V with -3.72V gate bias.

#### 4.4.2 Broadband Envelope Tracking Power Amplifier Implementation

Under envelope tracking, the constant drain supply was replaced with an envelope modulator to provide dynamically varying supply to the RFPA. Using the envelope tracking power amplifier test-bench, described in Chapter 1, the baseband fully modulated signal and the de-toughed envelope signal were generated. In the envelope path, the shaped envelope signal is passed directly to the envelope modulator where the signal is amplified by a voltage gain of 16 to provide a high voltage dynamic supply to the drain of the RFPA. As mentioned previously, as a result of stacking the FETs, the peak drain bias desired from the dynamic supply should be greater than 40V. Although even higher peak envelope voltages were desired for higher efficiency, the peak envelope voltage was limited to 42 V due to the maximum voltage operation of the high voltage envelope modulator. The RFPA had a gate bias at the same Class AB operating point,

while the drain bias was varied from 12 V to 42 V. As the carrier frequency was tuned across the band, the final stage GaN RFPA and the envelope modulator were left unchanged. It was necessary to use different driver amplifiers at the different carrier frequencies and modify the filters in the up-conversion and down-conversion chain to reduce LO leakage and eliminate unwanted images. Additionally, due to the wide bandwidth ( $\sim 5$ - $7$  times the signal bandwidth) of the envelope signal in the power supply “DC” path, the external bias tee at the drain of the RFPA was replaced with a custom bias tee designed to pass the envelope supply voltage through the DC path while blocking the RF output from reaching the supply modulator.

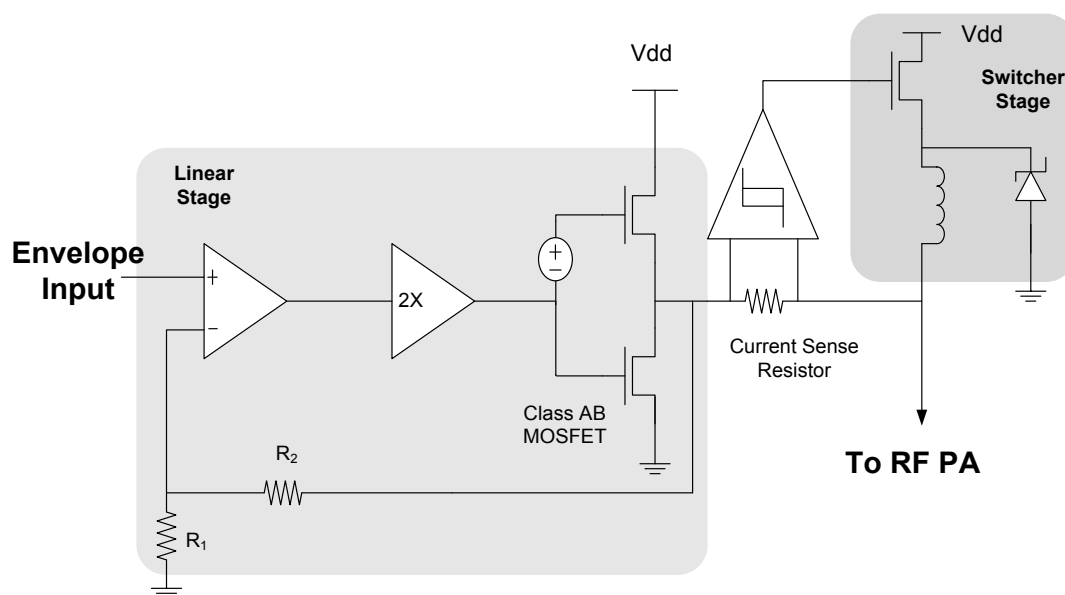


Figure 4.20: High voltage envelope amplifier block diagram.

The high voltage high efficiency wideband envelope modulator was achieved by operating a linear stage and a switcher stage in parallel, controlled by a hysteretic current sense stage, as shown in Figure 4.20 [14]. The high fidelity linear stage is designed to act as a voltage source using feedback to ensure that the output voltage is a linear function of

the input signal. The switcher stage acts as the main current source, providing majority of the current (>85%) with high efficiency (>90%). The switcher stage is essentially a buck converter whose input switching signal is determined by the net current out of the linear stage. Any differences between the current drawn by the load and the current provided by the switcher stage are sourced or sunk by the linear stage so as to minimize the overall error. The envelope modulator used in this experiment was designed to operate up to peak envelope voltages of 45 V [32].

Shown in Figure 4.21 are the measured average drain efficiency and average gain as a function of average output power of the envelope tracking power amplifier with a 6.6 dB PAPR WCDMA signal as the carrier frequency was tuned from 500 MHz to 1750 MHz. The peak overall envelope tracking system efficiency of 31% was measured at 752 MHz with a gain of 13.9 dB and an average output power of 4 W, corresponding to a peak output power of 18.3W and a peak power density as high as  $4.1 \text{ W/mm}^2$ . With the dynamic supply voltage operation, the PA operates at higher efficiency, allowing high power densities and low junction temperatures to be achieved. Across the entire frequency band, the average drain efficiency of the overall envelope tracking system, including the power consumption of the supply modulator, was measured to be 25% - 31% with more than 10 dB gain at output powers of 2 W - 4 W. Compared to the average drain efficiency (18.4% - 26.4%) under the WCDMA signal for the constant drain bias, an improvement in the overall efficiency was observed when the RFPA was placed under envelope tracking.

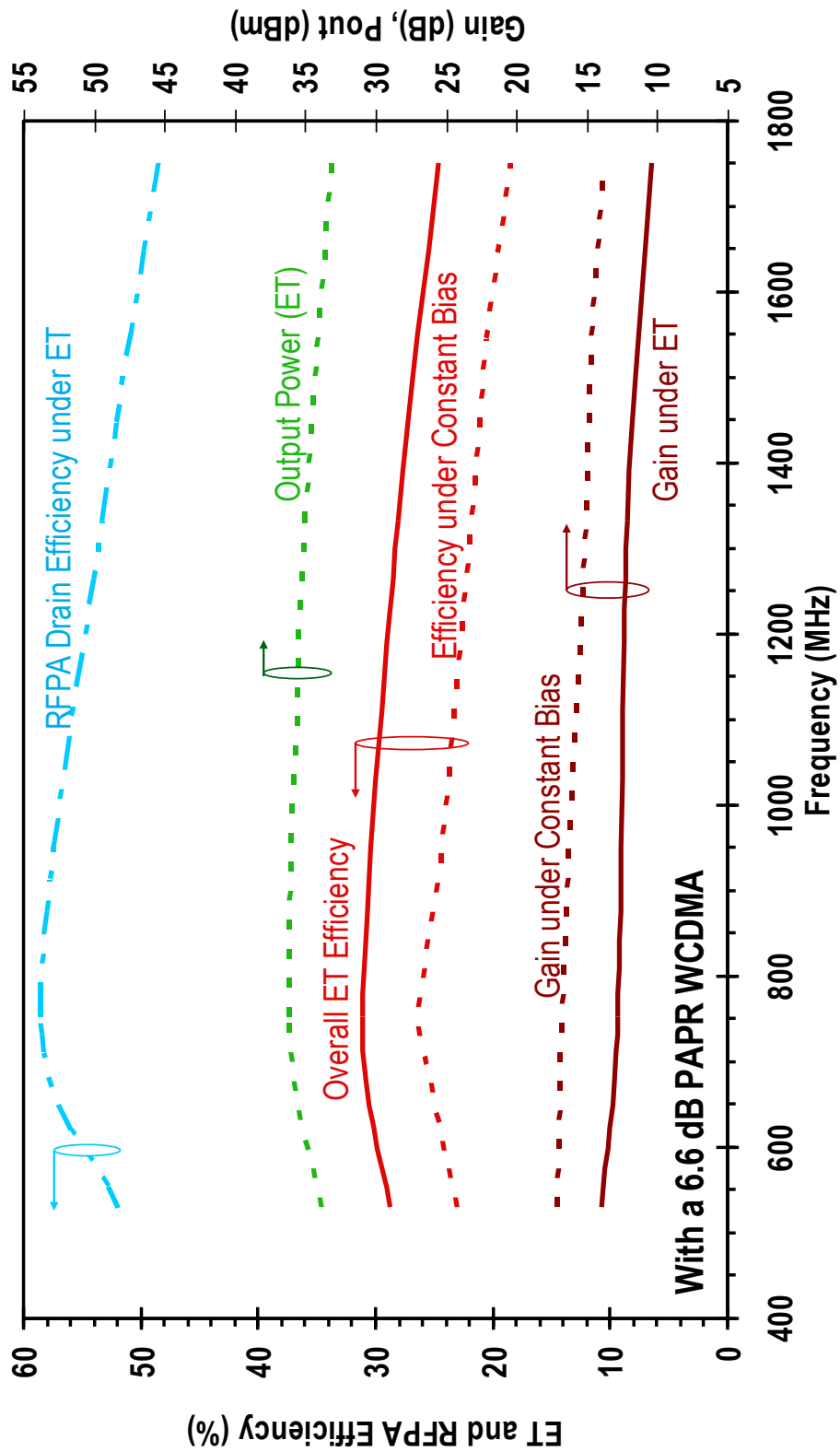


Figure 4.21: Measured average efficiency, gain, and output power of the GaN ETPA across frequency band of interest with -3.72 V gate bias.

### 4.4.3 Broadband Envelope Tracking Power Amplifier Performance Results

In envelope tracking, the average ETPA drain efficiency can be approximated as the product of the efficiency of the RFPA and that of the supply modulator, expressed as

$$\eta_{ETPA} = \frac{P_{out}}{P_{DC}} = \frac{P_{env}}{P_{DC}} \cdot \frac{P_{out}}{P_{env}} = \eta_{EA} \cdot \eta_{RFPA}. \quad (4.15)$$

By measuring the instantaneous envelope voltage and current provided to the drain of the RFPA, it is possible to determine the RMS envelope power. The efficiency of the modulator  $\eta_{EA}$  can be approximated as the RMS envelope power  $P_{env}$  divided by the average DC power  $P_{DC}$  into the modulator. Similarly, the efficiency of the RFPA  $\eta_{RFPA}$  is approximately the output RF power  $P_{out}$  divided by the RMS envelope power  $P_{env}$  into the RFPA. As shown in Figure 4.21, the measured RFPA efficiency and gain was found to be 48.5% - 58.5% and 10.4 dB - 13.9 dB, respectively, across the entire frequency band, around the same as the measured RFPA efficiency under single-tone excitation at the RMS drain supply voltage of 23V. Compared to the constant drain measurements with a modulated signal, shown in Figure 4.21, the efficiency of the RFPA has increased by more than 2 times as a result of operating in strong compression at most power ranges under the envelope tracking mode.

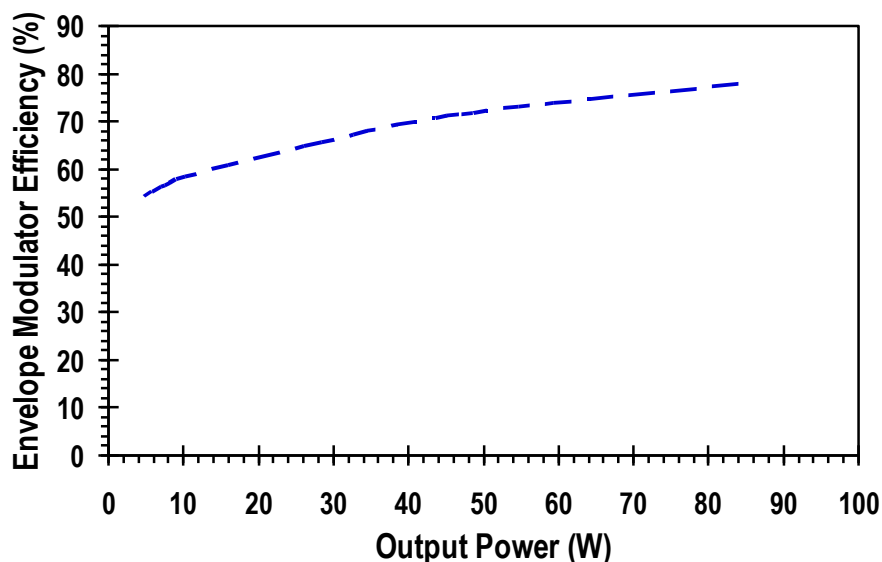


Figure 4.22: Measured envelope modulator efficiency as a function of output power, measured using the representative de-troughed envelope signal on various resistive loads.

The supply modulator efficiency during these experiments was between 51% and 55%, lower than the usual value (65 - 80%) measured in our laboratory for the modulators sized properly in accordance to the RFPA output power. The envelope modulator used in the experiment was designed for high output power applications (>40 W) with peak drain supply voltages at 45 V [32]. Figure 4.22 shows the measured efficiency of the supply modulator corresponding to different loading conditions (using resistive loading to emulate the RFPA). The change in efficiency as a function of output power is principally a result of the static power dissipation. At the RMS drain voltage of 23V, using the representative WCDMA signal, the average output power of the supply modulator corresponded to 4 W - 7 W. From Figure 4.22, the measured efficiency of the supply modulator at this supply power was 52% -56.4%. These results correspond well with the measured supply modulator efficiency when placed in envelope tracking mode with a RFPA as the load. As a result, we can infer that an efficiency reduction occurred

due to an oversized modulator. To achieve higher modulator efficiency, a scaled-down version, designed for supplying power below 10 W, would be required. Previous publications of a low power supply modulator of similar requirements have demonstrated efficiencies of around 70% [14] - [37]. For a properly sized modulator for lower output power applications, greater than 70% supply modulator efficiency is projected. Under this scenario, the projected overall ET efficiency would increase to 34% - 41%.

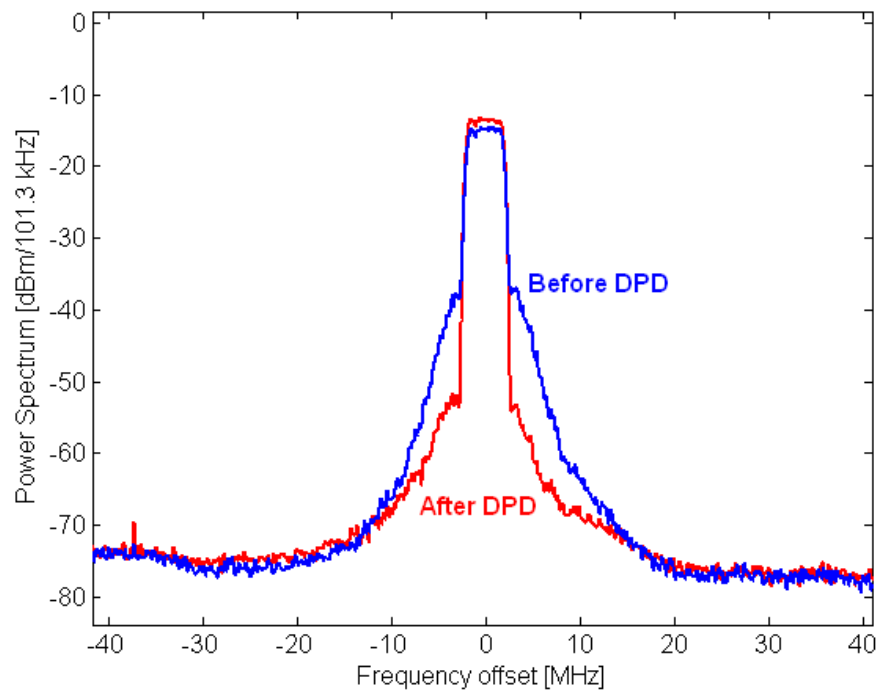


Figure 4.23: Output spectrum before and after DPD at 752 MHz.

Figure 4.23 illustrates the measured output spectrum before and after applying digital pre-distortion (DPD) at 752 MHz. The ACPR was measured to be -47.48 dBc and -52.22 dBc at 5 MHz and 10 MHz offset, respectively, after DPD, meeting the linearity specifications of the WCDMA base-station standard. The measured NRMSE (normalized RMS error) values before and after DPD were 9% and 2.8%, respectively. After DPD, the output signal was linearized as shown by the linear behavior of the AM-



AM plot and the flat phase of the AM-PM plot in Figure 4.24 and Figure 4.25, respectively. Table 4.3 summarizes the measured performance of the GaN ETPA presented in this paper. Table 4.4 shows the comparison of the CW performance of our broadband power amplifier IC with other broadband power amplifier designs. It can be observed that the RFPA IC offers broad bandwidths for high performance with much less area. Table 4.5 compares the performance of our broadband power amplifier under ET mode with other power amplifier designs, operated with high PAPR signals. This clearly shows that envelope tracking can be used to achieve good performance for future applications where extremely wide carrier bandwidths are desired.

Table 4.3: Summary of broadband ET PA results

<b>Under Envelope Tracking with a 6.6 dB PAPR WCDMA signal</b>		
Operating Frequency	500 MHz to 1750 MHz	
Output Power	2-4 W	
Gain	10.3-13.9 dB	
Total Drain Efficiency	25% - 31%	
RF PA Drain Efficiency	48.5% - 58.5%	
ACPR before DPD	-36.95 dBc at 5 MHz offset	-50.64 dBc at 10 MHz offset
ACPR after DPD	-47.48 dBc at 5 MHz offset	-52.22 dBc at 10 MHz offset

## 4.5 Summary

In this chapter, high efficiency power amplifiers designed to operate over a broad range of carrier frequencies were discussed. Leveraging the intrinsic characteristics of GaN, stacked FETs with RC feedback have been utilized to demonstrate efficiencies

greater than 50% with more than 12 W of output power was measured across the 3:1 bandwidth from 500 MHz to 1750 MHz while terminated directly to 50 ohms at both the input and the output. At around 750 MHz, the peak efficiency was 64.3% with a gain of 14.7 dB, corresponding to high power densities of  $\sim 3.7 \text{ W/mm}^2$ . The stacked RC feedback broadband matching concept was further demonstrated in a push-pull configuration with a low-loss broadband balun for better even harmonic terminations. Spanning from 500 MHz to 2.5 GHz, the broadband push-pull hybrid power amplifier demonstrated power added efficiencies (PAE) greater than 47% including the loss of the balun, with output powers range between 12.5-18.2 W and greater than 16 dB gain was measured across the band. These results demonstrate one of the best combinations of gain, bandwidth, output power, and PAE in this frequency range when compared to state of the art published broadband power amplifiers. To demonstrate high efficiency operation under the presence of signals with high PAPR, the broadband PAs were operated under envelope tracking and compared to its constant drain counterpart. As a representative modulated signal, a 6.6 dB PAPR single-carrier WCDMA signal was used as the carrier frequency was tuned across the band. The overall efficiency of the envelope tracking power amplifier was 25% - 31% with 10.3 dB - 13.9 dB gain from 500 MHz to 1750 MHz, including the dissipation of the modulator. Compared to its constant drain counterpart, using the same WCDMA signal, more than 2 times improvement in average efficiency in the RFPA was observed as a result of operating in envelope tracking (as compared to constant drain mode), along with higher power density. Under envelope tracking, linearity specifications, as defined by the WCDMA base-station standards, were met with

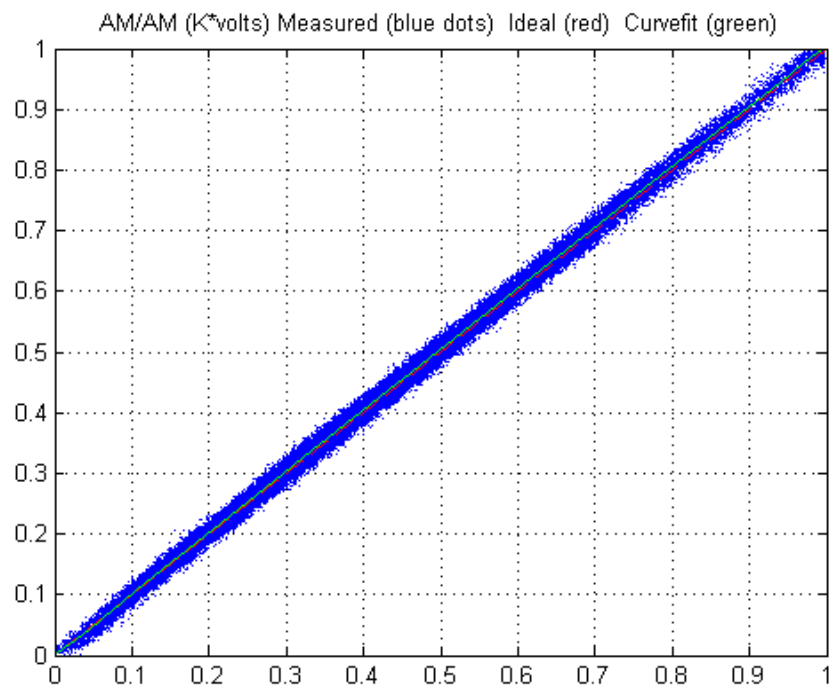


Figure 4.24: Measured AM-AM after DPD at 752 MHz.

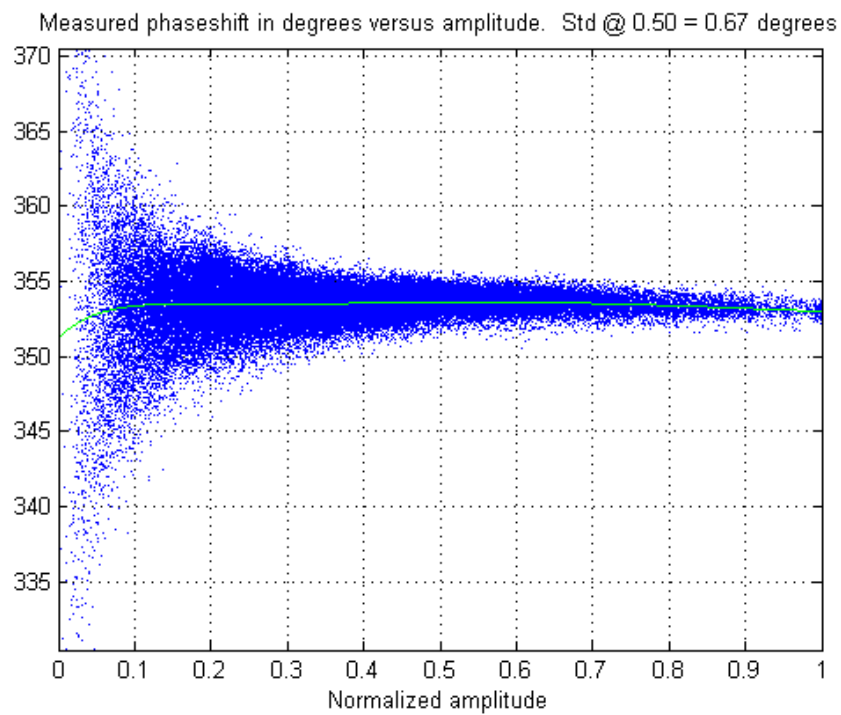


Figure 4.25: Measured AM-PM after DPD at 752 MHz.

Table 4.4: Comparison of reported broadband power amplifiers

**COMPARISON OF BROADBAND RF POWER AMPLIFIERS**

	Frequency (MHz)	Fractional BW (%)	Pout (dBm)	Efficiency (%)	Gain (dB)	Area	Output Match
[2]	20-2000	196	40	30-70	10-15	20.3mm x 12.7mm	Distributed
[5]	3500-10500	100	30	15-25	8	12.7mm x 10.2mm	Wideband Push-pull
[22]	2000-4000	67	40-42	52-72	9-11	65mm x 65 mm	Wideband Distributed
[23]	500-2500	133	42-44	30-40	9-11	-	Wideband Distributed
<b>This work</b>	<b>500-1750</b>	<b>111</b>	<b>40.6-41.0</b>	<b>56-64.3</b>	<b>12-16</b>	<b>1.125mm x 1.82mm</b>	<b>None</b>

Table 4.5: Comparison of reported broadband power amplifiers performance under high PAPR signals.

**COMPARISON OF BROADBAND PA PERFORMANCE UNDER HIGH PAPR SIGNALS**

	Frequency (MHz)	Fractional BW (%)	Pout (dBm)	Efficiency (%)	Gain (dB)	Topology	Modulated Signal
[22]	2000-4000	67	27.8-29.8	25-27	9-11	Constant Bias	11.2 dB PAPR 20 MHz LTE
[24]	1600-2100	27	27.5	30-36.3	-	Doherty	7.5 dB PAPR 10 MHz LTE
[25]	1.500-2140	35	42.1-44.5	31-44	11.5-13	Doherty	6-7 dB PAPR WCDMA
<b>This Work</b>	<b>500-1750</b>	<b>111</b>	<b>33-36</b>	<b>25-31</b>	<b>10.3-13.9</b>	<b>ET</b>	<b>6.6 dB PAPR WCDMA</b>

the use of digital pre-distortion. The results presented in this paper demonstrate the potential and applicability of envelope tracking power amplifiers in next generation broadband communication systems where high efficiency and high linearity in the presence of high PAPR signals are desired.

## 4.6 Acknowledgments

The author is very grateful to RF Micro Devices (Greensboro, NC) and Mitsubishi Electronics Inc. (Japan) for the GaN IC fabrication, and Dr. Young-pyo Hong for the design of the low-loss broadband balun, without which this work would not have been possible, and to Mr. Don Kimball, Shintaro Shinjo, Kenji Mukai, and Dr. Peter Asbeck for their discussions and suggestions.

Some of the materials in chapter 4 are as they appear in “Design of a 4-W Envelope Tracking Power Amplifier With More Than One Octave Carrier Bandwidth”, Jonmei J. Yan, Chin Hsia, Donald F. Kimball and Peter M. Asbeck, published in IEEE Journal of Solid-State Circuits, Vol. 47, No. 10 and in “Broadband High PAE GaN Push-Pull Power Amplifier for 500 MHz to 2.5 GHz Operation”, Jonmei J. Yan, Young-pyo Hong, Shintaro Shinjo, Kenji Mukai, and Peter M. Asbeck, submitted and accepted to the International Microwave Symposium 2013, June 2013. The contributions from the co-authors are appreciated. The author of this dissertation was the primary investigator and author for these publications.

# Chapter 5

## Adaptive De-troughing for Wide Modulation Bandwidth Signals

### 5.1 Introduction

Next generation communication systems use OFDM-based modulations with high peak-to-average power ratios (PAPRs), resulting in efficiency degradation in power amplifiers. Techniques such as the Doherty amplifier and envelope tracking (ET) have demonstrated high average efficiency in the presence of such signals. In the previous chapters, the ET architecture demonstrated advantages such as broad carrier bandwidths (Chapter 4), high efficiency under average power back-off operation (Chapter 3), and ease of implementation by substituting a static supply with a dynamic supply. However, one of the major challenges in implementing envelope tracking for next generation wireless systems lies in its ability to support wide modulation bandwidth signals. One of the main challenges in enabling such wider bandwidth signals for ET is the design of the envelope modulator, particularly at high output powers, where components in the

envelope modulator can be both bandwidth and slew-rate limited. In previous publications, signal-processing techniques have been made to limit the bandwidth REF and the slew-rate REF of the envelope modulator output (termed here supply waveform). However, both techniques resulted in significant efficiency degradation of the RFPA. Additionally, both efforts were demonstrated with a 5 MHz modulation bandwidth signal – which was within the regime, which the modulator was capable of producing without modification.

The envelope amplifier in discussion here is one designed for high power base-station applications, supporting up to 100 W of average power with peak envelope voltage of 30V. The switcher stage operates to provide mostly the RMS (root-mean-square) power. Its switching frequency is designed such that it contributes to most of the DC to low frequency components. The linear stage is designed as a high fidelity video amplifier with significantly larger bandwidth to accommodate the higher frequency components of the envelope supply waveform. In addition to providing linear voltage amplification of the VDD signal as a result of the linear stage feedback network, the linear stage also performs to reduce the error current by sinking and sourcing the necessary current as demanded by the RFPA. As a result of the high power demands from the RFPA, large devices are needed with intermediate driving stages in the linear stage, resulting in bandwidth and slew rate limitations and limiting maximum supported modulated envelope.

In this chapter, a DSP approach called “adaptive de-troughing” is introduced and used to extend the capabilities of the dynamic supply modulator in terms of its bandwidth and slew-rate capability to support wider modulation bandwidths with very little

efficiency penalty by reducing the supply waveform slew rate and bandwidth at selected time periods. We demonstrate the technique with 20MHz LTE signals, which is above the performance limit of the unmodified envelope amplifier. In addition, for a 10 MHz LTE signal, use of “adaptive de-troughing” showed that approximately 5-6% increase in the efficiency of the modulator can be achieved, compared to the “standard de-troughing” supply waveform.

## 5.2 Power Supply Waveform Engineering Implementation

Under envelope tracking, since the input of the RFPA is fed with a fully modulated signal, the drain supply voltage can be shaped to a wide range of voltage values without losing the amplitude information (provided the supply voltage remains high enough to avoid clipping). In much of our previous work, the drain (or collector) supply voltage was shaped to linearly track the envelope of the RF signal, except at low input voltages, for which the drain supply was “de-troughed” in order to reduce sensitivity to time misalignment and avoid gain collapse, according to:

$$V_{DD} = V_{DD,max} \left( |x_{RF}| + b \cdot e^{-\frac{|x_{RF}|}{b}} \right) \quad (5.1)$$

where  $|x_{RF}|$  is the normalized amplitude of the RF input signal and  $b$  is the approximately equal to the ratio of the RFPA knee voltage and the peak voltage of the envelope signal. By setting a low  $b$ , high average efficiencies were obtained by keeping the RFPA close to saturation. In this work,  $b$  was set to 0.1 ( $V_{DD,max} = 28V$  and  $V_{DD,min} = 2.8V$ ).



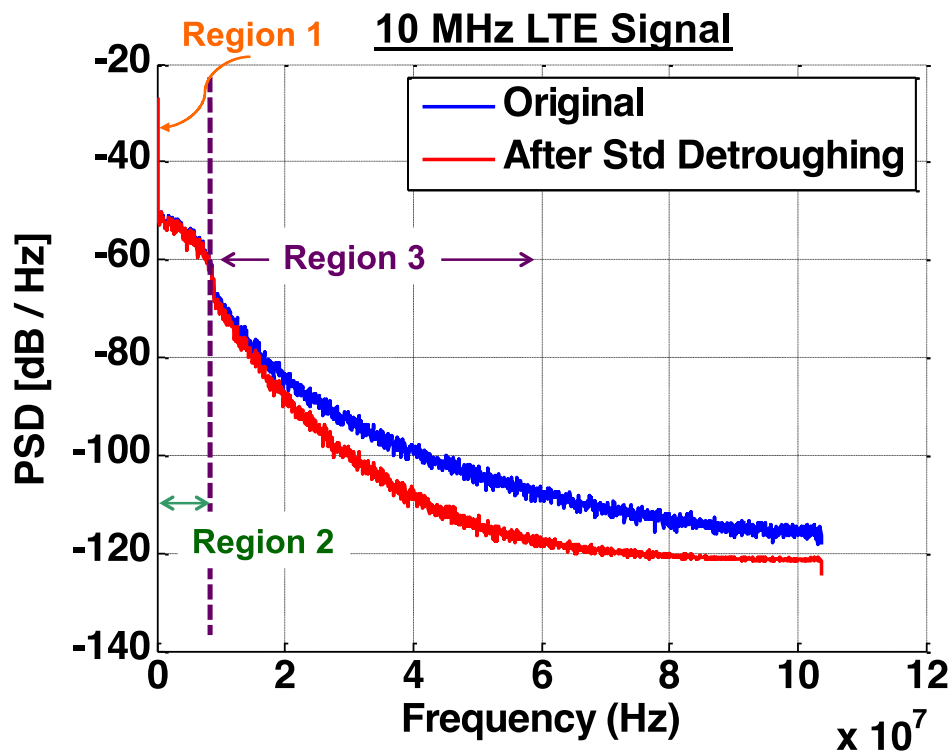


Figure 5.1: Spectral response of a 10 MHz LTE envelope signal.

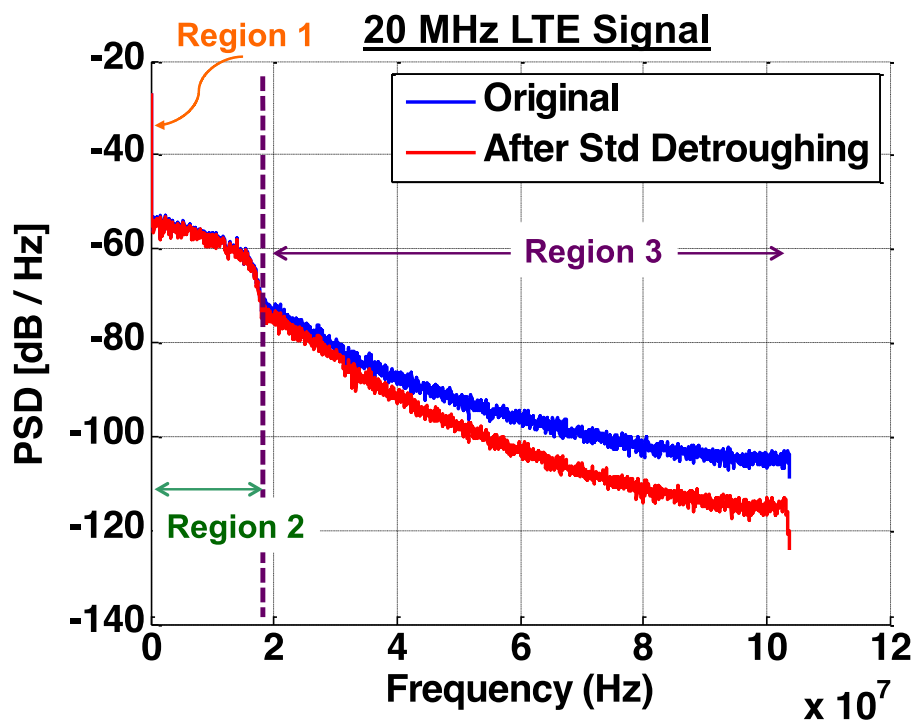


Figure 5.2: Spectral response of a 20 MHz LTE envelope signal.

As a result of de-troughing, the power spectrum of the envelope signal shows that the amount of power at high frequencies is reduced as shown in Figure 5.2. This alleviates the load on the linear stage at the high frequencies while the majority of the modulated supply voltage remains unperturbed within the modulation bandwidth. In this manner, the efficiency degradation due to de-troughing is also minimal (less than 1%) since the supply still follows the envelope of the RF signal and the RFPA is kept in saturation most of the time.

As mentioned in chapter 2, the supply modulator consists of two stages, the linear stage and the switcher stage, working in parallel. The finite rise and fall time of the switching transistor and the inductor of the converter place a limit on the switching frequency the switcher stage can provide. As a result, in the presence of high modulation bandwidth signals, the switcher stage ends up following more closely the RMS current than the envelope current waveform, leading to considerable ac current to be sourced or sunk by the linear stage. This requires high current capability for the linear stage and the larger devices are limited in bandwidth and slew-rate, which is essentially configured similar to a non-inverting feedback amplifier.

Figure 5.1 and Figure 5.2 above show the spectral response of the envelope waveform of LTE-A signals for various modulation bandwidths. We can divide the spectrum into three regions: region 1 (DC to a few hundreds of kHz), region 2 (a few hundreds of kHz to the modulation bandwidth), and region 3 (beyond the modulation bandwidth). The majority of the power of the envelope waveform (> 85%) is within 100 kHz, contained in region 1 and is provided by the switcher stage. However, there is a significant amount of power beyond the few kHz up to the modulation bandwidth of the

signal, namely region 2. For wide modulation bandwidth signals where the switcher stage provides mainly the RMS power, the linear stage must provide this additional region 2 power. This spectral region is critical to the accuracy of the envelope of the waveform and requires accurate large signal behavior of the linear stage of the modulator. In addition, a small amount of power extends beyond the modulation bandwidth (region 3), which is necessary in order to maintain the signal integrity of the overall envelope tracking power amplifier. However, since the power level of this portion is so low, its integrity is associated with the small signal response of the linear stage.

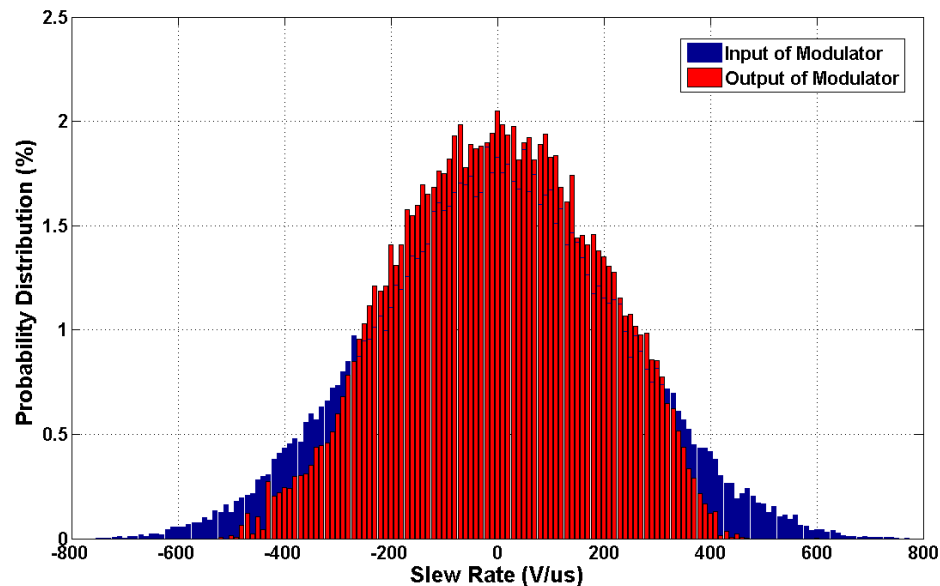


Figure 5.3: Histogram of the slew-rate into and out of the modulator.

For a 20 MHz LTE-A signal, power in region 1 is provided primarily by the switcher stage and in regions 2 and 3, it is provided by the linear stage. Region 3 extends from 20 MHz to 100 MHz, which is within the small signal bandwidth of the linear stage. In region 2, the  $V_{DD}$  output waveform is dominated by the large signal behavior of the linear stage and limited by two main properties: 1) large signal bandwidth and 2) slew-

rate of the op-amp. The large signal bandwidth of the linear stage is about 25-30 MHz, which is suitable for region 2 of the 20 MHz signal. However, the slew-rate requirements for the 20 MHz signal exceeds the capability of the linear stage.

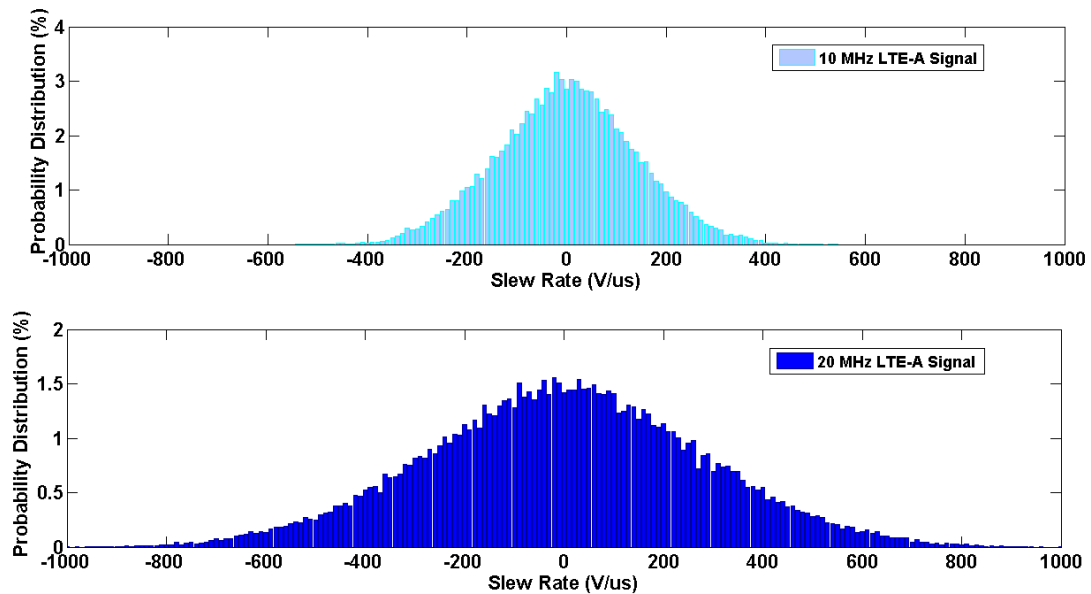


Figure 5.4: Histogram of the slew-rate of a 10 MHz and 20 MHz LTE supply envelope waveform.

To explore the slew-rate limitations of the supply modulator, we begin by examining its performance characteristics with a 15 MHz LTE signal. Figure 5.3 illustrates the histogram of the 15 MHz LT signal into and out of the supply modulator terminated with a resistive load. For the input signal, 95% of the slew-rate is contained within 600 V/us. However, measurement results at output showed that the higher slew-rates are unable to be replicated. As a result of the slew-rate limitation in the modulator, the output slew-rate was limited to about 425 V/us. By taking a histogram of the slew rate of the 10 MHz LTE signal, we find that 95% of the signal is contained within 400 V/us, as depicted in Figure 5.4, which is within the slew-rate capability of the high power

envelope amplifier. A histogram of the slew-rates of a 20 MHz signal shows that to cover 95% of the signal, the envelope amplifier would need to support 900 V/us, as shown in Figure 5.4, which is outside the supported range for this high power envelope amplifier.

In this work, we introduce power supply waveform engineering of the supply signal using a technique called “adaptive de-troughing”, which can reduce the slew-rate of the envelope waveform while still maintaining the bandwidth characteristics of the signal. In this manner, the efficiency degradation of the RFPA would be minimized. To properly modify the supply envelope waveform, certain conditions are required to maintain acceptable envelope tracking operation, namely:

1. To ensure the RF output isn't clipped, the proposed waveform must always be larger than the true envelope of the RF signal.
2. The supply waveform bandwidth should be maximized to make full use of the envelope modulator bandwidth.
3. The envelope modulator must operate within its slew-rate limits. We require that 95% of the waveform's slew-rate distribution be contained within modulator's range (up to 400 V/us).
4. In order to maintain high efficiency operation of the RFPA, the difference between the proposed VDD signal and the true envelope of the RF signal should be minimized.

Because, in the envelope tracking system, the envelope supply waveform is generated in DSP and converted into analog voltage via a digital-to-analog converter

(DAC) at a sampling frequency  $f_s$ , the time elapsed is computed in discrete time steps. An overall time period  $\Delta t$  is associated with the number of samples  $N_{\text{samples}}$ , expressed as

$$\Delta t = N_{\text{samples}} \cdot \frac{1}{f_s}. \quad (5.2)$$

For a given maximum slew-rate  $SR_{\text{max}}$  required for the adaptively de-toughed signal (condition #3), the slew-rate, rate of voltage or current change with time, of the signal must satisfy the expression,

$$SR = \frac{\Delta V_{\text{env}}}{\Delta t} \leq SR_{\text{max}}, \quad (5.3)$$

where  $\Delta V_{\text{env}}$  is the change in voltage. To determine the time window in baseband to which a compliant slew-rate ( $< SR_{\text{max}}$ ) will be found, we can express the maximum amplitude change  $\Delta V_{\text{env,max}}$  as the difference between the peak and minimum envelope supply voltage, given by

$$\Delta V_{\text{env,max}} = V_{DD,\text{max}} - V_{DD,\text{min}}. \quad (5.4)$$

The window or maximum time elapsed to which a compliant slew-rate will be found is a function of the maximum number of samples and expressed as

$$\Delta t_{\text{max}} = N_{\text{samples,max}} \cdot \frac{1}{f_s}. \quad (5.5)$$

Hence, for a given maximum voltage range and desired slew-rate, a compliant slew-rate can be determined within  $N_{samples,max}$  can be expressed as

$$N_{samples,max} = \frac{\Delta V_{env,max}}{SR_{max} \cdot 1/f_s} = \frac{V_{DD,max} - V_{DD,min}}{SR_{max} \cdot 1/f_s}. \quad (5.6)$$

To construct an adaptively de-troughed envelope supply waveform, the slew-rate of the supply envelope waveform is first calculated. For each non-compliant slew-rate, a modified envelope waveform is generated such that the slew-rate at each point complies with the maximum slew-rate. For a given initial non-compliant slew-rate, occurring on the downward slope of the envelope waveform, we will in general have

$$SR_{initial} = \frac{V_i - V_{i+1}}{t_i - t_{i+1}} < -SR_{max}. \quad (5.7)$$

The we choose the next incremental envelope waveform value of the original waveform at  $N_{samples}$  away, such that

$$|SR_{new}| = \left| \frac{V_i - V_{i+N_{samples}}}{N_{samples}/f_s} \right| \leq |SR_{max}|. \quad (5.8)$$

To smooth the transition between the values from the original envelope waveform and the modified values where the original slew-rate was not compliant, extra points at the end points are used to ensure a non-abrupt (continuous) change in slope between the adaptively de-troughed section and the rest of the original supply waveform. For this work, 3 extra points were used. A cubic spline interpolation was performed to determine

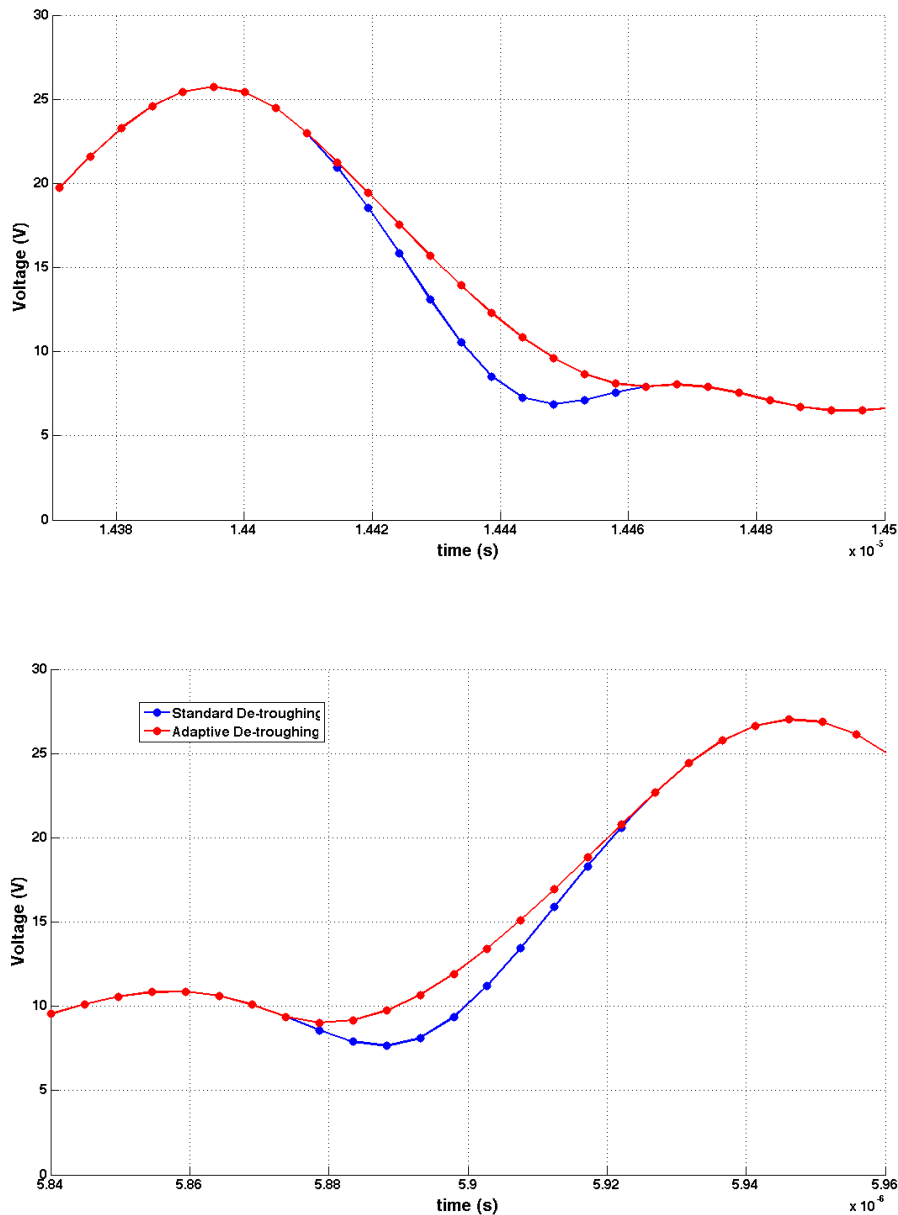


Figure 5.5: Example of a cubic spline interpolation used after “adaptive de-toughing” in the time domain; showing the original envelope, the new envelope supply waveform using cubic spline interpolation for a downward slope (top) and upward slope (bottom).

the modified envelope waveform corresponding to points between  $t_i$  and  $t_{i+N_{samples}}$  using the time values and corresponding voltages from  $t_{i-3}, \dots, t_i, t_{i+N_{samples}}, \dots, t_{i+N_{samples}+3}$ . Figure 5.5 illustrates an example of the cubic



spline interpolation between  $t_i$  and  $t_{i+N_{samples}}$  with 3 extra points at either end point with the corresponding modified envelope waveform value.

For an initial non-compliant slew-rate occurring on the upward slope of the envelope waveform, a similar algorithm is used except, rather than changing waveforms over a span with index  $N_{samples}$ , interpolation is performed using values  $N_{samples}$  back in time, such that

$$|SR_{new}| = \left| \frac{V_{i+1-N_{samples}} - V_{i+1}}{N_{samples}/f_s} \right| \leq |SR_{max}|. \quad (5.9)$$

This algorithm was used to produce “adaptively de-troughed” waveforms that are better suited to our present envelope modulators, and their characteristics were explored. While most of the envelope supply waveforms follow the standard de-troughing function, selected values were adaptively de-troughed to meet the previous criteria, resulting in values that no longer strictly depend on the amplitude of the RF signal. Relatively few points were perturbed, however, and no clipping was produced.

Figure 5.6 illustrates the relationship between the normalized envelope voltage and the normalized supply waveform for the adaptive de-troughed envelope waveform. With the original waveform, there was an one-to-one relationship between the supply waveform and the envelope waveform. This is no longer true for the adaptive de-troughing waveform. As a result of decoupling this relationship, the gain characteristic of the RFPA is determined by the surface defined by the supply voltage and the input power  $[G(t) \sim g(V_{DD}(t), V_{in}(t))]$ , rather than a single trajectory  $[G(t) \sim g(V_{in}(t))]$ , implying that an added parameter in the linearization of the ET PA under the presence of

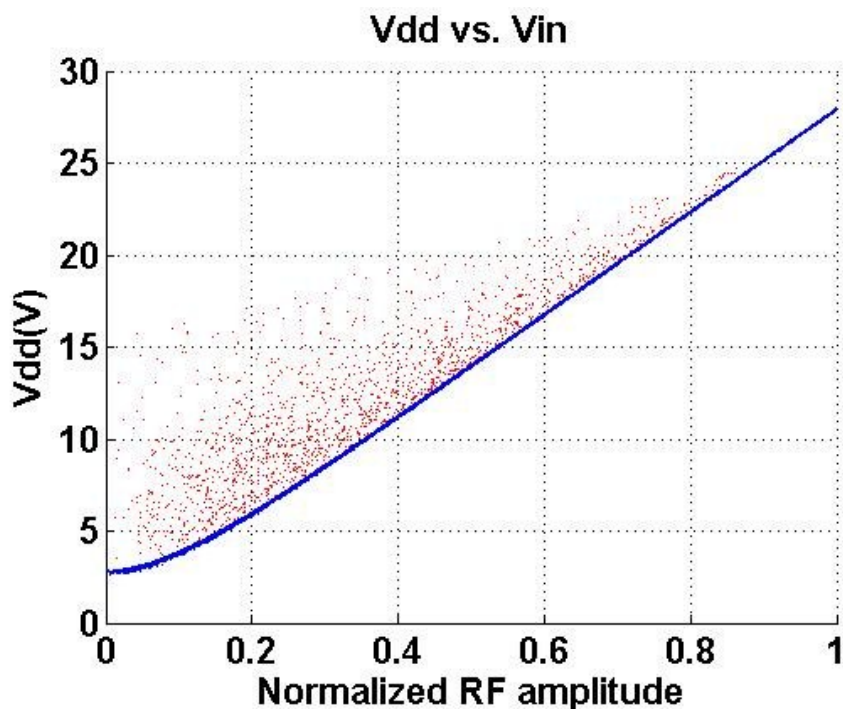


Figure 5.6: Normalized envelope versus normalized RF amplitude signal after adaptive de-troughing.

an adaptively de-troughed envelope supply is needed, as discussed in more details in section 5.5.

Figure 5.7 illustrates the corresponding power spectral density comparison showing that for the “adaptively de-troughed” supply waveform, the main lobe of the envelope is maintained, maximizing the bandwidth usage of the envelope amplifier. From the histogram shown in Figure 5.8, it is also observed that that the slew-rate of the “adaptively de-troughed” envelope is also contained within the modulator’s accessible range (400 V/us). Also, in envelope tracking, the efficiency of the RFPA is predominantly determined by the RMS voltage presented by the envelope amplifier. The voltage variation of the envelope signal remains approximately the same. As an example, with the representative 20 MHz LTE-A signal, the RMS voltage increased from 12.44 V

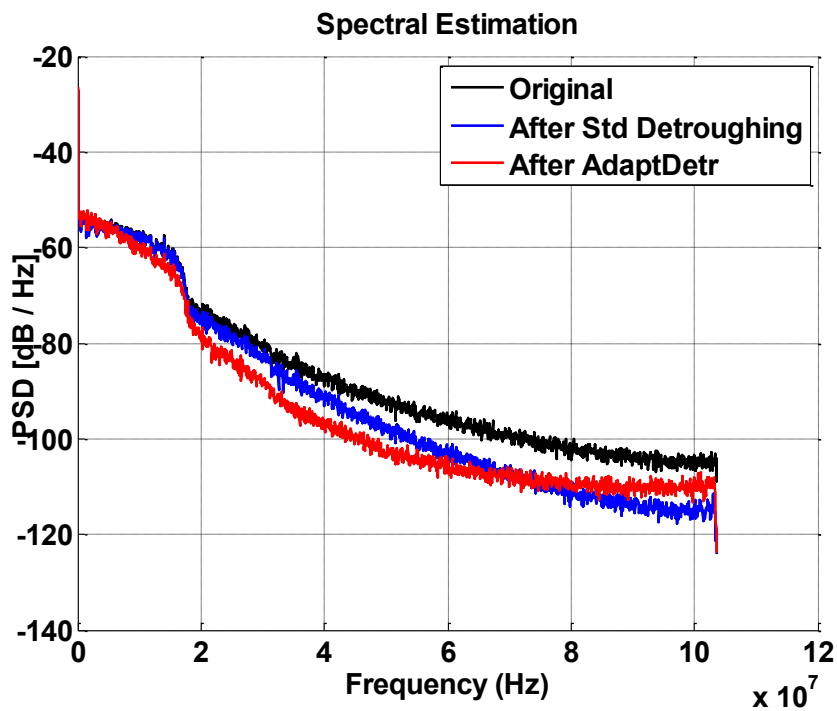


Figure 5.7: Power spectral density after adaptive de-trouching.

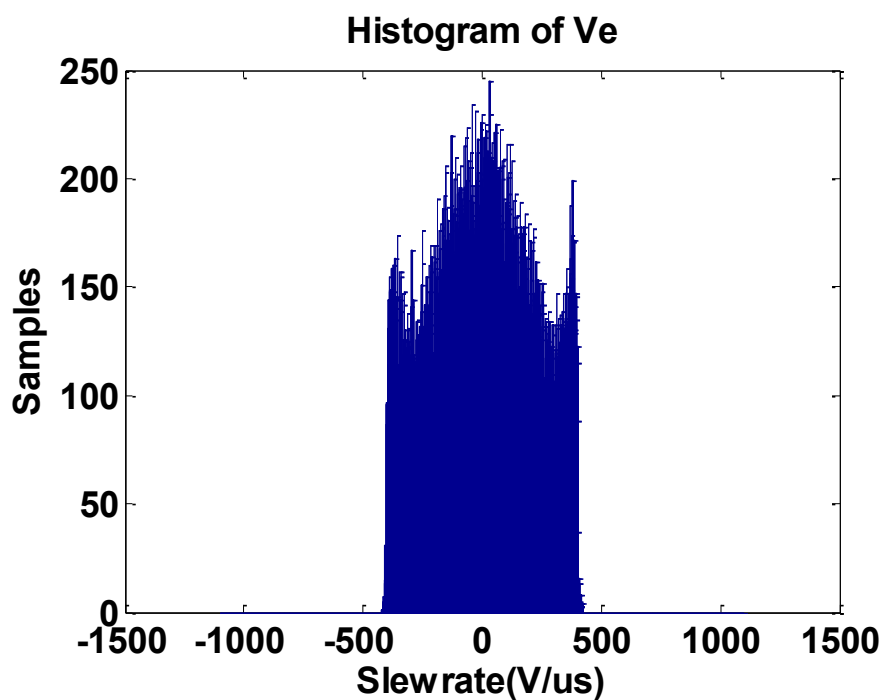




Figure 5.8: Histogram of a representative 20 MHz LTE-A signal after "adaptive de-trouching".

after “standard de-troughing” to 12.68 V after “adaptive de-troughing”. The RFPA, on average, is expected to behave similarly, with only a very subtle degradation in RFPA efficiency, when supplied by this adaptively de-troughed envelope, while the dynamic supply modulator is expected to behave slightly more efficiently.

## 5.3 Effects on Dynamic Power Supply Performance

Table 5.1: Measurements with a 6 Ohms resistive load.

	5 MHz	10 MHz	20 MHz
Std Detroughing	68%	61%	 BURN 
<b>Adaptive Detroughing</b>	73%	67%	<b>59%</b>

As mentioned previously, the efficiency of the dynamic modulator using the “adaptively de-troughed” waveform is expected to increase. This is a result of the reduced burden on the linear stage of the modulator. To demonstrate this, measurements were performed on the modulator with a resistive load of 6 Ohms. Comparing the measured efficiency while using the standard de-troughing and the adaptive de-troughing waveforms, about 5-6% efficiency improvement was obtained for a given bandwidth signal, as tabulated in Table 5.1. Due to the heat dissipation under such high power output conditions, the 20 MHz signal using the standard de-troughing scenario resulted in damage to the envelope modulator. By contrast, the 20 MHz LTE signal after adaptive de-troughing was found to achieve an efficiency similar to that of the 10 MHz LTE waveform under standard de-troughing (which had a similar maximum slew-rate). Figure

5.9 illustrates the measured power spectrum of the envelope amplifier output, demonstrating its capability to support a 20 MHz signal. Within the main lobe of the spectral response, the output spectrum closely resembles that of the input signal. To evaluate the linearity performance at the output of the modulator, a comparison of the modulator input and output was signals performed. As shown in Figure 5.10, a linear relationship was demonstrated and a normalized RMS error of 2.8% was achieved.

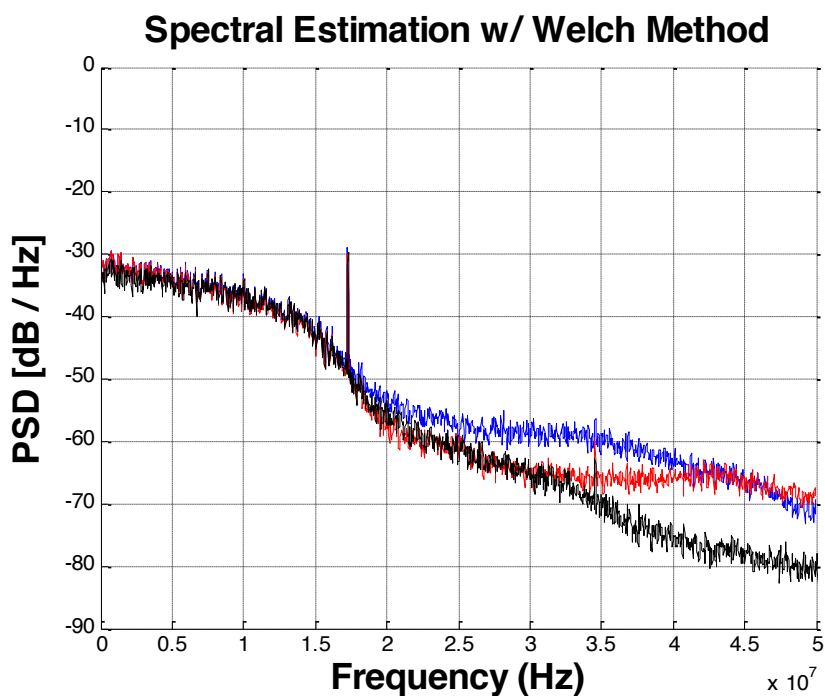


Figure 5.9: Power spectral density of the adaptively de-troghed envelope in MATLAB, input into the envelope amplifier, and output of the envelope amplifier to a 6 ohms load.

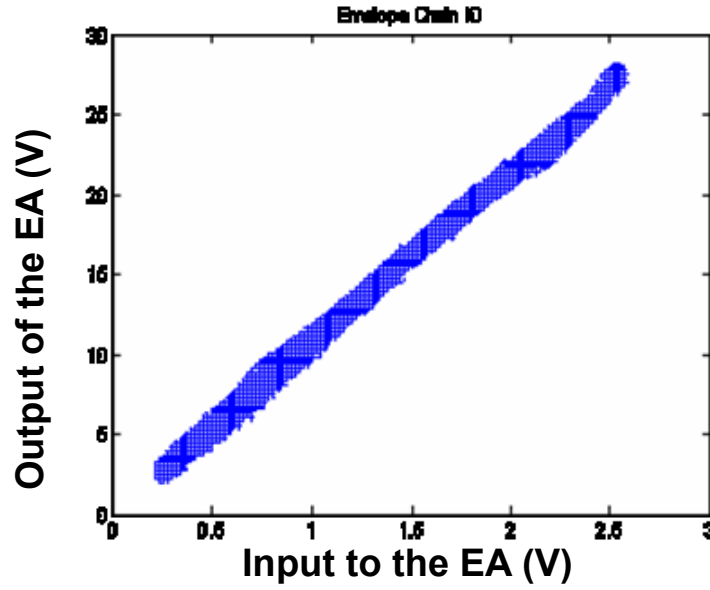


Figure 5.10: Comparison of the envelope amplifier input and output.

## 5.4 Effects on RF Power Amplifier Efficiency

As mentioned previously, because in the construction of the adaptively de-troughed envelope few values were modified and the RMS voltage of the envelope supply remained relatively the same, little degradation in the RF PA efficiency is expected. To analyze this quantitatively, we can evaluate the efficiency degradation factor  $k$ , the ratio between the RFPA efficiency using an adaptively de-troughed supply and the RF efficiency when supplied by the true envelope of the RF signal,  $k$  is given by

$$k = \frac{\langle \eta_{RFPA,AdaptDetr} \rangle}{\langle \eta_{RFPA,OrigEnv} \rangle} = \frac{\langle P_{out,AdaptDetr} \rangle / \langle P_{DC,AdaptDetr} \rangle}{\langle P_{out,OrigEnv} \rangle / \langle P_{DC,OrigEnv} \rangle}. \quad (5.10)$$

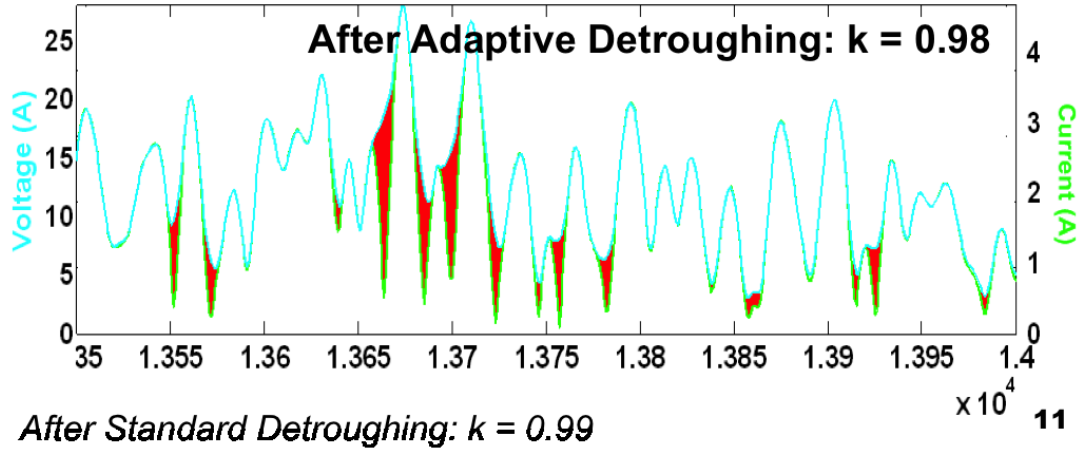


Figure 5.11: Time domain representation after adaptive de-troughing such that 95% of the waveform's slew-rate is contained within 400 V/us.

Since the voltage supplied to the RFPA does not clip and the average output power, dependent mainly on the RMS voltage of the envelope supply, remains predominantly the same, the RF PA output power  $P_{out}$  is the same for both cases. Also, in a Class B PA, the supply current can be expressed as a function of the true envelope of the RF signal divided by the optimal load impedance presented to the RFPA, namely

$$I_{DC} = \frac{V_{DC,OrigEnv}}{R_L}. \quad (5.11)$$

This leads to

$$k \approx \frac{\langle P_{DC,OrigEnv} \rangle}{\langle P_{DC,AdaptDetr} \rangle} \approx \frac{\langle I_{DC} \cdot V_{DC,OrigEnv} \rangle}{\langle I_{DC} \cdot V_{DC,AdaptDetr} \rangle}. \quad (5.12)$$

Hence, the efficiency degradation factor can be simplified as the average of the square of the true envelope divided by the average of the product of the true envelope and the “shaped” supply waveform, given by

$$k \approx \frac{\langle I_{DC} \cdot V_{DC,OrigEnv} \rangle}{\langle I_{DC} \cdot V_{DC,AdaptDetr} \rangle} = \frac{\langle V_{DC,OrigEnv} \cdot V_{DC,OrigEnv} \rangle}{\langle V_{DC,OrigEnv} \cdot V_{DC,AdaptDetr} \rangle}. \quad (5.13)$$

As an example, shown in Figure 5.11, for the “adaptively de-troughed” supply waveform of a 20 MHz LTE-A signal, a  $k$  factor of 0.98 (or 2% degradation) was calculated. Under the “standard de-troughing”, a  $k$  factor of 0.99 was calculated for the same signal. Therefore, in comparison to other techniques such as direct bandwidth reduction, the new adaptively de-troughed signal has a low penalty cost to the RFPA efficiency.

## 5.5 Digital Pre-distortion for “Adaptively De-troughed” ET Power Amplifiers

The power amplifiers must have high linearity in order to meet the physical air interface requirements imposed by regulatory agencies. Power amplifiers are typically allocated only a portion of the spurious output levels allowed by the specifications. Nonlinearities in power amplifiers may be characterized as amplitude (AM-AM) distortion, phase (AM-PM) distortion, intermodulation distortion (IMD), and spectral regrowth. Amplitude distortion occurs when the output amplitude is not a linear function of the input signal. This effect is due to the gain expansion or compression at the fundamental frequency. Amplitude distortion leads to the rise of harmonic and intermodulation distortions. Harmonic distortion is the creation of harmonics of the fundamental frequency at the output. Intermodulation distortion occurs when multi-tone signals are present at the input. Due to the mixing of the input frequencies, other



frequency components are present at the output. Unlike harmonic frequencies, intermodulation products can fall in-band and on the fundamental frequency, making it impossible to filter out. Digital pre-distortion can be used to cancel the distortion products near the signal of interest. In addition to AM-AM distortion, an amplifier also typically exhibits phase (AM-PM) distortion. AM-PM distortion represents the change in phase of the transfer characteristics as the drive level increases towards compression.

Memoryless digital pre-distortion (DPD) was carried out by measuring the output data via the feedback down-converter chain, synchronizing the output data with its corresponding input, and fitting the data (amplitude and phase) with an appropriate polynomial. With envelope tracking power amplifiers using supply waveforms using standard de-toughing, the supply voltage and the amplitude of the input RF signal are strongly coupled by the relationship expressed in (4.3). In this case, a 2-dimensional look-up-table (LUT) with the input amplitude of the RF signal as the independent variable can be used to model the output of the ET-HPA such that

$$P_{out} = f(x_{RF}, V_{env}) = f[x_{RF}, g(|x_{RF}|)], \quad (5.14)$$

where  $x_{RF}$  is the RF input signal and  $V_{env}$  is the supply voltage, as depicted by the solid blue line in Figure 5.12. However, in the case where “adaptive de-toughing” is used, particular values of the supply voltage are no longer coupled to the amplitude of the RF signal, as illustrated in Figure 5.6. Hence, the ET-HPA behavior tracks along a surface (in the  $x_{RF}, V_{env}$  space) rather than a single trajectory, whose output is now dependent on both the amplitude of the RF PA,  $x_{RF}$ , and the supply voltage  $V_{env}$ , as shown in Figure 5.12. This results in additional memory effects at the RF output.

Thus, a modified LUT-based pre-distortion linearization approach is needed to correct for the additional memory effects caused by “adaptive de-troughing”. One necessary condition of the pre-distorted envelope supply is that sufficient supply voltage be provided to the RFPA such that desired linearized output power be achievable. Under “adaptive de-troughing”, the supply envelope generated is always larger than the envelope of the RF signal. Hence, for these particular values of the supply voltage, the RFPA is no longer operated in compression, resulting in gain expansion. Since less than 10% of the original envelope was adaptively de-troughed, one approach is to first perform LUT-based inversion of the AM-AM and AM-PM to achieve memoryless linearization such that the sufficient supply is provided. The new supply waveform with “adaptive de-troughing” is then generated from the resulting pre-distorted input signal. With sufficient supply voltage provided and memoryless linearization achieved, we can then determine the “deterministic memory” effects, memory components that are repeatable, due to the inherent memory in the RFPA as well as the self-induced memory as a result of “adaptive de-troughing”. The deterministic component can be extracted from the repeatable measurements after subtracting out the memory-less components. Iterative adjustments are made to the pre-distorted RF input signal while keep the “adaptively de-troughed” envelope supply the same.

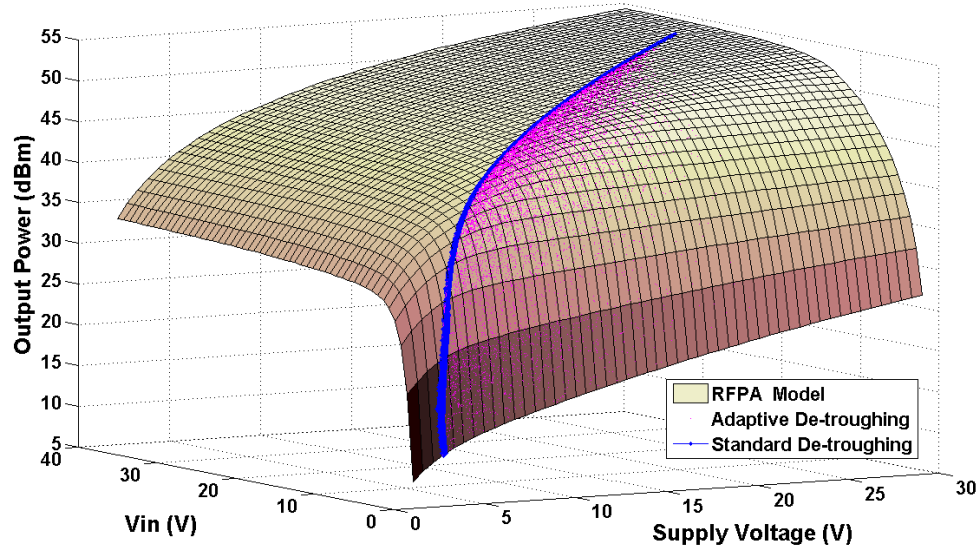


Figure 5.12: Relationship surface between output power, input voltage, and supply voltage of a RFPA with “standard de-troughing” (blue) and under “adaptive de-troughing” (magenta).

## 5.6 Adaptively De-troughed Envelope Tracking Power Amplifier Performance

The ET-HPA architecture, comprising the dynamic supply modulator and the RF power amplifier, was demonstrated to maintain high efficiency for high PAPR signals. Signal generation, de-cresting/de-troughing, time alignment, and pre-distortion algorithms are performed with DSP at baseband, with a sampling rate of 207.36 MHz. The RF signal was generated with a digital IF at 51.84 MHz. The envelope tracking system was implemented using a GaAs High Voltage HBT as the RF final stage. Measurements were done with 10 MHz and 20 MHz LTE signals centered at 2.14 GHz. To demonstrate envelope tracking with an RF PA, measurements were made using a 120W Triquint GaAs HVHBT biased in Class AB at 2.14 GHz in conjunction with an envelope modulator capable of supporting up to 10 MHz modulation bandwidth with

conventional envelopes. The GaAs HVHBT was operated at a peak envelope voltage of 29.5V and a minimum supply voltage of 2.95V. Proper time alignment is critical between the supply voltage and the RF signal at the RFPA. In this work, sub-sample time alignment was performed digitally.

Table 5.2 shows the summary of results with a 10 MHz LTE 64-QAM signal with a conventional envelope and a 20 MHz LTE 64-QAM signal, adaptively de-troughed to the same maximum slew rate. The overall ET efficiency with the adaptively de-troughed 20 MHz LTE signal was measured to be around 48% with 27 W of output power and 12.6 dB of gain. These results are comparable to the 10 MHz LTE under the standard de-troughing function. The subtle efficiency difference between the two sets of results is due to both a lower efficiency in the EA and the RFPA as a result of using a wider modulation bandwidth signal. Comparing the 10 MHz LTE signal with and without adaptive de-troughing, as we had predicted, very little penalty in terms of efficiency was observed using this technique. As previously calculated, about 2% RFPA efficiency degradation was expected as result of adaptive de-troughing. Although subtle degradation in the RFPA efficiency occurred in the adaptive de-troughing scenario, the overall ET efficiency increased due to the larger increase in the modulator efficiency. Hence, “adaptive de-troughing” can also be used to enhance the efficiency of the overall ET system where slightly higher EVM and memory effects can be tolerated.

After pre-distortion, the EVM of the 64QAM / LTE signal obtained with “adaptive de-troughing” reduced to 3.8%. From the AM-AM and AM-PM plots in Figure 5.13, it can be observed that a significant spread is present. This spread is due primarily to:

1. changes in the gain characteristics of the RFPA with different drain biases and
2. changes in output power dependent on the past history of the drain bias (conventionally referred to as ‘memory effects’).

As a result of the first effect, a modified linearization routine will be necessary to achieve better linearity in the presence of these adaptively de-troughed supply waveforms.

## 5.7 Summary

Envelope tracking power amplifiers offer many benefits such as high average efficiency for high PAPR signals, and broad carrier tunable bandwidths. In this work, adaptive de-troughing is used to extend the capabilities of an existing envelope amplifier in terms of its bandwidth and slew-rate capability beyond its original abilities with very little efficiency penalty in the RFPA efficiency, as evident by the 2% efficiency degradation factor. In addition, comparing waveforms with the same modulation bandwidth, measurement results show that approximately 5-6% increase in modulator efficiency was measured as a result of using “adaptive de-troughing”. Additionally, as a result of the minimal RFPA efficiency degradation, the overall ETPA efficiency increases by 3.5-4% after “adaptive de-troughing”. For further linearity improvements, it can be observed that a modified linearization routine is needed to account for changes in gain characteristics as a result of the adaptively de-troughed VDD signal.

Table 5.2: Summary of measurement results of a 10 MHz LTE signal and an “adaptively de-troughed” 20 MHz LTE signal

		Gain (dB)	Output Power (W)	Efficiency (%)	PAE (%)	EVM (%)
10 MHz 64 QAM LTE (after standard de-troughing)	Before DPD	12.45	28.3	50.3	47.5	3.7
	After DPD	12.5	30.6	51.1	48.2	1.8
10 MHz 64 QAM LTE (after adaptive de-troughing)	Before DPD	12.5	28.7	53.9	50.86	4.2
	After DPD	12.55	30.8	54.7	51.66	2.3
20 MHz 64 QAM LTE (after adaptive de-troughing)	Before DPD	12.6	26.8	47.9	45.25	6.9
	After DPD	12.6	27.4	48.2	45.5	3.8

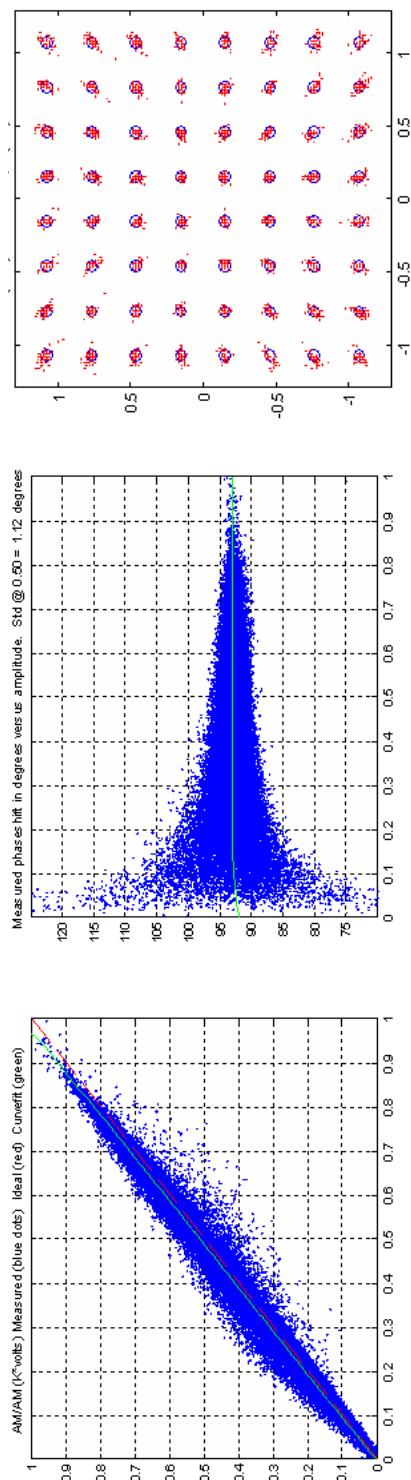


Figure 5.13: Measured AM-AM, AM-PM, and constellation of the adaptively de-troughed 20 MHz signal after digital pre-distortion.

## 5.8 Acknowledgements

The author is very grateful to Triquint Semiconductors for providing GaAs HVHBT power amplifier used in this work, to Nokia-Siemens Networks for valuable discussions, and to Mr. Paul Draxler, Mr. Don Kimball, Mr. Hayg Dabag, and Dr. Peter Asbeck for their valuable discussions and suggestions.

Some of the materials in chapter 5 are as they appear in “Enabling Wide Modulation Bandwidth for Envelope Tracking Power Amplifiers Through the Use of DSP”, Jonmei J. Yan, Paul Draxler, Donald F. Kimball and Peter M. Asbeck, published in GoMACTech Conference 2012. The contributions from the co-authors are appreciated. The author of this dissertation was the primary investigator and primary author for this publication.

# Chapter 6

## Conclusion and Future Work

### 6.1 Dissertation Summary

In order to accommodate the increasing demand for higher data rates while remaining within limits of the frequency allocation mandated by the FCC, advances in wireless communications have led to signals with complex non-constant envelopes with high peak-to-average ratios and stringent in-band and out-of-band linearity requirements in order to maintain spectral efficiency. Among the various proposed power amplifier architectures for high efficiency operation for these high PAPR signals, the envelope tracking power amplifier is one of the more promising candidates for high efficiency when various system requirements such as linearity, power, bandwidth, and dynamic range are considered simultaneously. In this dissertation, the design of broadband envelope tracking power amplifiers for micro- and macro- base-station applications for wireless communication systems was investigated. The study of the envelope tracking power amplifiers in both simulation and experiment in terms of practical performance



factors such as bandwidth, efficiency, linearity, and back-off operation has led to solutions for better overall performance.

The dissertation began with an analysis of the envelope tracking power amplifier. In order to evaluate broadband envelope tracking power amplifiers under full power and average back-off operation, a broadband power amplifier test-bench was implemented. A calibration equalization route was developed in order to obtain a flat linear response over the entire 100 MHz instantaneous bandwidth of the system. Envelope tracking power amplifiers ranging from UHF to mm-wave were measured and their performances (including efficiency, gain, and output power) were evaluated, with record efficiencies demonstrated at each band.

Next, in efforts to demonstrate the performance advantage of envelope tracking under practical scenarios where the average power demanded of the power amplifier fluctuates with the load demands over time, the envelope tracking power amplifier under average power back-off was analyzed. Monte-carlo simulations based on a projected time-varying power profile were used to determine the long-term efficiency of the ET power amplifier. Comparisons of the long-term efficiency with other architectures were made. In a comparison with a 2-way ideal Doherty with the same peak efficiency as the ET PA, analysis showed that the ET PA achieved more than 1.4x reduction in the overall energy consumed, making ET a promising architecture in the presence of practical field applications where the average power fluctuates over time.

Thirdly, envelope tracking power amplifiers are fundamentally immune to variations of the frequency of the carrier since the envelope of the RF signal remains the same, independent of the carrier. Hence, the same supply modulator, capable of

supporting such modulation bandwidths, can be used for multi-band power amplifiers to achieve high efficiency in the presence of high PAPR signals and over average power back-off. Single-ended and push-pull stacked power amplifiers were designed to demonstrate broad bandwidth operation. A compact GaN stacked power amplifier with R feedback, demonstrating multi-octave operation, was placed under envelope tracking. In comparison with its constant supply counterpart, using the same modulation signal, the novel amplifier demonstrated more than 2 times average efficiency improvement over the entire bandwidth.

Finally, a technique called adaptive de-troughing for enhancing the modulation bandwidth capability of the supply modulator was investigated. Effects of this technique on the supply modulator and the RF power amplifier were studied. A digital pre-distortion technique for the adaptively de-troughed envelope signals was described. Measurement results demonstrated that approximately 5-6% increase in overall efficiency was provided when compared to conventional VDD supply waveforms. For a supply modulator capable of supporting ~10 MHz modulation bandwidths conventionally, the technique extended the modulator's ability so that it could support 20 MHz modulation bandwidth signals with 48% ET efficiency, used with a GaAs HVHBT PA.

## **6.2 Future Work**

### **6.2.1 Envelope Tracking Power Amplifier Modeling**

A SPICE-based full-scale model of the dynamic supply modulator needs to be developed for further optimizing. A constant impedance load can be used to initially

model the power amplifier for the design and development of the SPICE-based supply modulator model. With the recent advancements of microwave simulators, multi-platform simulations can also be made possible. To accurately model the envelope tracking power amplifier, integration of the SPICE-based supply modulator with power amplifier design in simulators like Agilent ADS or AWR Microwave Office can be realized to obtain a more realistic response of the envelope amplifier and optimization of the overall system. In addition, a more accurate prediction of the nonlinearities may lead to better DPD algorithms specified for envelope tracking power amplifiers.

### **6.2.2 Reconfigurable Broadband Envelope Tracking Power Amplifier**

In chapter 4, broadband power amplifiers were designed for envelope tracking. The designed was based on class AB operation. On the other hand, harmonic tuning can be used to achieve even high power amplifier efficiency. Traditional harmonic tuning has been viewed as a relatively narrowband technique for achieve high efficiency. However, in most practical applications, the power amplifier is not operated over a multi-octave bandwidth instantaneously. Hence, reconfigurable harmonic tuning networks at the output can be used to achieve high efficiency at the desired carrier frequency with the use of high voltage varactors. Additionally, reconfigurable network can be placed at the input of the ET PA to boost the gain and PAE of the ET PA.

### **6.2.3 Hybrid Supply Modulator for Broad Modulation Bandwidth Signals**

In chapter 5, the need for modulators with broad modulation bandwidth was discussed. In conjunction with using the adaptive de-toughing technique to extend the bandwidth of the modulator, a hybrid design of the modulator utilizing faster switching devices can be used to realize a more efficient modulator. With recent developments of enhancement-mode GaN devices, faster high voltage switching stages can be realized. Further innovations for reducing the power demanded by the linear stage and reducing the delay through the switcher path remains a key to the design of an efficient broadband modulator.

### **6.2.4 Envelope Supply Path Equalizer and Linearization**

In chapter 5, to mitigate the self-induced memory effects as a result of adaptive de-toughing, the pre-distortion of the envelope supply path was decoupled from the RF path. We can further extend this to a separate pre-distortion algorithm for the envelope path for better linearity. This involves an additional ADC path for tapping off the supply at the drain of the RFPA for analysis and signal processing. In addition, the envelope supply path contains filters and various components that cause frequency dependent amplitude and phase variations. Similar to an equalization routine presented in chapter 2, a calibration equalization can be added to the supply path for better response and fewer memory effects.

# References

- [1] R.M.Smith, J. Lees, P. Tasker, J. Benedikt, and S.C.Cripps, , "A 40W push-pull power amplifier for high efficiency, decade bandwidth applications at microwave frequencies," *Microwave Symposium Digest (MTT), 2012 IEEE MTT-S International* , 17-22 June 2012.
- [2] P. Draxler, et. al, "Memory effect evaluation and pre-distortion of power amplifiers," in *Proc. IEEE MTT-S Int. Microw. Symp.*, June. 2005
- [3] Draxler, P.J.; Anding Zhu; Yan, J.J.; Kolinko, P.; Kimball, D.F.; Asbeck, P.M.; , "Quantifying distortion of RF power amplifiers for estimation of predistorter performance," *Microwave Symposium Digest, 2008 IEEE MTT-S International* , June 2008.
- [4] S. C. Cripps, *RF Power Amplifiers for Wireless Communications*. Norwood, MA: Artech House, 2006.
- [5] Raab, F.H.; Asbeck, P.; Cripps, S.; Kenington, P.B.; Popovic, Z.B.; Pothecary, N.; Sevic, J.F.; Sokal, N.O.; , "Power amplifiers and transmitters for RF and microwave," *Microwave Theory and Techniques, IEEE Transactions on* , vol.50, no.3, pp.814-826, Mar 2002.
- [6] Lashkarian, N.; Tarn, H.; Dick, C., "Crest Factor Reduction in Multi-carrier WCDMA Transmitters," *Personal, Indoor and Mobile Radio Communications, 2005. PIMRC 2005. IEEE 16th International Symposium on* , vol.1, no., pp.321,325, 11-14 Sept. 2005.
- [7] Braithwaite, R.N., "Implementing crest factor reduction (CFR) by offsetting digital predistortion (DPD) coefficients," *Integrated Nonlinear Microwave and Millimetre-Wave Circuits (INMMIC), 2012 Workshop on* , vol., no., pp.1,3, 3-4 Sept. 2012.
- [8] Braithwaite, R.N., "A Combined Approach to Digital Predistortion and Crest Factor Reduction for the Linearization of an RF Power Amplifier," *Microwave Theory and Techniques, IEEE Transactions on* , vol.61, no.1, pp.291,302, Jan. 2013.
- [9] Jau-Horng Chen; Kenney, J.S., "A Crest Factor Reduction Technique for W-CDMA Polar Transmitters," *Radio and Wireless Symposium, 2007 IEEE* , vol., no., pp.345,348, 9-11 Jan. 2007.
- [10] Baxley, R.J.; Chunming Zhao; Zhou, G.T., "Constrained Clipping for Crest Factor Reduction in OFDM," *Broadcasting, IEEE Transactions on* , vol.52, no.4, pp.570,575, Dec. 2006.

- [11] Steinbeiser, C.; Landon, T.; Suckling, C.; Nelson, J.; Delaney, J.; Hitt, J.; Witkowski, L.; Burgin, G.; Hajji, R.; Krutko, O.; , "250 W HVHBT Doherty With 57% WCDMA Efficiency Linearized to -55 dBc for 2c11 6.5 dB PAR," *Solid-State Circuits, IEEE Journal of* , vol.43, no.10, pp.2218-2228, Oct. 2008
- [12] Ildu Kim; Junghwan Moon; Seunghoon Jee; Bumman Kim, "Optimized Design of a Highly Efficient Three-Stage Doherty PA Using Gate Adaptation," *Microwave Theory and Techniques, IEEE Transactions on* , vol.58, no.10, pp.2562-2574, Oct. 2010.
- [13] Jeong, J., et. al; "Modeling and Design of RF Amplifiers for Envelope Tracking WCDMA Base-Station Applications," *MTT, IEEE Transactions on* , vol.57, no.9, pp.2148-2159, Sept. 2009.
- [14] Wang, F., et.al; "Design of wide-bandwidth envelope-tracking power amplifiers for OFDM applications," *MTT, IEEE Transactions on* , vol.53, no.4, pp. 1244-1255, April 2005.
- [15] Asbeck, P., et.al; , "High dynamic range, high efficiency power amplifiers for wireless communications," *BCTM 2005, IEEE*, Santa Barbara, CA, 2005.
- [16] Yang, Y., et. al ; "High efficiency CDMA power amplifier with dynamic current control circuits," *CSICS, 2004. IEEE* , Monterey, CA, Oct. 2004
- [17] Bumman, K., et.al; "Efficiently Amplified," *Microwave Magazine, IEEE* , vol.11, no.5, pp.87-100, Aug. 2010.
- [18] R.M.Smith, J. Lees, P. Tasker, J. Benedikt, and S.C.Cripps, , "A 40W push-pull power amplifier for high efficiency, decade bandwidth applications at microwave frequencies," *Microwave Symposium Digest (MTT), 2012 IEEE MTT-S International* , 17-22 June 2012.
- [19] X Chenggang; Pavio, Anthony; "Development of GaN HEMT based High Power High Efficiency Distributed Power Amplifier for Military Applications," *Military Communications Conference, 2007. MILCOM 2007. IEEE*, vol., no., pp.1-4, 29-31 Oct. 2007.
- [20] Meliani, C.; Behtash, R.; Wiirfl, J.; Heinrich, W.; Trankle, G.; "A Broadband GaN-MMIC power amplifier for L to X Bands," *Microwave Integrated Circuit Conference, 2007. EuMIC 2007.*, Oct. 2007.
- [21] Patterson, Howard; Scarpitto, Forrest; Bielick, Brian; "Broadband Characterization of GaN Transistors for Software Defined Radio Power Amplifier Applications," *Military Communications Conference, 2007. MILCOM 2007. IEEE* , vol., no., pp.1-7, 29-31 Oct. 2007
- [22] Jong-Wook Lee; Webb, K.J.; "Broadband GaN HEMT push-pull microwave power amplifier," *Microwave and Wireless Components Letters, IEEE* , vol.11, no.9, pp.367-369, Sep 2001
- [23] Pornpromlikit, S.; Jinho Jeong; Presti, C.D.; Scuderi, A.; Asbeck, P.M.; "A Watt-Level Stacked-FET Linear Power Amplifier in Silicon-on-Insulator CMOS,"

*Microwave Theory and Techniques, IEEE Transactions on* , vol.58, no.1, pp.57-64, Jan. 2010.

- [24] Jinseong Jeong; Kimball, D.F.; Myoungbo Kwak; Chin Hsia; Draxler, P.; Asbeck, P.M.; , "Modeling and Design of RF Amplifiers for Envelope Tracking WCDMA Base-Station Applications," *Microwave Theory and Techniques, IEEE Transactions on* , vol.57, no.9, pp.2148-2159, Sept. 2009
- [25] A. Ezzeddine, and H. Huang, "Broadband MMIC power amplifier for multiple wireless systems," *Wireless and Microwave Technology Conference (WAMICON), 2010 IEEE 11th Annual*, 12-13 April 2010.
- [26] W. M. Fathelbab and M. B. Steer, "New classes of miniaturized planar Marchand baluns," *IEEE Trans. Microw. Theory Tech.*, vol. 53, no. 4, pp. 1211–1220, Apr. 2005.
- [27] Grebennikov, A.; , "A high-efficiency 100-W four-stage Doherty GaN HEMT power amplifier module for WCDMA systems," *Microwave Symposium Digest (MTT), 2011 IEEE MTT-S International* , vol., no., pp.1-4, 5-10 June 2011.
- [28] Steinbeiser, C.; Landon, T.; Suckling, C.; Nelson, J.; Delaney, J.; Hitt, J.; Witkowski, L.; Burgin, G.; Hajji, R.; Krutko, O.; , "250 W HVHBT Doherty With 57% WCDMA Efficiency Linearized to -55 dBc for 2c11 6.5 dB PAR," *Solid-State Circuits, IEEE Journal of* , vol.43, no.10, pp.2218-2228, Oct. 2008.
- [29] Iwamoto, M.; Williams, A.; Pin-Fan Chen; Metzger, A.G.; Larson, L.E.; Asbeck, P.M.; , "An extended Doherty amplifier with high efficiency over a wide power range," *Microwave Theory and Techniques, IEEE Transactions on* , vol.49, no.12, pp.2472-2479, Dec 2001
- [30] Godoy, P.A.; Chung, S.; Barton, T.W.; Perreault, D.J.; Dawson, J.L.; , "A highly efficient 1.95-GHz, 18-W asymmetric multilevel outphasing transmitter for wideband applications," *Microwave Symposium Digest (MTT), 2011 IEEE MTT-S International* , vol., no., pp.1-4, 5-10 June 2011
- [31] van der Heijden, M.P.; Acar, M.; Vromans, J.S.; Calvillo-Cortes, D.A.; , "A 19W high-efficiency wide-band CMOS-GaN class-E Chireix RF outphasing power amplifier," *Microwave Symposium Digest (MTT), 2011 IEEE MTT-S International* , vol., no., pp.1-4, 5-10 June 2011
- [32] Chin Hsia; Kimball, D.F.; Asbeck, P.M.; , "Effect of maximum power supply voltage on envelope tracking power amplifiers using GaN HEMTs," *Power Amplifiers for Wireless and Radio Applications (PAWR), 2011 IEEE Topical Conference on* , vol., no., pp.69-72, 16-19 Jan. 2011
- [33] Jonmei J. Yan.; Kimball, D.; Chin Hsia; Hsuan-yu Pan; Ricketts, S.; Ghajari, H.; , "High-efficiency, high-linearity envelope tracking power amplifier for mobile UHF applications," *MILITARY COMMUNICATIONS CONFERENCE, 2010 - MILCOM 2010* , vol., no., pp.1572-1576, Oct. 31 2010-Nov. 3 2010

- [34] Joon Hyung Kim; Gwan Do Jo; Jung Hoon Oh; Young Hoon Kim; Kwang Chun Lee; Jae Ho Jung; , "3.54GHz 10W envelope tracking amplifier with 43% efficiency utilizing the 1.5 bit-high efficiency envelope amplifier," *Power Amplifiers for Wireless and Radio Applications (PAWR), 2011 IEEE Topical Conference on* , vol., no., pp.21-24, 16-19 Jan. 2011
- [35] Wang, F., et.al; "Design of wide-bandwidth envelope-tracking power amplifiers for OFDM applications," *MTT, IEEE Transactions on* , vol.53, no.4, pp. 1244-1255, April 2005.
- [36] Yan, J.J.; Hsia, C.; Kimball, D.F.; Asbeck, P.M.; , "GaN Envelope Tracking Power Amplifier with More Than One Octave Carrier Bandwidth," *Compound Semiconductor Integrated Circuit Symposium (CSICS), 2011 IEEE* , vol., no., pp.1-4, 16-19 Oct. 2011.
- [37] Myoungbo Kwak; Kimball, D.; Presti, C.; Scuderi, A.; Santagati, C.; Jonmei Yan; Asbeck, P.; Larson, L.; , "Wideband high efficiency envelope tracking integrated circuit for micro-base station power amplifiers," *Radio Frequency Integrated Circuits Symposium (RFIC), 2011 IEEE* , vol., no., pp.1-4, 5-7 June 2011.
- [38] Ezzeddine, A.; Ho Huang; "Broadband MMIC power amplifier for multiple wireless systems," *Wireless and Microwave Technology Conference (WAMICON), 2010 IEEE 11th Annual* , vol., no., pp.1-3, 12-13 April 2010.
- [39] P. Saad, C. Fager, H. Cao, H. Zirath, K. Andersson, "Design of a Highly Efficient 2–4-GHz Octave Bandwidth GaN-HEMT Power Amplifier," *Microwave Theory and Techniques, IEEE Transactions on* , vol.58, no.7, pp.1677-1685, July 2010
- [40] Jaewoo Sim, Jaeyeon Lim, Myoungkyu Park, Wenwoo Kang, Bak-II Mah, "Analysis and design of wide-band power amplifier using GaN," *Microwave Conference, 2009. APMC 2009. Asia Pacific*, 7-10 Dec. 2009
- [41] Daehyun Kang; Dongsu Kim; Yunsung Cho; Jooseung Kim; Byungjoon Park; Chenxi Zhao; Bumman Kim; , "1.6–2.1 GHz broadband Doherty power amplifiers for LTE handset applications," *Microwave Symposium Digest (MTT), 2011 IEEE MTT-S International* , vol., no., pp.1-4, 5-10 June 2011.
- [42] Bathich, K.; Markos, A.Z.; Boeck, G.; , "A wideband GaN Doherty amplifier with 35 % fractional bandwidth," *Microwave Conference (EuMC), 2010 European* , vol., no., pp.1006-1009, 28-30 Sept. 2010.